UNIVERSIDAD DE INVESTIGACIÓN DE TECNOLOGÍA EXPERIMENTAL YACHAY

Escuela de Ciencias Físicas y Nanotecnología

TÍTULO: Adsorption of Glyphosate in water by Fe₃O₄@TiO₂ Nanocomposite

Trabajo de integración curricular presentado como requisito para la obtención del título de Ingeniero en Nanotecnología

Autor:

Paredes Carranza Edison Patricio

Tutor:

Dra. Sarah Elisa Briceño Araujo, PhD.

Urcuquí, Junio del 2021

SECRETARÍA GENERAL
(Vicerrectorado Académico/Cancillería)
ESCUELA DE CIENCIAS FÍSICAS Y NANOTECNOLOGÍA
CARRERA DE NANOTECNOLOGÍA
ACTA DE DEFENSA No. UITEY-PHY-2021-00003-AD

A los 7 días del mes de mayo de 2021, a las 11:30 horas, de manera virtual mediante videoconferencia, y ante el Tribunal Calificador, integrado por los docentes:

Presidente Tribunal de Defensa	Dr. CHACON TORRES, JULIO CESAR , Ph.D.
Miembro No Tutor	Dra. GONZALEZ VAZQUEZ, GEMA , Ph.D.
Tutor	Dra. BRICEÑO ARAUJO, SARAH ELISA , Ph.D.

El(la) señor(ita) estudiante **PAREDES CARRANZA, EDISON PATRICIO**, con cédula de identidad No. **1805195771**, de la **ESCUELA DE CIENCIAS FÍSICAS Y NANOTECNOLOGÍA**, de la Carrera de **NANOTECNOLOGÍA**, aprobada por el Consejo de Educación Superior (CES), mediante Resolución **RPC-SO-13-No.156-2015**, realiza a través de videoconferencia, la sustentación de su trabajo de titulación denominado: **Adsorption of Glyphosate in water by Fe3O4@TiO2 Nanocomposite**, previa a la obtención del título de **INGENIERO/A EN NANOTECNOLOGÍA**.

El citado trabajo de titulación, fue debidamente aprobado por el(los) docente(s):

Tutor	Dra. BRICEÑO ARAUJO, SARAH ELISA , Ph.D.

Y recibió las observaciones de los otros miembros del Tribunal Calificador, las mismas que han sido incorporadas por el(la) estudiante.

Previamente cumplidos los requisitos legales y reglamentarios, el trabajo de titulación fue sustentado por el(la) estudiante y examinado por los miembros del Tribunal Calificador. Escuchada la sustentación del trabajo de titulación a través de videoconferencia, que integró la exposición de el(la) estudiante sobre el contenido de la misma y las preguntas formuladas por los miembros del Tribunal, se califica la sustentación del trabajo de titulación con las siguientes calificaciones:

Tipo	Docente	Calificación
Presidente Tribunal De Defensa	Dr. CHACON TORRES, JULIO CESAR , Ph.D.	9,8
Miembro Tribunal De Defensa	Dra. GONZALEZ VAZQUEZ, GEMA , Ph.D.	10,0
Tutor	Dra. BRICEÑO ARAUJO, SARAH ELISA , Ph.D.	10,0

Lo que da un promedio de: **9.9 (Nueve punto Nueve)**, sobre 10 (diez), equivalente a: **APROBADO**

Para constancia de lo actuado, firman los miembros del Tribunal Calificador, el/la estudiante y el/la secretario ad-hoc.

PAREDES CARRANZA, EDISON PATRICIO
Estudiante

Firmado electrónicamente por:
JULIO CESAR CHACON TORRES

Dr. CHACON TORRES, JULIO CESAR , Ph.D.
Presidente Tribunal de Defensa

Firmado electrónicamente por:
SARAH ELISA BRICENO ARAUJO

BRICEÑO ARAUJO, SARAH ELISA , Ph.D.
Tutor

GEMA GONZALEZ VAZQUEZ
Digitally signed by GEMA GONZALEZ VAZQUEZ
Date: 2021.05.07 13:23:09 -05'00'

Dra. GONZALEZ VAZQUEZ, GEMA , Ph.D.
Miembro No Tutor

AUTORÍA

Yo, **EDISON PATRICIO PAREDES CARRANZA**, con cédula de identidad 1805195771, declaro que las ideas, juicios, valoraciones, interpretaciones, consultas bibliográficas, definiciones y conceptualizaciones expuestas en el presente trabajo; así cómo, los procedimientos y herramientas utilizadas en la investigación, son de absoluta responsabilidad del autor del trabajo de integración curricular. Así mismo, me acojo a los reglamentos internos de la Universidad de Investigación de Tecnología Experimental Yachay.

Urcuquí, Junio del 2021.

_____

Edison Patricio Paredes Carranza

CI: 1805195771

AUTORIZACIÓN DE PUBLICACIÓN

Yo, **EDISON PATRICIO PAREDES CARRANZA,** con cédula de identidad 1805195771, cedo a la Universidad de Investigación de Tecnología Experimental Yachay, los derechos de publicación de la presente obra, sin que deba haber un reconocimiento económico por este concepto. Declaro además que el texto del presente trabajo de titulación no podrá ser cedido a ninguna empresa editorial para su publicación u otros fines, sin contar previamente con la autorización escrita de la Universidad.

Asimismo, autorizo a la Universidad que realice la digitalización y publicación de este trabajo de integración curricular en el repositorio virtual, de conformidad a lo dispuesto en el Art. 144 de la Ley Orgánica de Educación Superior

Urcuquí, Junio del 2021.

Edison Patricio Paredes Carranza

CI: 1805195771

Acknowledgments

I would like to thanks my friends who were there for me in this career. I like to thank them for the time that we spend in the university, for every night of study and also for every other night that we just hang out. You were the immediately people to listen to my stories, tears, laughs, and gave me their best. In a special way to my best friends Selena, Jenny, Carito, Fabian and my friend from Brazil Claudemir. Also, big thanks to my brother Carlos, who was my greatest support in my entire career. Finally, I would like to thank my family, without their support this could not be possible.

Edison Patricio Paredes Carranza

Dedication

I want to dedicate this work to my family, who with their patience and love have accompanied me during this project. To my angel Milton Edison who blesses me all the time. To my parents Elvia and Hugo for motivating me to study what I am passionate about, for teaching me to be persevering, for supporting me in my studies, and for being so generous with their advice and experiences. To my twin brother for teaching me to share happy moments, and to tolerate bad moments. Finally, I dedicate this work to my grandmother Evita who has been very attentive and generous to me, always supporting me in my studies and in my life.

Edison Patricio Paredes Carranza

Resumen

Los recursos naturales son el principal sustento del desarrollo y el avance de las poblaciones del mundo. El tratamiento de aguas contaminadas con métodos no destructivos, eficientes y amigables con el medio ambiente es uno de los temas más relevantes en los estudios de investigación. El glifosato es un pesticida organofosforado ampliamente utilizado en la industria agrícola para controlar especies de plantas. Su uso común ha provocado la liberación no deseada de glifosato en aguas residuales, ríos y otras fuentes de medios acuosos. La presencia de glifosato en aguas residuales y fuentes de agua afecta la salud humana y del ecosistema debido a su toxicidad. Por lo tanto en este trabajo, diseñamos un nanocompuesto magnético basado en TiO_2 con nanopartículas de magnetita (Fe_3O_4) para investigar el proceso de adsorción de glifosato comercial en agua. Las síntesis de nanocompuestos magnéticos son fácilmente atraídas por un campo magnético externo, lo que demuestra una rápida recuperación después de su funcionamiento. Los nanomateriales se caracterizaron mediant espectroscopía infrarroja por transformada de fourier (FTIR), XRD, mapeo de color EDS y SEM. Los espectros de FTIR demuestran la presencia de los picos característicos de las NP de TiO_2 y Fe_3O_4. Los patrones de XRD confirman la estructura de las NP de Fe_3O_4 y TiO_2 con un mayor porcentaje de la fase cristalina de anatasa que la de rutilo. Las micrografías de mapeo elemental SEM y EDS confirman la presencia de ambos materiales y revelan la agregación de nanopartículas de hierro. El tamaño medio de partícula del nanocompuesto fue de 100 ± 20 nm. Nuestros resultados demuestran que la tasa máxima de eliminación (R) alcanzada fue del 26 %. El mecanismo de adsorción/desorción investigado en este trabajo sostiene que el glifosato comercial con presencia de magnetita está relacionado con la formación de un complejo glifosato/metal que inhibe el desempeño del nanocompuesto como absorbente.

Palabras Claves: Nanotecnología, glifosato, adsorción, nanocompositos, $Fe_3O_4@TiO_2$.

Abstract

Natural resources are the main support of development and advancement of the populations in the world. The treatment of polluted waters with non-destructive, efficient and environmentally friendly methods are one of the most relevant topics in research studies. Glyphosate is an organophosphate pesticide widely used in the agricultural industry to control plant species. Its common use has led to the unwanted release of glyphosate in wastewater, rivers, and other sources of aqueous media. The presence of glyphosate in wastewater and water sources affect human and ecosystem health due to its toxicity. In this work, we design a magnetic nanocomposite based on TiO_2 with magnetite nanoparticles Fe_3O_4 to investigate the adsorption process of commercial glyphosate in water. The synthesis of magnetic nanocomposite are easily attracted by an external magnetic field, demonstrating the easily recover after the adsorption process. The nanomaterials were characterized using fourier-transform infrared spectroscopy (FTIR), XRD, EDS color mapping, and SEM. The FTIR spectra demonstrate the presence of the characteristic peaks of TiO_2 and Fe_3O_4 NPs. XRD patterns confirm the structure of Fe_3O_4 NPs and TiO_2 with a higher percentage of the anatase crystalline phase than the rutile one. SEM and EDS elemental mapping micrographs confirm the presence of both materials and reveal the aggregation of iron nanoparticles. The average particle size of the nanocomposite was 100 ± 20 nm. Our results demonstrate that the maximum removal rate (R) reached was 26%. The adsorption/desorption mechanism investigated in this work argues that the commercial glyphosate with the presence of magnetite is related to the formation of a glyphosate/metal complex inhibiting the performance of the nanocomposite as absorbent.

Keywords: Nanotechnology, adsorption, glyphosate, nanocomposite, $Fe_3O_4@TiO_2$.

Contents

List of Figures

List of Tables

Chapter 1

Introduction

Increasing global demand for organic food and the farmers action in order to increase crop yields, has made that pesticides such as Glyphosate, has a high adverse impact on health and the environment to be used. Glyphosate (N-phosphonomethyl glycine) (PMG) is a commercial organophosphate herbicide with a highly effective, non-selective, non emergent, broad spectrum pesticide.[1] PMG is widely used around the world in agriculture for weed control and other species different than what is being grown.[1,2] Its use has recently increased exponentially due to its efficient nondiscriminatory weed removal and the widespread planting of PMG resistant genetically modified crops.[1,3] However due to the large scale use of PMG, it has generated a level of concern because the half life of the PMG and its main metabolism aminomethylphosphonic acid (AMPA) can last several days with ranges of 0.8-151 days and 10-98 days, respectively.[1,4]

According to Yong et al.,[2] microorganisms and plants could degrade PMG to produce AMPA and sarcosine, which in turn could further degrade into water, carbon dioxide and phosphate, but this degradation is slow because it is made in a natural way.[2,5] Furthermore, Peerawas et al.,[6] in they research mention that there is concern about the harmful effect of PMG on human health, since there are several adverse effects of PMG, including teratogenesis, carcinogenesis and mutagenesis.[6] In Ecuador, the use of PMG in fumigation aircraft to delimit the borders between Ecuador and Colombia has been of great concern, since it represents a chronic threat to humans and the ecosystem in that part of the border country. Therefore, an effective and ecological degradation strategy is needed for PMG and AMPA.[7] Considering that PMG is highly soluble in water and could contaminate the aquatic environment through various mechanisms such as: spray drift, runoff, spills, or drainage and many degradation methods that have been intentionally sought many times.[1] As mentioned above, the biological processes of PMG degradation generally requires a long time and depend on environmental conditions,[1] due to the degradation of PMG in the environment is mainly by biotic pathways mediated like bacteria and fungi. In view of the strong soil binding properties of the PMG and the abundance of soil microorganisms, the biodegradation of PMG is more appropriate for soil environments.[1] Therefore, seeking a new form for degradation of PMG and AMPA in aqueous solutions with high efficiency, low cost and friend with the environment is the main objective of this research.

Several chemical techniques have been widely used to decontaminate glyphosate from aqueous environments. Biological of microbial degradation[8], photocalysis using semiconductors or oxidative reagents such as O_3, H_2O_2 and UV radiation is know as advanced oxidation processes (AOPs) which can mineralize organic compounds during the photoreaction and specially adsorption process.[1,9] Recent investigations,[10] explain that the AOPs processes for the degradation of PMG in water usually use several mechanisms such as: electrochemical processes, ozone, ultraviolet spectral region (UV), H_2O_2/UV and heterogeneous photocatalysts such as: TiO_2, MnO_2, MnO_2/graphite and magnetite are used for that.[9–11] However, despite of the fact that AOPs processes can be used for degradation of organic pollutants, there are some limitations for their application in wastewater treatment, especially in large scale application.[9] The high cost of UV light source reactors and separation-recovery of the catalyst are the main problems for scale up this processes. Fortunately, it has been demonstrate that the adsorption process, which is preliminary step to photocatalysis, can be an optimal path for pollutant water treatment.[11] Also the adsorption process is an important physicochemical process used for pollution control and its economical application depends on regenerating and reusing the spent adsorbents.[12] On the other hand application of magnetic nanoparticles as the support for heterogeneous catalysts or adsorbents provides favorable conditions for circumvents recycling problems.[13] Ferromagnetic materials such as iron oxides often show super-paramagnetic behavior and use as support for recycling the photocatalysts or adsorbents after catalytic reactions or treatment processes.[1]

Of all the oxide semiconductors, Titanium Dioxide (TiO_2) is one widely used in semiconductors as a adsorbent/photocatalyst for its chemical as well as commercial properties, such as its high stability in water, non toxic by ingestion, and low cost.[6,14]. According to Jian et al.,[14] the use of TiO_2 for the decomposition of organic and inorganic compounds is based on the following factors; a) the adsorption and photocatalytic reaction occurs at normal air pressure and temperature, b) unlike the direct photolysis process, degraded organic pollutants are completely mineralized into non toxic substances, c) TiO_2 is a semiconductor with capabilities to be reusable, d) photogenerated holes and electrons are extremely oxidized and reduced enough to produce superoxides from dioxygens, due to the interaction of the conduction band photoelectrons with O_2.[14] However, the efficiency of using TiO_2 as adsorbent or photocatalyst agent for degradation processes is not high and one of the difficulties is its separation and recovery. For this reason, the development of magnetic nanocomposites with TiO_2 has proven to be a good way to overcome these limitations. Therefore in order to increase the degradation efficiency and its rapid recovery, doping with (Magnetic Nanoparticles, Magnetite (Fe_3O_4)) is one of the best options.[14]

There are some reports,[13,15] in which nanocomposites of Fe_3O_4 have been synthesized with a coating of TiO_2 used in photocatalysis.[13,15] Magnetic separation marks a highly sustainable process since it prevents loss of catalyst mass and the use of additional solvents.[15] According to Sawsan et al.,[13] magnetic nanoparticles (Fe_3O_4) are ideal materials as nuclei, for several reasons; a) its biocompatibility and low toxicity, b) low Curie temperature, c) high coercivity and magnetization, d) efficient photon absorption capacity and e) presents strong dipole-dipole bonds in its molecules.[13] Also Sawsan et all.,[16] synthesized titanium dioxide nanoparticles on a magnetite core, in a kind of core shell using the co-precipitation method for Fe_3O_4 synthesis and the non-thermal method for the synthesis

of TiO_2, those synthesis was at 80°C and they evaluated its adsorption/photocatalytic activity for the removal of methylene blue from water.[13,16] In that research, they obtained a photodegradation efficiency of 96 % under solar irradiation, using a concentration of 70 ppm of methylene blue and 40 mg of the synthesized photocatalizer, for 140 minutes, at 34 °C.[13] On the other hand, another group of researchers deposited the titanium dioxide on metallic nanoparticles such as: Au, Co, Pt and noble metals in order to increase photocatalytic activity. They reports that the Titanium dioxide doped with metallic nanoparticles decrease the band gap and achieve a light absorbance with larger wavelengths.[13] Therefore the use of magnetic nanoparticles with TiO_2 is one of the best recovery options for adsorption and photocalaysis process.

Thus, in this work we propose to study of the adsorption efficiency of commercial glyphosate by using a $Fe_3O_4@TiO_2$ nanocomposite. The synthesis of the nanocomposite was done by a chemical co-precipitation method and combines two types of TiO_2; 1) commercial one at micrometer scale and 2) nanostructured TiO_2 modified using an ultrasound assistant method. The nanocomposite was characterized by UV-vis spectroscopy, X-ray diffraction (XRD), EDS color mapping and Scanning Electron Microscopy (SEM). The adsorption process was followed using UV-vis spectroscopy in order to quantify the absorbance of the Glyphosate.

Chapter 2

Motivation

2.1 Problem Statement

Natural resources are the support of development and advancement of the populations in the world. The treatment of polluted waters with non-destructive, efficient and environmentally friendly methods are one of the most relevant topics in research studies. The main water pollutants caused by human activities that stand out are: microbes and pathogens, heavy metals, organic matter, suspended sediments and the use of pesticides.[1,3] In urban areas where various industries such as textiles, food and laboratories are located, there are many chemical compounds that need treatments before disposing them to a large water body. On the other hand wastewater of agricultural origin is those generated by pesticides and fertilizers. The harmful effects of pesticides in water are given according to the toxicity expressed in the lethal dose, that is, in the persistence, which refers to the time it takes for the initial concentration to decrease in percentages tolerable by the environment.[17]

Pesticides, among them Glyphosate (N-phosphonomethyl glycine) (PMG), contaminate the water either by leaching, evaporation or runoff from rain or irrigation, and can reach groundwater, rivers and even oceans as thirsty or chemical loads carried by rivers.[17] In Ecuador, the production of crops such as banana plantations heavily use pesticides to control diseases, weeds and others in order to have an impeccable production of the product. The continued inadequate use, irrigation and drainage that the plantations possess, will be key to the magnitude of damage that can cause to the bodies of water and also to the organisms that are present including humans. PMG is one of the most widely used pesticides and with a high probability of affecting the health of living beings.[7] Since its commercial introduction, PMG has become the dominant herbicide worldwide. And its use is likely to increase further, as crops are genetically modified and develop tolerance for this herbicide.[18] Currently its commercial form not only contains PMG, but also a large amount of additives that prevent decomposition and that in contrast increases the toxicity of this product. Due to the increase in its use worldwide, it has generated high concern, because the action time of this herbicide can last approximately up to 151 days.[1,4] For all this, new processes have been developed in recent years as a viable and novel alternative for the treatment of liquid effluents contaminated with highly toxic compounds.

Although a range of conventional methods can be applied to remove PMG, which include oxidation, adsorption, ozonation, photolysis and photocatalytic degradation etc, an efficient and cost-effective method is still desirable.[11] From the structural formula of PMG, it is known that the glyphosate is a kind of organic phosphate in nature.[11] Fortunately, it has been demonstrated especially in the recent years that TiO_2, can be used as a low-cost adsorbent and photocatalyst for some pollutants degradation like pesticides. However this material as photocatalyst involves the use of highly strong and expensive UV light reactors for its activation and the difficulty of separation and recovery. In fact, we propose to degrade commercial glyphosate by adsorption process using a composite $Fe_3O_4@TiO_2$. This project has advantages over conventional methods of degradation of this type of herbicide by the low-cost adsorption mechanism using a $Fe_3O_4@TiO_2$ nanocomposite, and the easy recovery of the sample by applying a magnetic field.[15]

2.2   General and Specific Objectives

2.2.1   General Objective

- To study the adsorption of commercial glyphosate using a magnetic nanocomposite based on $Fe_3O_4@TiO_2$.

2.2.2   Specific Objectives

- To synthesize a magnetic nanocomposite based on $Fe_3O_4@TiO_2$.

- To characterize the nanocomposite using Fourier Transform Infrared Spectroscopy, X-ray diffraction, EDS color mapping and Scanning electron microscopy (SEM).

- To verify the efficiency of glyphosate adsorption using the nanocomposite based on $Fe_3O_4@TiO_2$.

Chapter 3

Theoretical Background

This chapter aims to introduce the general concepts, definitions, methodology, theoretical bases and processes that are of great help in understanding this research work. The first part of this chapter focuses on describing the emerging contaminant, such as commercial glyphosate, that is being to degraded in this work. Then, some alternatives that can be used for the degradation of contaminants in aqueous media are summarized. Mainly, an in-depth review of adsorption processes, their kinetics and models. On the other hand we discuses about the recent field of research such as Nanotechnology. What is Nanotechnology and its principles? What types of nanomaterials exist? What are Magnetic Nanoparticles? What are hybrids materials? among others. Finally, the chapter ends by describing some reported studies of glyphosate degradation.

3.1 Glyphosate

Glyphosate (N-phosphonomethyl glycine) (PMG) is an organophosphate herbicide, non selective, broad spectrum and the most widely used in history to remove undesirable weeds in agricultural and forest environments.[1] Its chemical molecule consists of a fraction of glycine and another of phosphomethyl (N-phosphonomethyl glycine) $C_3H_8NO_5$ according to Figure 3.1.[1] It is a herbicide that inhibits the synthesis of amino acids in plants, bacteria, algae, fungi and parasites, through inhibition of growth enzymes.[17] Since PMG became a generic compound, its cost has been drastically reduced. Within its components PMG has very complicated toxicity mechanisms. Its commercial form not only contains glyphosate but also several salts and commercial formulations containing surfactants, which vary in concentration and performance. Commercial formulations have different amounts of PMG concentration ranging from 1% to 41% for domestic use. Commonly these formulations contain an isopropylamine glyphosate salt alloy, surfactants, and several minor components including defoaming agents and inorganic ions. Therefore degradation of commercial PMG toxicity in aqueous solutions is difficult, since the contribution of surfactants and additives help increase toxicity.[18]

Regarding history, as reported by Stephen et al.,[19] glyphosate was first synthesized in 1970 by researcher Jhon
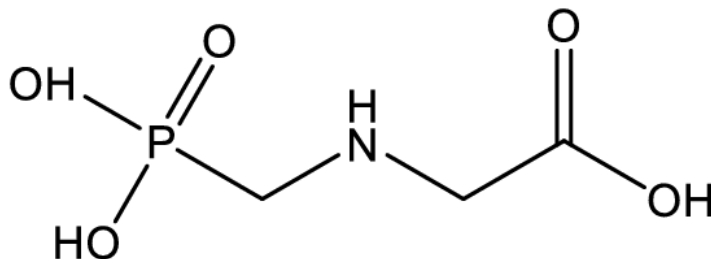
Figure 3.1: Chemical structure of glyphosate [N-(phosphonomethyl) glycine].[18]

Franz. Later, it was patented and put on the market.[19] During the last 30 years PMG has been chemically evolving, looking for alternatives for more selective use. Taking into account the widespread use of glyphosate worldwide, it is important to study its physicochemical properties, interactions with the components of water and soil, toxicity with the environment, as well as its detection, quantification, and degradation in natural samples.[1] Every pesticide product contains, in addition to the active ingredient, other substances whose function is to facilitate its handling or increase its effectiveness. In general, these ingredients, misleadingly called inert, are not specified on product labels. In the case of glyphosate herbicides, many inert ingredients have been identified. To help PMG penetrate plant tissues, most of its commercial formulas include a surfactant chemical.[20]

Action Mechanism

Glyphosate exerts its herbicidal action through the inhibition of an enzyme, 5-enol-pyruvil-shikimate-phosphate synthetase (EPSPS), thus preventing plants from making three essential aromatic amino acids for their growth and survival.[18] Advantageously, these three amino acids are not present in mammals, including humans. PMG mechanism of action is slow, making it effective in perennials, because it is transported through the plant before killing growing tissue.[18] Therefore the insufficient production of aromatic amino acids within plants is the main factor that PMG does, causing the death of this species of living beings.[18]

Ecuadorian Legislation

Several countries and international organizations have established a regulation for the use of glyphosate, which is presented in order to safeguard human health and conserve fragile species of fauna, flora and ecosystems. According to the World Health Organization (WHO) says there is sufficient scientific evidence to consider GPM as a probable carcinogen since 2015. Suggesting that the control of this product be more controlled by governments.[21]

The regulations in Ecuador stipulate in Annex 1 "Norma de calidad ambiental y descarga de efluentes: recurso agua" of the reform "Libro VI del Texto Unificado de Legislación Ambiental Secundaria del Ministerio del Ambiente del 2013" that a concentration of 200 μg/L is the maximum permissible limit for glyphosate in waters for human consumption and domestic use that only require conventional treatment.[22] This is the only value found within the legal regulations for the use of glyphosate in water in our country. On the other hand, ministerial agreement 0.21 of "Ministerio del Ambiente y la Norma Técnica Ecuatoriana INEN 1078/2013" establishes comprehensive management methodologies and final disposal of plastic waste from pesticides and related products, however, glyphosate is not specifically mentioned.[23,24] It is important to clarify that Ecuador has diplomatic problems with Colombia over the use of glyphosate. In order to eradicate the production of illegal plantations on the borders of Colombia, its government implements containment systems using aerial spraying on the illegal plantations. However, these fumigations have a negative effect in terms of environmental contamination in Ecuadorian soil. There are several researches showing diseases due to this herbicide with citizens at Ecuadorian borders.[7] According to the press, both governments have so far disputed about this international issue.

3.2 Alternatives for removal treatment of emerging pollutants

Wastewater treatments using conventional methods are, in general, not suitable for the elimination of emerging compounds, since many of them persist without any alteration even in the effluents of treatment plants. For this reason, it is important to identify and evaluate the efficiency of other technologies, in order to propose alternatives to minimize the presence of emerging pollutants in waters with a low economic, energy and environmental cost. In addition, it should be noted that these contaminants (residual water, pharmaceuticals, personal care and pesticides) possess very diverse chemical properties and, therefore, the success of their elimination varies greatly depending on their particular properties. The usually proposed technologies for elimination of emerging pollutants are summarized below.

3.2.1 Advance Oxidation Processess (AOPs)

Advanced oxidation process (AOPs), are the most studied in wastewater treatment, offering an option for cleaning contaminated water with previous organic products from industrial and municipal effluents that cannot be efficiently removed with conventional techniques.[25] In general AOPs induce the generation of several oxidative species among them are the creation of superoxids $\bullet O_2^-$, hydrogen peroxide H_2O_2, ozone O_3 and hydroxyl radicals ($\bullet OH$). The latter is the strongest oxidant since it has an oxidation potential equivalent to E = 2.8 v, which being very energetic, is able to oxidize organic compounds, generating free radicals that in turn react with other molecules and initiating a series of reactions of oxidation.[25] Although the treatment of wastewater or water contaminated by chemicals is the main focus of the AOPs, applications have also been found for groundwater treatment, odor control, production of purified water and treatment of organic compounds.[26] AOPs use expensive reagents or consume large amounts of energy. But it has been shown that when combined with different processes, such as biological processes or

adsorption, it increases their potential in terms of economic efficiency. These processes are classified into two: 1) non-photochemical processes through the transformation of mimic species or by using different forms of energy without including the light and 2) the photochemical processes that work by the action of a photocatalyst under the use of a light source.[27] Considering the topic studied in this work, we are going to focus on AOPs with photochemical action. The main photochemical processes used for the wastewater treatment consist of UV applications and the combination of H_2O_2, O_3 or the use of a photocatalizer. Among these you will find:

3.2.2   UV photolysis

Photolysis is the process by which compounds are degraded by the breaking of chemical bonds by the effect of light, and is defined as the interaction of one or more photons with a target molecule. In this process, the effect of UV light can trigger phenomena of degradation or inactivation by direct or indirect photolysis. With respect to direct photolysis, the molecules absorb UV radiation generating an increase in its energy, which causes bond breakage, followed by degradation or decomposition; on the other hand, in indirect photolysis through the generation of highly reactive radicals that allow the inactivation of pathogenic and non-pathogenic microorganisms, such as glyphosate.[26]

O_3/UV

O_3 is a powerful oxidant whose oxidation potential is 2.07 v. In this case ozonation as AOPs is an indirect oxidation process (O_3 does not act directly as an oxidant), which through an electrophilic mechanism oxidizes and destroys organic compounds toxic by effect of OH radicals that are oxidizing agents.[26] The reaction mechanism of this process in saturated aqueous systems involves UV light irradiation at a wavelength equivalent to 254 nm. Because ozone is very poorly soluble, the transfer of ozone mass in aqueous medium is primarily limiting factor for large scale use of this process. However this problem is being solved by increasing the reaction time in the reactor or increasing the pressure in order to increase its solubility.[28] The O_3/UV processes are complex because to generate •OH radicals they have to go through different reaction pathways according to Equation 3.1.[28]

$$O_3 + hv \rightarrow O^1D + O_2 \tag{3.1}$$

$$^1D + H_2O \rightarrow H_2O_2 \tag{3.2}$$

$$H_2O_2 + hv \rightarrow OH + OH \tag{3.3}$$

H_2O_2/UV

Where a new process of hydroxyl radicals generation is given thanks to H_2O_2 photolysis under UV irradiation as shown in Equation 3.3. Then, different radicals formed as OH• can react with H_2O_2, resulting the next sequence of reactions Equation 3.4-3.6. [27]

$$OH + H_2O_2 \rightarrow OH + H_2 + O_2 \tag{3.4}$$

$$2OH \rightarrow H_2O_2 \tag{3.5}$$

$$HO_2 + OH \rightarrow H_2O + O_2 \tag{3.6}$$

However, there is drawback of this second H_2O_2/UV process, due to the molar extinction coefficient of H_2O_2, in which the organic substrates act as internal filters. To solve this problem it has been determined that the photolysis rate of H_2O_2 depends strictly on pH conditions, i.e. to more alkaline conditions increases its OH• radical formation process. [28]

3.2.3 Fenton and Photo-Fenton Oxidation

The generation of reactive oxygen species through the catalytic decomposition of hydrogen peroxide by ferrous ions is know as fenton reaction. This process is mainly based on a series of chain reactions between iron salt species Fe^{2+} / Fe^{3+} and hydrogen peroxide H_2O_2, especially at an acidic pH value, that provides an important source of hydroxyl radicals (Equation 3.7). In addition, the fenton process it is considered a potentially convenient and economical process due to the low cost of hydrogen peroxide for the generation of oxidizing species and in effect the degradation of various compounds. Furthermore, the added benefit in improved hydroxyl radical production when iron species are employed further points to these advantages. [29]

On the other, the addition of a light source (solar or ultraviolet) in the fenton process, generates a new process called photo - fenton (Fe salts / H_2O_2 / UV). The photo - fenton process is basically the combination of fenton reagents and UV radiation (<600 nm). The photo-reduction of Fe^{3+} to Fe^{2+} ions and the photolysis of H_2O_2 through a shorter wavelength (<310 nm) ensures, in fact, an extra production of hydorxyl radicals (Equation 3.8). [27–29]

$$Fe^{2+} + H_2O_2 \rightarrow Fe^{3+} + OH^- + \bullet OH \tag{3.7}$$

$$Fe^{3+} + H_2O + hv \rightarrow Fe^{2+} + H^+ + \bullet OH \tag{3.8}$$

3.2.4 Photocatalysis

Photocatalysis is a term that implies the combination of photochemistry with catalysis. Both radiation and catalyst are necessary for a chemical reaction to take place under the presence of a UV radiation source. In other words,

photocatalysis is defined as the mechanism to accelerate chemical reactions through the presence of a photocatalyst.[30] Within photocatalysis there are two types of processes: heterogeneous processes and homogeneous processes. On the other hand, heterogeneous processes use solid semiconductors in the aqueous or gas phase to obtain catalysis.[31] On the other hand, homogeneous processes where the oxidation system is used in a single phase, that is, dissolved catalyst.[30] Heterogeneous photocatalysis is the finest method to remove organic species in the environment, since the process gradually breaks down the pollutant molecules without leaving any residue of the original molecule. The catalyst does not undergo any changes during the process and no additional chemicals are required to fulfill its function. It is important to clarify that after the degradation process, in many cases the catalyst is fully recovered.[32]

Reaction Mechanism

Photocatalysis consists of the generation of an electron / hole pair (e^- / h^+) respectively, by excitation of the electron from a semiconductor by means of a radiation source.The process starts when the semiconductor (SC) absorbs energy greater or equal of its bandgap value, which is defined as the energy difference between the valence band and the conduction band of the photocatalyst. This difference in energy causes that electrons in the valence band to jump into the conduction band (e^-) and, as a result, a gap (h^+) is generated in that band,[30] like is shown in Equation 3.9.

$$hv + SC \rightarrow e^- + h^+ \tag{3.9}$$

The electrons and holes that have not recombined migrate to the semiconductor surface to carry out a series of reactions with the adsorbed chemical species. The holes react with water and the hydroxide ion, to generate hydroxyl radicals ($\bullet OH$) and the electrons are transferred to the adsorbed molecular oxygen, generating superoxides ($\bullet O^{2-}$). Hydroxyl radicals are the most abundant, making their generation the most important stage for the degradation of pollutants.[30] As shown in the following Figure 3.2.

Photocatalyst

The catalysts used for photodegradation must be semiconductor materials, since the degradation process requires an energy gap that generates electron / hole pairs.[33] Its effects can be very appreciable with low amounts of catalyst in order to achieve large increases in the speed of the reaction.[34] In addition to being a semiconductor, photocatalysts must have a high gap energy, so that electrons can jump from the valence band to the conduction band under some source of irradiation. In truth it must be a chemically stable material and resistant to compression, abrasion and photo-corrosion.[30] Photocatalyst, as Ibhadon explains in his article,[32] takes advantage of UV radiation from sunlight or any other artificial light source and uses that energy to decompose or disintegrate substances that include organic materials, organic acids, estrogen, pesticides, dyes, microbes, and chlorine resistant organisms.[32]
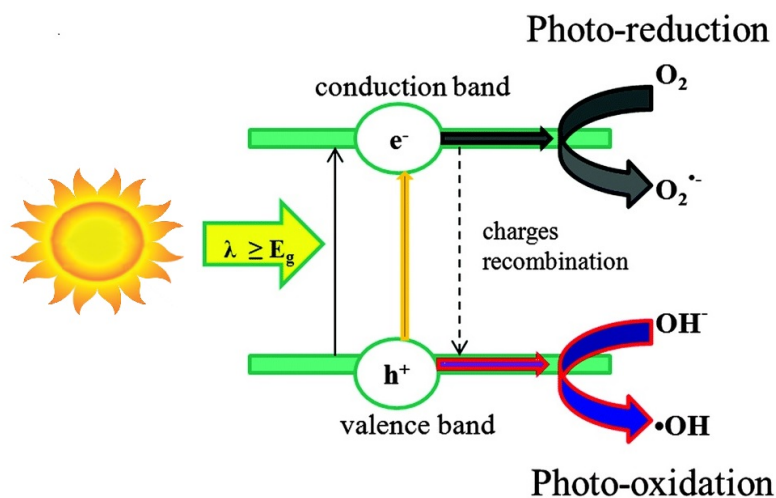
Figure 3.2: Reaction mechanism of photocatalysis[30]

3.2.5   Adsorption

Adsorption is a matter transfer process that involves the concentration of one or more compounds in a gas or liquid on the surface of a solid. Likewise, desorption is the phenomenon by which a molecule adsorbed on the surface of a solid, detaches itself from the solid surface and returns to the fluid. It is, therefore, the reverse process of adsorption.[35–37] If the interaction between the solid surface and adsorbed molecules has a physical nature, the process is known as physisorption. On the other hand, if forces of a covalent nature are formed between the solid and the adsorbed substances, we are talking about chemisorption.[38–40] Under favorable conditions, both processes occur simultaneously or alternatively, but the physisorption appears to be the predominant mechanism.[35] However, generally, is very difficult to distinguish between physisorption and chemisorption. Thus Table 3.1 summarizes the fundamental characteristics of both processes.[36–41]

Physisorption	Chemisorption
Its arises due to Van der Waalls' Forces.	Its arises due to the chemical bond formation.
No appreciable activation energy is required.	High activation energy is sometimes required.
It is reversible.	It is irreversible.
It decreases with increase in temperature and occurs at lower temperature.	It increases with temperature and occurs at high temperature.
It is not specific in nature, i.e. all gases are adsorbed in all solids to some extend.	It is specific in nature and occurs only when a chemical bond is formed between the adsorbate and adsorbent.

No electron transfer, although polarization of sorbate may occur	Electron transfer leading to bond formation between sorbate and surface
Multilayer adsorption occurs	Only the monolayer adsorption occurs
Endothermic or Exothermic process	Only Exothermic process

Table 3.1: Characteristics of the Physisorption and Chemisorption.

3.2.6   Adsorption Equilibrium

One of the most common forms of representing the adsorption equilibrium is through the relationship between the amount adsorbed and the pressure, in the case of gases or vapors, or the concentration in the liquid phase, in the case of liquid adsorption, for a given temperature. This relationship is known as adsorption isotherm for a determined adsorbate-adsorbent system.[38] Gas adsorption isotherms, widely used in the characterization of the porous structure materials, can be classified in six types, according to the classification proposed by Brunauer et al., in 1938 and which is currently recommended by the IUPAC.[38] This classification is shown in Figure 3.3.

a) Type I Isotherm (Figure 3.3 I): is typical for characterize the sorption caused by predominantly microporous structure. It appears in saturated monolayer adsorption. This Isotherms is related with Langmuir isotherm and is commonly used to describe monolayer adsorption.[39]

b) Type II isotherm (Figure 3.3 II): is typical for a non-porous or macroporous adsorbent representing limited monolayer-multilayer adsorption.[39]

c) Type III isotherm (Figure 3.3 III): is typical for weak adsorbate-adsorbent interactions. These isotherm are found with microporous or mesoporous adsorbents and is convex at the high relative concentration.[40]

d) Type IV isotherm (Figure 3.3 IV): has a hysteresis loop associated with capillary condensation taking place in mesoporous adosorbents. The initial part is attributed to monolayer-multilayer adsorption since it follows the same path as the corresponding part of a Type II isotherm.[40]

e) Type V isotherm (Figure 3.3 V): indicate weak adsorbate-adsorbent interactions and are applied for mesoporous with a weak interaction.[39]

f) Type VI isotherm (Figure 3.3 VI): is primarily introduced as a hypothetical isotherm and might associate with layer by layer adsorption on a uniform surface.[39]

In order to perform a thorough study of water pollutant removal, is necessary to know the mechanism that takes place in that process, as well as how the conditions of the reaction medium influence it. In the specific case of
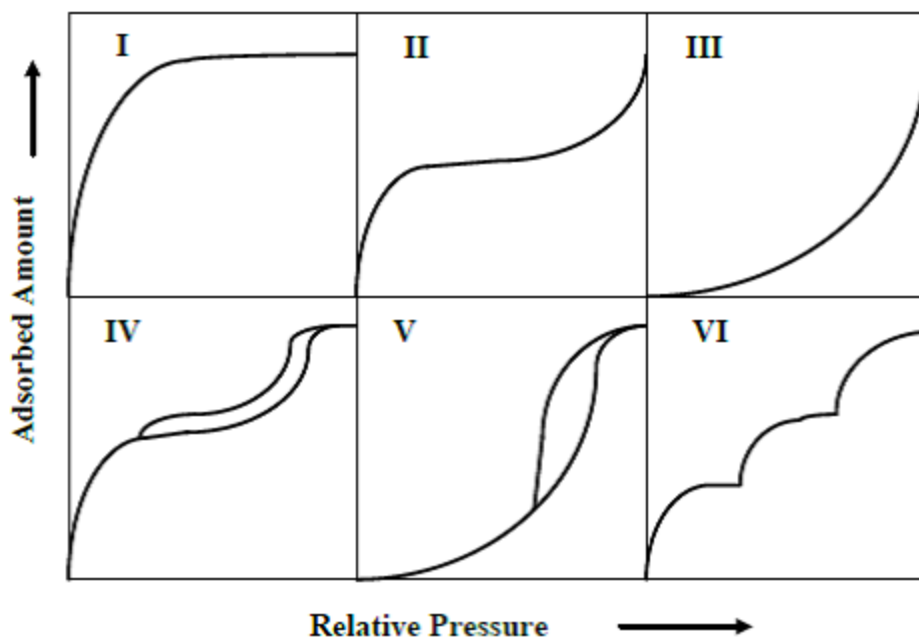
Figure 3.3: Classification of adsorption isotherms recommended by IUPAC.[38]

adsorption processes, variables such as the pH of the medium, the presence of other contaminants or temperature, are decisive for their development and to understand their mechanism.[40] Pollutant adsorption processes in water are based on the distribution of a solute (the contaminant) between a liquid phase (the contaminated effluent) and a solid phase (the adsorbent).[40] To describe the equilibrium distribution of the solute between the two phases, various mathematical models have been developed that allow to interpret the experimental data and describe them quantitatively.

One of the fundamental objectives that this type of process has, is the determination of the adsorption capacity of the adsorbent. The adsorption capacity (Q_t) is calculated from a mass balance and represents the amount of species adsorbed per unit mass of adsorbent (Equation 3.10).[43] The adsorption capacity is one of the most important parameters of an adsorbent and depends on its characteristics (pore size, specific surface or functional groups on the surface) and for certain conditions of the reaction medium such as pH or temperature.[43]

$$Q_t = \frac{V(C_i - C_e)}{m} \tag{3.10}$$

where V is the volume of the solution that is contact with the adsorbent, C_i is the initial concentration of the contaminant in the solution, Ce is the concentration of the contaminant at equilibrium, and m is the mass of the dry

adsorbent.[43]

In the adsorption processes, the pollutant or adsorbate is attracted to the adsorbent through different mechanisms until equilibrium is reached.[42] The characterization of the equilibrium process is carried out by obtaining its adsorption isotherm.[42] The adsorption isotherm is the relationship between the amount of pollutant adsorbed per unit of adsorbent (Q_t), and the concentration of the pollutant in the liquid phase (C_e) at a given temperature.[42] Most mathematical models used to study adsorption equilibrium are based on the concept of solid phase adsorbent, where adsorption takes place by deposition of adsorbate over the physical pores of the adsorbent surface.[39] However these concepts cannot be strictly applied to adsorption with some low-cost materials such as biomaterials, whose structure is much more complex. Nevertheless, they are useful for interpreting experimental data and are therefore used frequently. Among the most used models are the Langmuir and Freundlich.[39,40,42]

Langmuir isotherm model

This model proposed by Langmuir 1918, seen in Equation 3.11, is the simplest theoretical model for monolayer adsorption system, and it presumes monolayer sorption onto a homogenous surface with a finite number of identical sites. The Langmuir model is based on four basic premises: 1) molecules are adsorbed at a fixed number of defined localized sites, 2) all sites are energetically equivalent, 3) there is no interaction between molecules adsorbed on the neighbouring site and 4) each site can hold one adsorbate molecule.

$$\frac{1}{Q_e} = \frac{1}{Q_{max}b}\frac{1}{C_e} + \frac{1}{Q_{max}} \tag{3.11}$$

where C_e is the equilibrium adsorption concentration in the solution (mg/L), Q_t is the equilibrium adsorption capacity (mg/g), Q_{max} in the Langmuir model is the saturated monolayer adsorption capacity or maximum solid-phase concentration (mg/g) and b is the Langmuir adsorption coefficient, related to the binding energy of the sorption system (mg/L). Plotting C_e/Q_e versus $1/C_e$ the slope and intercept of the linear plot gives the values of b and Q_{max}. The Langmuir isotherm constant b can be used to indicate the affinity, that is to say, combining capacity of adsorbent toward the ions to be adsorbed. High value of b indicates for a strong affinity of adsorption.[41]

Freundlich isotherm model

The Freundlich isotherm is an empirical nature model Equation 3.12. It is normally applied to adsorbents with heterogeneous surfaces or that have adsorption sites with different affinities. But it should be noted that it can only be used at lower and intermediate solute concentrations; it lacks of physical meaning because it does not include a maximum adsorption capacity.[41,44]

$$log(Q_e) = logk_f + \frac{1}{n}logC_e \tag{3.12}$$

where k is the Freundlich adsorption coefficient that represent the adsorption capacity and n is the Freundlich

exponent that is related to the adsorption intensity and surface heterogeneity. This values gives an indication of how favourable is the adsorption processes. Plotting log Q_e versus log C_e the slope and intercept of the linear plot give the values of the Freundlich isotherm parameters such as: n and k, respectively. It is important to clarify that if the values of n are from 0.1 to 0.5 adsorption is favourable, if the values are between 0.5 and 1.0 the adsorption is quite difficult and if n is greater than 1 the adsorption is difficult.[41][44]

3.2.7 Adsorption Kinetics

Kinetic studies are essential to obtain a detailed knowledge of adsorption process. Consequently the adsorption kinetics process is defined as the rate of the adsorbate-adsorbent system in reaching adsorption equilibrium. In other words, the adsorption rate is limited by mass transfer mechanisms, also depending on the adsorbate and adsorbent properties.[45]

The adsorption process of pollutants in a solution can be divided into four stages: 1) the transport of the adsorbate to the outer surface of adsorbent, 2) external film diffusion, associated with the transport of adsorbate from dissolution through the stationary layer surrounding the particle, 3) internal (pore) diffusion or intraparticle diffusion, which is the transfer of the adsorbate from the particle surface to the active sites (porous) within it, and 4) adsorption, which the adsorbative adhers to the adsorbent surface on available sites. It is important to emphasise that the adsorbate transport to the adsorbent is usually, under the right conditions, the limiting stage of the process.[43,45] However, changes in the conditions of the process (stirring, mixing ...) may lead to the limiting stage of the reaction rate being intraparticle diffusion, that is, the diffusion of the adsorbate between the pores of the adsorbent, or that the determining stage in this process is the interaction of the adsorbate with the adsorbent.[45,46] On the other hand desorption, occurs in the reverse manner; it begins with desorption and ends with transport from the concentration boundary layer around the adsorbent into the solution.[45,46]

The design and application of an adsorption system need knowledge of adsorption equilibrium and kinetics.[43] The development of kinetics understanding is limited by the theoretical complexity of adsorption mechanisms.[43] There are a large number of theoretical models used for the study of adsorption kinetics and the limiting stage of the reaction rate.[43] The models used to describe the kinetics studies carried out for this thesis are: the pseudo-first order model and the pseudo-second order.

Pseudo Fist Order Model

The pseudo-first-order (PFO) equation was proposed by Largergren in 1898 for adsorption of oxalic and malonic acid onto charcoal.[43] It is the first kinetic model that describes the adsorption processes based on the capacity of the adsorbent used.[43] It has the following differential form Equation 3.13 and linearized form Equation 3.15:

$$\frac{dq}{dt} = k_1(Q_e - Q_t) \tag{3.13}$$

where Q_t is the adsorption capacity (mg/g), Q_e is the equilibrium adsorption capacity (mg/g); t is the time (min) and k_1 = rate constant (1/min). The integation with the initial condition Q=0 and t=0 yields Equation 3.14 and its linearized form Equation 3.15.

$$Q_t = Q_e(1 - exp(-kt)) \tag{3.14}$$

$$ln(Q_e/(Q_e - Q_t)) = k_1t \tag{3.15}$$

If we plot $ln((Q_e - Q_t)/ Q_e)$ vs. t we can have a straight line that passes through the origin with a slope k_1 for systems that obey this model.[43]

Pseudo Second Oder Model

The pseudo second order (PSO) model based on sorption equilibrium capacity, is also widely used since it is a well defined representation of the experimental data. The model can be used to predict the behaviour over the whole range of adsorption and assumes that the uptake rate is second order with respect to the available surface sites.[43,47] It has the following differential form Equation 3.16 and linearized form Equation 3.16:

$$\frac{dq}{dt} = k_2(Q_e - Q_t)^2 \tag{3.16}$$

$$\frac{t}{Q_t} = \frac{1}{k_2Q_e^2} + \frac{t}{Q_e} \tag{3.17}$$

where k_2 is the pseudo-second-order (PSO) rate constant. Other values have the same meanings as in in the previous model. If we plot t/Q_e vs t we can have a straight line that is compatible with PSO. Most environmental kinetic adsorption can be modeled well using PSO model, thereby indicating its superiority to other models.[43]

The kinetics analysis in these type of works, in which the experimental data are fitted to Pseudo First Order and Pseudo Second Order models, serve merely to complement the adsorbent evaluation.[43] Acoording to Tan K. et al.,[43] the kinetics analysis of adsorption process need strong knowledge of the origins, strengths, and limitations of these models.[43] And also said that the model parameters are merely empirical constants that have no distinct theoretical significance.[43]

3.3   Nanotechnology

Nanotecnology is the study of phenomena and the manipulation of matter at atomic, molecular and macromolecular scales, where properties differ significantly from those at a larger scale.[48] The importance of nanotechnology is that allow the creation of new materials with outstanding properties. These new materials can be design and produce to have numerous advantages in relation with preexisting materials. According to Brushan,[49] he reports that this term refers to any technology that can be applied and used in the real world at a nano level (a nanometer is a unit of length that denotes one millionth of a meter that is, 10^{-9} m),[50] that is, that matter can be controlled and used at atomic and molecular levels with a size in the range of 1 to 100 nm.[49] Since it is in this range where quantum effects dependent on the particle size are produced, making the properties of matter at the nanoscale level different from the large scale ones. On the other hand, in the book "Nanotechnology: health and environmental risks" it is mentioned that a key criterion for defining Nanotechnology is that its creation has to be artificial. In other words, a nanoparticle, nanocomposite or nanomaterial will be synthetically produced. Because otherwise they would have a define as biomolecule or a particle which is naturally formed. Regarding history, the author of the book explain that Nanotechnology term was proposed by Norio Taniguichi, from Tokyo University in 1974, who use this term to describe the thin film size deposited on a semiconductor.[51] But it was in 1959 that one of the brightest physicists in history gave a lecture to the American Physics Society called "There's plenty of room at the bottom—an invitation to enter a new field of physics". Where he argued the benefits we could have from making very small things.[52,53] With all this it is clear to know that nanotechnology has been and will remain present in future years.

The integration of nanotechnology in the current world according to Brushan,[49] explains that he has managed to penetrate and solve various problems efficiently in areas such as: medicine, the environment and especially technology.[49] Drug delivery, electronics, energy and water, biotechnology and others are some field where the nanotechnology is applied.[50] Nanotechnology represents the breakthrough in current research as it has made great discoveries that have helped social, economic and technology in the world.[53] Therefore, once we have already defined the concept of nanotechnology, we can clarify that this thesis project is based on synthesis and characterization a nanocomposite based on magnetite and titanium dioxide to evaluate its adsorption activity and degrade pesticides.

3.4   Nanoparticles (NPs)

Some of the most notable advances in materials science and chemistry is the production of new and improved materials at the nanometric level. NPs play an important role in the development of technology and its applications range from the field of health, industrial production branches and even in the incorporation of various materials such as cosmetics or clothing with manometric technology.[49,54] According to Ibrahim Khan,[55] NPS are materials that have a dimension less than 100 nm and that depending on their overall shape, NPs can adapt different dimensions. In addition, he argues that size at the nanometric level can influence the physicochemical properties of materials, such as optical properties.[55] Gold NPs, for example, present different color according their size at the nano level scale and this, at the same time, will depend on the amount of reagents and the time spent in their synthesis.[56]

Considering that the size effect plays an important role in particles, we can define that the quantum size effect describes the physics of solids by improving their properties when the size reaches nanometers.[57] The quantum effects present, dominate the behavior of matter at the nanometric level, particularly inside the particle, which is where optical, electrical, magnetic and other behavior are affected. Also, nanoscale materials could be produced, according to the number of dimensions present can be divided into: a) zero dimension nanomaterials (0D), where all the dimensions present in the material are measured at the nanometric level such as quantum dots, b) one dimensional nanomaterilas (1D), where one of the dimensions is outside the nanoscale level, in these type are included nanotubes and nanorods, c) two dimensional nanoaterials (2D) where two of the dimensions are outside the nanoscale range, for example graphene, nanofilms and nanocoatings and d) three dimensional nanomaterials (3D) where all the dimensions of the materials are outside the nano region, such as bulk powders, nanoparticle dispersions and multiple nanolayers.[58] According to Khan, et al.,[55] these materials are made up of several layers: firstly, there is the surface layer, which allows the particle to functionalize with a variety of smaller molecules such as surfactants, polymer or metal ions.[55] On the other hand there is the cover layer, which is a very different layer to the core as a whole. Finally there is the nucleus, which is the main part that defines a nanoparticle.[55,59] There are two techniques to create them: one using top-down techniques and the other using Bottom-up techniques. Top-down is a destructive technique of producing nanomaterials, breaking down large molecules into very small structures. The most common methods in this synthesis are: mechanical milling, chemical etching, sputtering and others.[55] We have a clear example of this method in the mechanical production of graphene from graphite sheets.[60] On the other hand, bottom-up technique employs in the opposite sense to the previous one, that is, small structures are created from simpler substances. The most common methods in this type of synthesis are: sol gel, precipitation, sedimentation and reduction techniques, among others. An example of this type of synthesis is the creation of silver NPs by chemical methods from their precursor ions.[61]

3.5   Iron Oxide Nanoparticles

The growing number of scientific publications focused on the synthesis of metal and metal oxide nanoparticles has brought great interest in physics, chemistry, biological, medicine, mechanics and material engineering where new techniques are being developed to investigate and manipulate atoms and molecules at nanometric scale.[37] Metal and metal oxides nanoparticles have a high surface area and high fraction of atoms, which is responsible for their fascinating properties such as magnetic activity.[62] In addition these nanoparticles after being superficially modified, may possess excellent biocompatibility, which is suitable for applications in the field of medicine.[63] Currently, magnetic nanoparticles mainly include metal NPs, metal oxide NPs, and metal alloy NPs; the more common NPs are silver, iron, cobalt, gold, and nickel.[63]

Magnetite (Fe_3O_4) is a magnetic iron oxide that has a cubic reverse spinel crystalline structure centered on the faces with oxygen and iron cations that occupy the Tetrahedral Interstitial Sites Fe_{tet} and Octahedral Fe_{oct} as is shown in Figure 3.4.[64] According to Andrade et al.,[65] electrons can jump between Fe^{2+} and Fe^{3+} in octahedral sites even
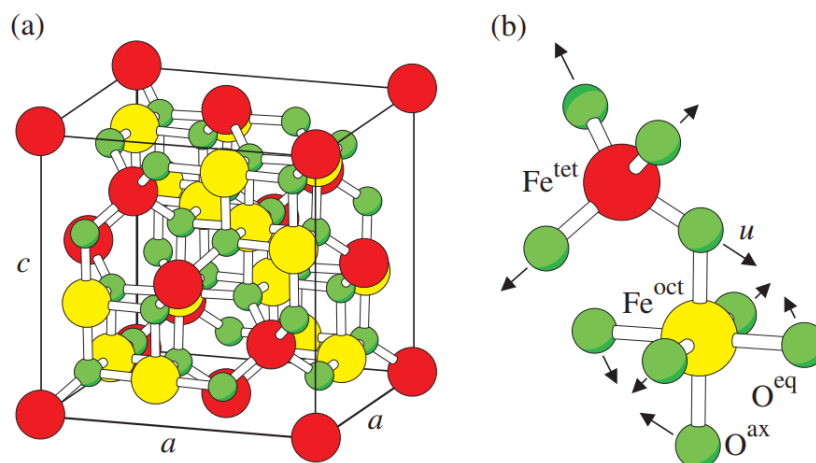
Figure 3.4: Crystalline structure of magnetite (a) Face centred cubic spinel structure of magnetite. (b) Magnification of one tetrahedron Fe^{tet} and one adjacent octahedron Fe^{oct} oct sharing an oxygen atom.[64]

at room temperature, making magnetite an important metallic material medium.[65] Depending on the size, Fe_3O_4 exhibits different behaviors when a magnetic field is applied to them.[66] From micrometric to nanometric level, these particles have been shown to have had abrupt changes in their magnetic properties.[67] Since when these are in sizes at the nano level, the surface effects begin to dominate the magnetic behavior of the particles.[66] A wide variety of methods for synthesis of magnetic nanoparticles are described in the literature, the most important being the microemulsion, sol-gel and co-precipitation processes.[64,66] According to Dresco et al.,[68] the most common process to synthesize magnetic iron nanoparticles is the co-precipitation method, starting from salts of Fe (II), Fe (III) and using an alkali metal hydroxide as a reducing agent.[68]

In the figure 3.5 the process of formation of magnetic nanoparticles can be observed using the homogeneous co-presipitation method assisted sonochemically.[66] Figure 3.5 (a), shows the solution in which the two iron salts and the reducing agent are placed. Figure 3.5 (b), shows the nucleation process, which is the starting point for the formation of Fe_3O_4 nanoparticles at the time of ultrasound is applied. Consequently, the co-precipitation process, where the nanoparticles are separated from the solution and form a homogeneous precipitate, takes place when the solution turns a different color, as can be seen in figure 3.5 (c) and (d). Finally the complete formation of magnetic nanoparticles is verified when the initial solution turns black figure 3.5 (e). The corresponding chemical reaction of this process is explained in Equation 3.18.[66]

$$Fe^{2+} + 2Fe^{3+} + 8OH^- \rightarrow Fe_3O_4 + 4H_2O \qquad (3.18)$$

$$Fe^{2+} + 2Fe^{3+} + 8OH^- \qquad \text{Nucleation} \qquad \text{Homogeneous Coprecipitation} \qquad Fe_3O_4 + 4H_2O$$
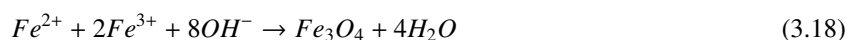
Figure 3.5: Synthesis of Fe_3O_4 nanoparticles using co-precipitation method sonochemically assisted.[66]

3.6 Nanocomposites

In recent years, research on the synthesis of nanomaterials has been expanded to the development of more complex structures than conventional single-phase nanostructures, because it is 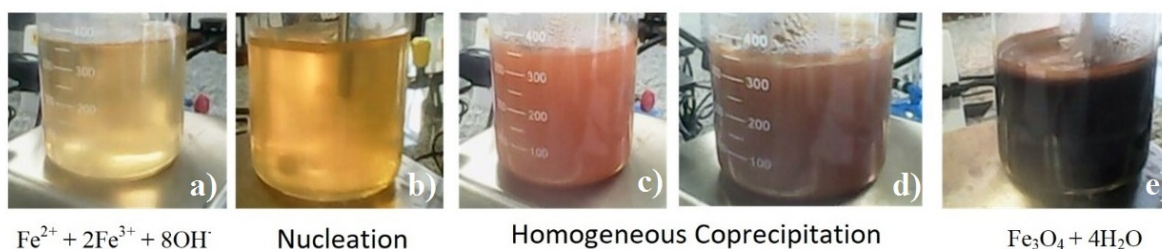possible to combine a wide range of building blocks (attached to through their chemical interfaces) generating new materials with improved characteristics and properties, combined into a single multifunctional platform. This class of materials is commonly known as nanocomposites or hybrid nanomaterials (since they have more than one component), and they emerge as an attractive alternative for scientific and technological applications in which conventional nanomaterials cannot compete. In fact, nanocomposites are those compounds that have at least one phase of their internal structure, a morphology in the range of nanometers; such as nanoparticles, nanotubes or lamellar nanostructures. The result of adding materials at the nanometric level is the radical improvement in their properties in which they can include mechanical resistance, thermal stability, chemical resistance, toughness, electrical conductivity or also two functions that can provide another function like magnetic properties.[69] The nanocomposites can be composed of several materials such as: metals, non-metals or polymers that provide an additional advantage to the properties of its main material. Also, it is important to mention that with the extensive research that is given to this field, now-a-days, it has been possible to generate new materials with great novel properties through innovative synthetic approaches. Therefore, the main idea behind the nanocomposite is to create new hybrid materials with dimensions in the nanometer range and provide more than one function or increase its physical properties to the material for the development of science.[69]

Nanocomposites materials can be classified into three groups by their matrix materials such as: (1) ceramic matrix nanocomposites (CMNC), (2) polymer matrix nanocomposites (PMNC) and (3) metal matrix nanocomposites (MMNC).[69] Ceramic matrix nanocomposites are those materials in which one or more different ceramic phases are intentionally added, to improve wear resistance and chemical and thermal stability. Polymer matrix nanocomposites are polymers or co-polymers that contain nanoparticles or nanofillers dispersed in their polymeric composition and are commonly called poly-nanocomposites. Finally, metal matrix nanocomposites are those multiphase materials that are formed by a ductile metal or alloy matrix in which some nanosized reinforcement material is implanted in order to enhance its toughness, modulus, strength and ductility and are commonly called inorganic nanocomposites.[69] For example, in the field of heterogeneous photocatalysis, it is common to use metal matrix nanocomposites using TiO_2,

or another photosensitive semiconductor, with some metals like silicon, gold, silver, nickel and iron nanoparticles in order to increase its photocatalytic properties in the visible spectrum and also in its easy recovery applying an external magnetic field .[15,70,71]

3.6.1 Fe_3O_4@TiO$_2$ Nanocomposite

It is widely reported in the literature that TiO_2 nanoparticles have a large surface area and good efficiency in the adsorption and photocatalytic process for degradation of various chemical compounds; in which there are included pesticides, phenolic compounds, organic colorants and also in mechanisms for treatment of wastewater.[2] This has made researchers look many options to improve these materials using nanoengineering as the basis for their construction. One of the main problems they currently face is the recovery and reuse after its utilization when works as absorbent and photocatalyst. The separation process is critical not only for reusability, but also to prevent the harmful biological effects of many semiconductor NPs even when light is not present.[72] Novel alternatives such as recovery, centrifugation and filtration have been proposed but most of these techniques involve additional processes that complicate operation, maintenance and represent an unwanted waste of energy and resources. For this reason, it is sought to remedy this problem by developing materials by adding superimposed layers on a single particle to form nano-hybrids that are composed of a core coated by a "shell" of a different material.[13] That is, TiO_2 nanoparticles with a magnetite core that facilitates recovery by adding a external magnetic field. In this way, it is possible to separate the catalyst from the contaminant in a simple and efficient way, avoiding the use of additional energy and materials.[13,73]

Consequently, in recent years, several researchers have been involved to improve the adsorption and photocatalytic activity using novel nanocomposites based on Fe_3O_4@TiO_2. Magnetic components integrated into TiO_2 nanoparticle-based catalysts have proven to be an effective way to solve the problem mentioned above, as they can prevent catalyst particle agglomeration during recovery and improve catalyst durability.[74] The magnetic oxide nanoparticles (Fe_3O_4), on the other hand, are much more sensitive and unstable than titania, particularly in acidic conditions. A magnetic photocatalyst, consisting of a magnetic core coated with a photoactive titanium dioxide layer, has been designed to solve the problem.[74] The magnetic core was used to improve the photocatalyst's separation properties from the treated water, while the outer titanium oxide coating was used to degrade organic pollutants.[74] Fortunately, a lot of work was put into synthesising core@TiO_2 structures. For example, a high specific surface area and a mesoporous structure are sought to increase adsorption/photocatalytic activity. In this sense, researchers like Vinod Kumar et al.,[10] have some works on photocatalytic oxidation of pesticides and organic compounds for wastewater treatment through TiO_2@$CoFe_2O_4$ NPs decorated reduced graphene oxide in the presence of UV light.[10] Their studies showed good results in the degradation of chlorpyrifos pesticide and they clarify that nanocomposite was separated from the solution by a magnet and reused after the photodegradation.[10] In this way recyclable of the nanocomposite is economically significant in the industry. In point of fact hybrid nanocomposites based on TiO_2@Fe_3O_4 are a good choice for glyphosate degradation processes thanks to high efficiency and their magnetic properties for rapid recovery.
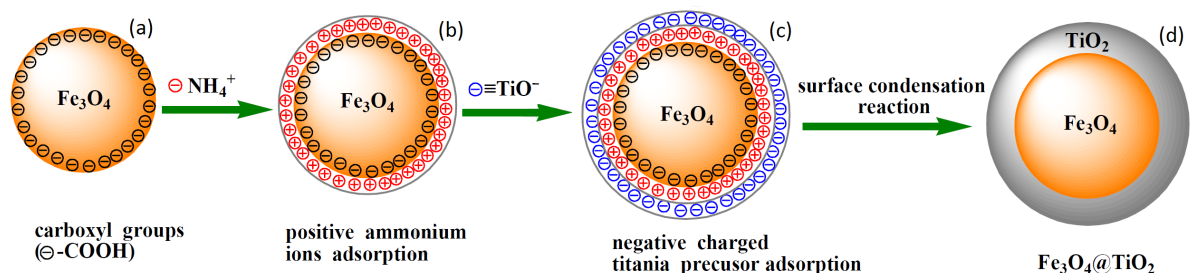
Figure 3.6: Scheme of forming process of titania coated core@shell nanocomposites. [74]

Figure 3.6 shows an example the formation process of the titanium dioxide coating on the surface of the magnetic nanoparticles reported by Tiejun Xin et al. [74] The formation mechanism of the titania coating include the following steps: Figure 3.6 (a) the NH_4^+ species are formed in the reaction system, Figure 3.6 (b) via electrostatic interaction, the NH_4^+ species can be retained by the negatively charged surface of Fe_3O_4 cores terminating in carboxyl groups, Figure 3.6 (c) the negatively charged titania precursor is adsorbed by the NH_4^+ species onto the surface of the Fe_3O_4 core as NH_4^+ species accumulate on the surface and Figure 3.6 (d) the surface condensation reaction catalyzed by NH_4^+ species can easily occur on the surface of Fe_3O_4 core to form $TiO_2@Fe_3O_4$ nanocomposites with a core-shell structure. [74] According with Tiejun Xin et al., [74] the ammonia ions (NH_4^+) are thought to play a significant role in the coating reaction based on the above study. The key is that the carboxyl groups on the particle surface attract the positively charged NH_4^+, which attracts the negatively charged TiO^- species, making titania coating in an ethanol/acetonitrile mixed solvent easier. [74]

3.7 Reported studies of glyphosate degradation

Glyphosate degradation processes are reported in the literature, many of them have achieved very efficient degradation. On the one hand there are metabolic processes that the plants themselves develop using their microorganism for glyphosate degradation, these are processes with long time of action in soil environments. On the other hand, there is the advancement of technology and its innovative degradation processes in which include electrochemical, photochemical and chemical processes, that are used in aqueous environments. However, it is important to clarify that many of these processes have been carried out with highly pure glyphosate reagents, that is, within the composition they have no additives.We will now describe some of the research done with reference to glyphosate degradation. Nam Tram, et al., [75] analyze the electrochemical oxidation capacity for the degradation and mineralization of glyphosate herbicide using a Ti/PbO$_2$ type anode.The electrolyte used was Na$_2$SO$_4$, in order to eliminate toxic by-products during the electrolysis. Furthermore, they mention that pH, treatment time, current intensity and concentration of catalyst are the parameters that influence glyphosate degradation by electrochemical method. They conclude mentioning that their research had a degradation efficiency of 90% - 95%, showing that electrochemical

treatment is a good option for glyphosate degradation.[75]

Rui Huo et al.,[76] show their results regarding glyphosate degradation in aqueous phase. In this research they develop Bismuto Vanadato nanoparticles ($BiVO_4$) in a range of 30-100 nm, which are powered by light to develop photocatalytic activity. In addition, they mention that factors such as crystal structure, crystallization temperature and particle size of the nanoparticles are indispensable in the percentage of degradation. In this work they conclude that $BiVO_4$ sample, which has a morphology of sphere nanoparticles calcinated at 400 °C, is the sample that presented the highest rate of photocatalytic degradation of glyphosate under irradiation. Specifically they have achieved the degradation of the herbicide by 50% during 180 min.[76]

Eduardo Vidal et al.,[77] developed a mathematical and experimental model to study the oxidative degradation of glyphosate using hydrogen peroxide and UV radiation based on the sequence of reactions. Refering to mathematical part they considered all the experimental values gathered in the laboratory reactor in order to develop the respective calculus. On the other hand, the experimental part was developed using glyphosate acid and glyphosate isopropylamine salt from a commercial formulation under the UV/H_2O_2 reactor to assess degradation process. The conclusions shown that both the mathematical and experimental model of UV/H_2O_2 can become an suitable and very simple process for treatment of wastewater with the presence of glyphosate, since they obtained 80% efficiency under 12h reaction. However, they emphasize that in practical applications there are factors such as the presence of organic matter or inorganic salts that cause changes in the reaction environment.[77]

Peerawas Kongsong, et al.[6] develop a thin film with TiO_2 to treat glyphosate contaminated water under UV and solar irradiation. In this research, they synthesized various thin film coatings of SnO_2/TiO_2 that were deposited on glass fibers in order to study its photoactivity. The doping of the nanocomposite with nitrogen was one of the key points of this study, since it produced changes in absorption wavelengths and narrowing of band gap, obtaining a high percentage of glyphosate degradation. They conclude that the SnO_2/TiO_2 sample, which has a narrow band energy and a small crystalline size, has very good results of photocatalytic degradation on herbicide glyphosate. In addition, they explain that it would take 11 h to degrade glyphosate by 90%. However, this depends on the UV intensity, the surface area of the catalyst and the concentration of glyphosate.[6]

Chapter 4

Characterization Techniques

Nanoparticles (NPs) have attracted attention due to their large physical, chemical and mechanical properties depending on the size of the particles. NPs are increasingly used because they have unique properties, making materials stronger, more durable and more effective in their application. Because the size of a nanoparticle is in the range of 1 to 100 nm, standardized methods of manometric analysis are rare. Various techniques to characterize these materials, where the crystalline structure, elemental composition, morphology, particle size and dispersion are studied with several sophisticated equipment.[78] The characterization of nanomaterials plays an important role in the study of materials at nanometric level. More complete NPs characterization is necessary, requiring a comprehensive approach, combining techniques in a complementary way.[79] In this chapter we will describe the definition, mechanisms, utility and problems of some characterization techniques that we will use in this study.

4.1   UV-vis Spectroscopy

Ultraviolet visible spectroscopy (UV-vis) is considered to the most widely used spectrophotometric technique for the analysis of a variety compounds.[80] This technique encompasses absorption spectroscopy and reflectance spectroscopy in the UV-vis spectral region, to quantify how much a chemical absorbs light, relating the absorption of light from a sample to a reference or blank sample.[81] For this, it involves electromagnetic radiation with matter at a particular wavelength, causing that the molecules experimenting electronic transitions, i.e. electrons jump from lower to higher energy levels.[80,82] The amount of absorbance at any wavelength has a direct relationship with the chemical structure of the molecule. Depending on the amount of light and its wavelength, valuable information can be obtained from the sample such as: purity, amount and presence of materials.[81] Furthermore, UV-vis spectroscopy is used to quantitatively determine the elemental concentrations of a solution using Lambert Beer's law.
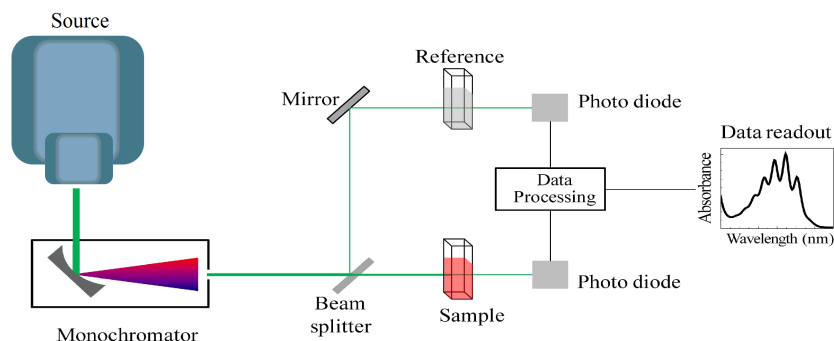
Working Principle

Figure 4.1: Illustration of Ultraviolet visible spectroscopy (UV-vis) experiment cuvette-based.

When a photon hits a molecule and is absorbed, the molecule is promoted to a more excited energy state.[87] Visible light has enough energy to promote electrons to a higher electronic state, since there is a particular energy that is associated with each wavelength of light.[82] Chemically, this jump goes from a high occupied molecular orbital HOMO to a lower unoccupied molecular orbital LUMO, making that the energy difference between these two molecular orbitals to be considered as "Band Gap".[82] It is important to clarify that the Band Gap and the absorption spectrum will be different for each molecule because each one has different chemical structure. Another important fact is that the resulting spectrum from the UV-vis technique represents a graph of absorbance as a function of wavelength.[88] The height of the absorption peaks is directly proportional to the concentration of the species present in the sample. The calculation of the concentration is governed by Lambert Beer's law Equation 5.6, where b is the length of the optical path and C is the concentration. ϵ is the molar attenuation coefficient, which describes the characteristic that the compound has in order to absorb light at a given wavelength.[87]

$$A = \epsilon * b * C \tag{4.1}$$

In a typical cuvette based UV-vis experiment Figure 4.1, in which you want to determine the concentration of a sample solution of unknown concentration, you must first create a calibration line. This line is made by measuring the light absorption of at least three standard solutions with different known concentrations and at a predefined fixed wavelength.[87] These concentrations must be above and below the estimated concentration of the unknown sample. Before a measurement a reference blank or sample needs to be done in order to record a zero in the measurement.[88] It is important to know that each solvent has a cut-off wavelength of UV-vis absorbance. The solvent limit is the wavelength below which the solvent itself absorbs all light. Among the limitations of this process is the type of material that you want to measure.[82] Most UV-vis instruments can analyze solid samples or suspensions with a diffraction apparatus or an integrative sphere, however this is not common. Commercial equipment of this type of
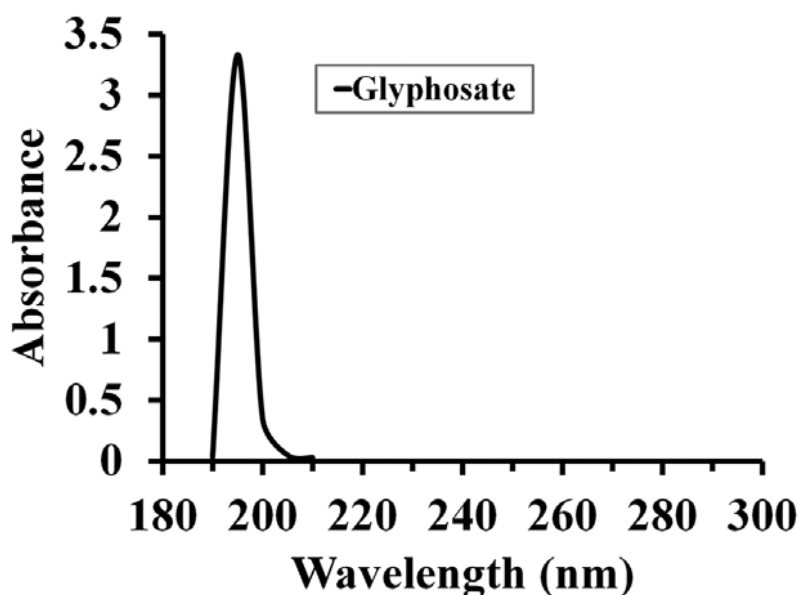
Figure 4.2: Example of a Glyphosate UV-vis Spectrum.[90]

characterization generally analyzes liquid samples and solutions more efficiently.[87]

In order to understand the results obtained with UV-vis, we must distinguish two types of analysis: qualitative and quantitative. On the one hand, the qualitative analysis, in which the absorption spectra are analyzed identifying the amount of peaks and their intensity, can determine substance in reference to the wavelength. Specifically, the position of each peak allows to identify characteristic compounds of the sample, since each sample has a unique spectrum. In addition, the size and peak width define how pure a material is present in the sample.[82] On the other hand, the quantitative analysis that involves the use of mathematical formulas, such as Lambert Beer's law, to determine the concentration of the compound.[89] These include the analysis of concentration as a function of time, very useful in processes of degradation or release compounds, due to the time plays an important role in this type of study.[82] An example of UV-vis spectrum of glyphosate is shown in figure 4.2.[90]

Figure 4.2 shows the UV-vis absorption spectrum of glyphosate, with a PMG concentration of 100 μg/ml, which presents a maximum absorption peak at the wavelength equal to 195 nm.[90] According to several reports presented in the literature,[91,92] the range between 195 nm and 220 nm is the wavelength range that organic acids, such as glyphosate, are expected to absorb UV radiation.[91] They also explain that the variations in pH increase and decrease the absorption spectra.[91]

4.2   Scanning Electron Microscopy (SEM)

SEM amplified images from approximately 10 times to 300000 times with a resolution from 30 nm to 1 nm, depending of the electron source and the equipment, providing information related to topographic characteristics, elemental composition, morphology, phase distribution, composition differences, crystal orientation, and the presence and location of electrical defects.[93,94] The ability to examine even the most minute details in high resolution way is crucial, especially when talking about materials at the manometric level. The characteristics found at this level consist of a small number of atoms, which can generate only weak signals, so measurements in SEM must be fully optimized to these conditions in order to obtain the desired information.[95]

SEM uses a focused beam of high-energy electrons that are generated by an electron gun, processed by magnetic lenses, focused on the sample surface and picked up by a detector to form an image.[94] Specifically, electrons are generated at the top of the microscope column. They are then accelerated and attracted by the positively charged anode downwards, and pass through the combination of electromagnetic lenses and openings to produce a focused and controlled beam of electrons that hits the surface of the sample.[96,97] The position of the electron beam in the sample is controlled by scanning coils. These coils, that are located below of objective lens as in the Figure 4.3 i), allowing to scan the beam on the sample surface generating an electron/sample interaction.[94] It is important to clarify that, the entire electron column has to be under vacuum in order to protect against contamination, vibrations and noise. In the absence of vacuum, other atoms and molecules present can interact with bombarded electrons, reducing image quality.[93,97]

Working Principle

When the beam hits the sample there is an electron/sample interaction where a series of results occur. In other words, when some electrons bounce from the sample are called backscattered electrons (BSE), others hit atoms and displace electrons that, in turn, come out of the sample are called secondary electrons (SE), or are simply characteristic X-rays, cathodoluminiescence, auger electrons, light or heat can be result of these interactions Figure 4.3 iii).[94,98] Specific signals given by BSE and SE are the single information that can be taken on external morphology, topography, chemical composition, crystalline structure and orientation from the materials by Scanning Electron Microscopy (SEM) detectors. On the one hand BSE are formed from elastic scattering of electrons in the incident beam by atoms in the sample. These electrons are used to generate images with a contrast, that varies with the atomic number of different constituent elements in the sample and give information about the chemical composition of it. On the other hand SE, which are formed from inelastic dispersion process, are useful for having topographic information of the sample surface, because they have a very low intensity and cover only a small part of the sample that is related to the beam angle.[96,99]

The information of BSE and SE is collected by an electron detector that converts this information into photons through a scintillator. This signal is then amplified and converted into electrical signals and used to modulate the
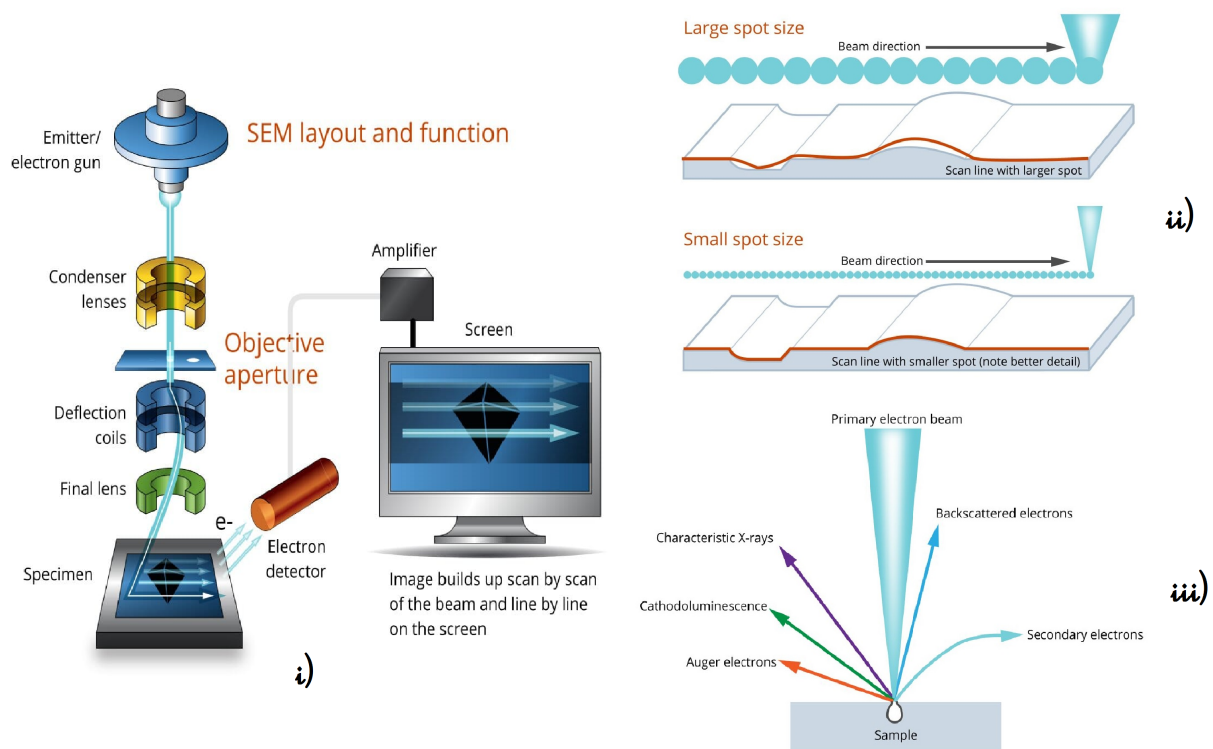
Figure 4.3: Scanning Electron Microscopy (SEM) i) Parts of electron microscope, ii) effect of probe size and spot size on sample scanning and iii) interaction scheme of electron/sample.[94]

intensity of the image on the display screen by computer programs.[94] SEM images are made up of lines of image points, i.e. each electron beam interaction with the sample is considered as a point.[100] In addition, the equipment ability to display clear images depends on the spot size, which in turn depends on the number of electrons contained in the probe. When we have a large spot size, we will have little time at each point in the sample and therefore the scanning of the image is very superficial around the original morphology. Whereas when we have a smaller spot size, the scanning of the image takes longer, but it manages to have a better image result in terms of the morphology in the analyzed sample. Therefore, as we decrease the probe size, we can have detailed result of each points taken as we can see in Figure 4.3 ii).[94,100]

Several parameters in the initial configuration before developing the measurements affect SEM images. For example: acceleration voltage, spot size, Z depth, filament current, magnification, and astigmatism are parameters that need to be considered to get high quality SEM images.[99] Regarding the sample preparation before measurement, it is important to know that they must be conductive or covered by a conductive layer, in order to eliminate any accumulation of electrons in the surface of the sample and avoid charging.[94] Figure 4.4 presents an example of SEM
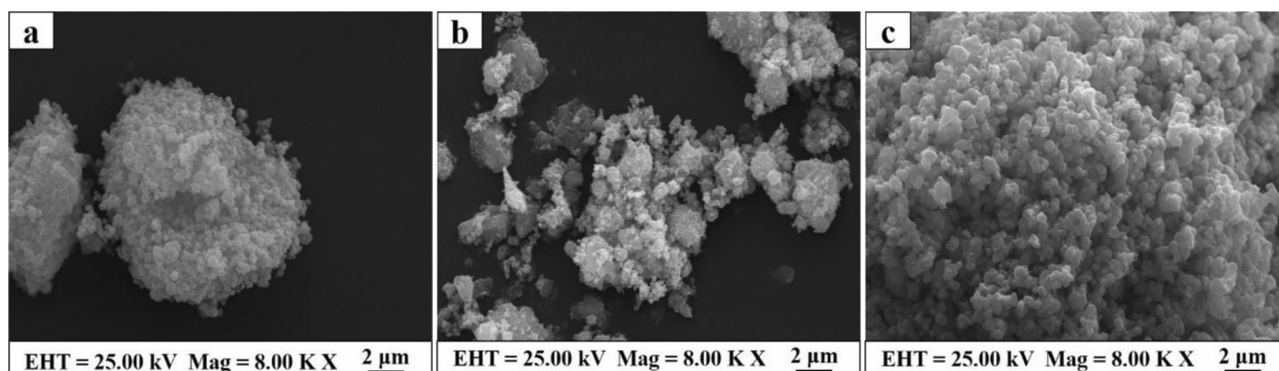
Figure 4.4: SEM micrograph example of TiO_2 (a), Fe_3O_4 NPs (b) and Fe_3O_4@TiO_2 Nanocomposite (d). [101]

micrograph of TiO_2 (a), Fe_3O_4 NPs (b), Fe_3O_4@TiO_2 Nanocomposite (c). [101]

Figure 4.4 (a) shows the SEM image of TiO_2 which is aggregated by nano-sized spherical particles after the heat-drying procedure. The SEM micrograph Figure 4.4 (b), which corresponds to Fe_3O_4 nanoparticles, shows a rough surface with agglomerated irregular particle due to its magnetic properties. Finally, Figure 4.4 (c) present the SEM micrograph of Fe_3O_4@TiO_2 magnetic nanocomposite, which present the similar surface morphology than the TiO_2 sample, indicating that the TiO_2 has successfully wrapped onto the Fe_3O_4 NPs during the synthesis process. In this case, the increase in the specific surface area by having numerous dispersed magnetic nanocomposites, due to the deposition of the TiO_2 particles on the external surface of Fe_3O_4, should be beneficial for the rapid diffusion of TiO_2 towards all the active sites of the adsorbent. [101]

4.3   X-ray diffraction (XRD)

XRD is a non-destructive technique used to reveal structural sample information such as: chemical composition, crystalline structure, crystalline size, deformation, preferred orientation, and layer thickness. [94] XRD is based on the constructive interference of monochrome X-rays and a crystalline sample. X-rays are used in this technique because they are on the same scale of length in interatomic space and network parameters. [102] To describe a material using XRD, two stages are required; the first by studying the elements present using chemical analysis techniques and the second determined as these are organized in their crystalline phases. [94] The identification of the phases is achieved by comparing the acquired data with reference bases, based on the diffraction pattern obtained. [103] Therefore, materials researchers use this characterization technique in order to study materials ranging from x-ray powder diffraction to thin films, solids, and nanomaterials including semiconductors and polymers. [104]
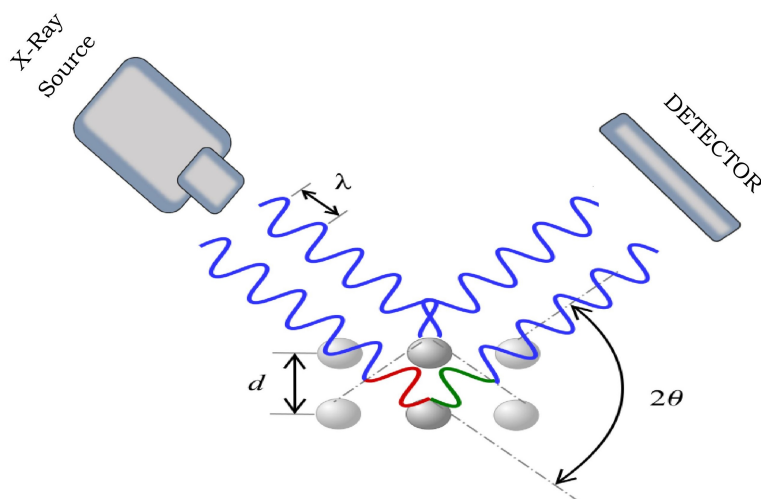
Figure 4.5: Illustration of X-ray diffraction mechanism as a reference of Bragg's Law.[107]

Working Principle

This test method is performed by directing an X-ray beam to a sample and measuring the scattered intensity as a function of the output direction. Specifically, when an X-ray beam hits the sample, they interact with the electrons in the atoms, causing the reflected x-ray photons to be deflected from their original trajectory.[105,106] It is important to clarify that in regular structure materials, such as crystallines ones, the diffraction beams cancel each other, producing constructive interference, which in turn create detectable intensity peaks as seen in Figure 4.5.[107] The intensity of the scattered X-rays is plotted as a function of dispersion angle, i.e. the material structure is determined from the analysis of the location, angle and intensities of the scattered peaks. We have to take into account that the diffraction direction depend on the size and shape of the unit cell, and the diffraction intensity depend on the type and arrangement of the atoms in the crystalline structure.[103] All of this is given by Bragg's Law according to Equation 4.2. Where λ is the wavelength of X-rays, d_{hkl} is the space between a particular set of planes, θ is the angle of incidence at which a diffraction peak is measured, and n is an integer representing the harmonic order of the diffraction.[105,106]

$$n\lambda = 2d\sin(\theta) \tag{4.2}$$

In a typical XRD experiment, in reflection mode, the X-ray source is directed to a fixed position and the sample rotates with respect to the X-ray beam on θ. Then, diffraction rays are collected by a detector, which rotates over a range of 2θ, recording the x-ray intensity signal reflected by the crystal in each position Figure 4.5. Consequently, when observing intensity peaks, Bragg's law is fulfilled, causing that network parameters can be calculated and the crystal direction can be identified.[105,106] All of this is done using an available database, in reference to the XRD
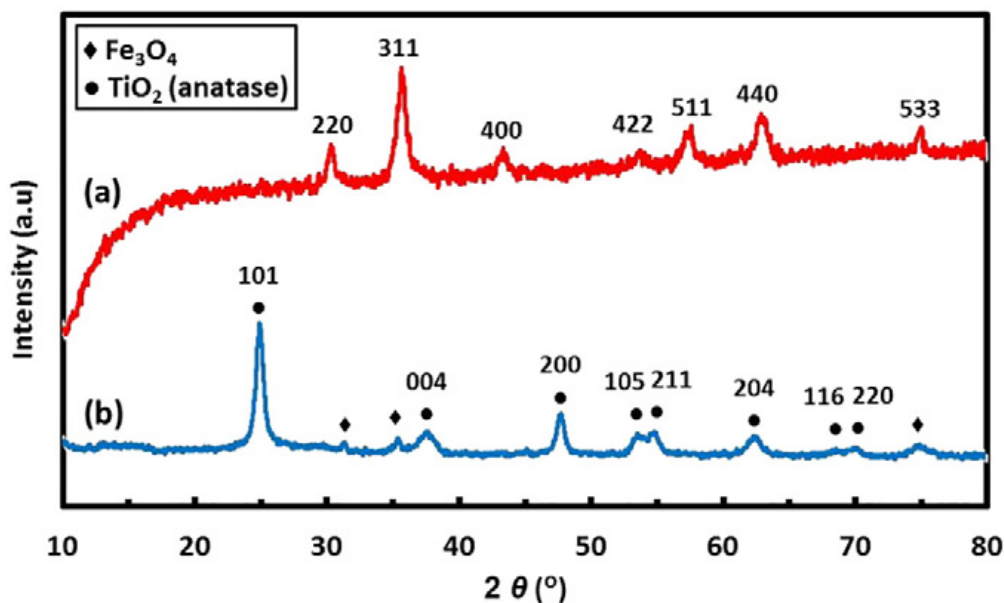
Figure 4.6: Example of XRD patterns for Fe_3O_4 NPs (a) and Fe_3O_4@TiO_2 Nanocomposite (b). [108]

software that it is using. Among the factors that contribute to the patterns intensity is the dispersion contribution, i.e. the number of X-ray photons that enter and leave the sample. This contribution strictly depends on material aspects such as absorption and structural factor. On the one hand the absorption factor, who has the ability to receive and release X-rays, does not depend on theta but rather on the thickness of the sample. On the other hand the structural factor directly affects the intensity of peaks as a result of the material structure. [102,107]

Finally a plot of intensity as a function of 2θ is the result of XRD experiment. With presence and absence of peaks, the crystal type and the parameters of the unit cell, associated with the material, can be determined. Furthermore, the size of each peak determines the particle size of the sample, including nanometers. This process is carried out comparing values with databases, using deduction and elimination process. It is clear to emphasize that this comparison is very simple nowadays, since a variety of software linking to numerous databases, which contain information of crystalline structures, are very affordable. [102,107] An example of XRD patterns of Fe_3O_4 NPs (a) and Fe_3O_4@TiO_2 Nanocomposite (b), with 2 in the range of 10–80 is shown in Figure 4.6. [108]

Figure 4.6 (a) shows the diffraction peaks, obtained from Fe_3O_4 NPs, at around 2 of 30.1°, 35.5°, 43.2°, 53.4°, 57.2°, 62.8° and 75 which are related to the reflection of (220), (311), (400), (422), (511), (440) and (533) planes. [108] According to Khashan et al., they explain that is possible to demonstrate the well crystallized structure of Fe_3O_4

with typical cubic inverse spinel structure, due to the peaks are sharp and intense.[108] On the other hand, Figure 4.6 (b) shows the XRD pattern of Fe_3O_4@TiO_2 nanocomposite. The diffraction peaks at around 2 equal to 25.3°, 37.8°, 48.2°, 54.2°, 55.3°, 69 and 70 are assigned to the (101), (004), (200), (105), (211), (116) and (220) planes of TiO_2, respectively.[108] It is important to mention that the decrease of diffraction peaks intensities of Fe_3O_4 NPs is observed as a result of TiO_2 coating, due to the absorption of X-ray through the TiO_2 shell.[108]

4.4 Fourier transform infrared spectroscopy (FTIR)

FTIR is a well-established characterization technique for identification and structural analysis of chemical compounds.[83] The peaks in its spectrum represent the exitation of vibrational modes of molecules in the sample, which are associated with various functional groups and chemical bonds in the molecules.[83] Specifically, this characterization technique allows to study the absorbent and emitting properties of materials. Because, in order to study the chemical bonds that connect the atoms it is necessary to know the different wavelengths of the infrared spectrum.[84] Well it is here, that these bonds tend to vibrate with frequencies that correspond to infrared wavelength light and hence can easily be excited with such a radiation.[85] The clear alterations in the characteristic pattern of absorption bands affirm a change in the material composition.[86] It is very common in IR spectroscopy to use wavelengths that cover numbers ranging from 200 to 4000 cm -1.[84] In general FTIR spectroscopy is used to identify unknown material, finding additives, detecting contaminants, new compounds formations and identify decomposition and oxidation.[86]

Working Principle

IR spectroscopy is a method that studies the absorption and emission of energy caused by infrared interaction and the material. The basic principle behind molecular spectrometry is that molecules absorb energy from light at specific wavelengths, known as their resonance or vibration frequencies. For example, water molecules resonate/vibrate around the wave number of 3450 cm-1 in the infrared region of the electromagnetic spectrum.[83]

The instrument that is used for this characterization produces a beam from an infrared source as can be seen in Figure 4.7. This beam passes through an interferometer where spectral coding takes place. Inside the interferometer there are several devices such as: Figure 4.7 a) a collimating mirror, which collects the light from the source and makes the beam's rays parallel, Figure 4.7 b) a fixed mirror, which remains fixed in one position, Figure 4.7 c) a moving mirror , which has the function of moving to the left and right and Figure 4.7 d) beamsplitter, designed to transmit and reflect at the same time part of the incident light on it. In general, a light source with various IR wavelengths, emitted by the beamsplitter, travels towards the fixed mirror and the light reflected by the beamsplitter travels towards the moving mirror. The resulting rays are reflected off these mirrors, then travel back to the ray splitter and recombine, see the schematic in the figure. This recombination in the interferometer of beams with different trajectories creates a constructive and destructive interference called an interferogram. This interference pattern or interferogram is then sent to the sample and the transmitted part of the interferogram is sent to a detector. After comparison with a reference sample beam spectrum at the detector, a Fourier transform is performed to obtain the

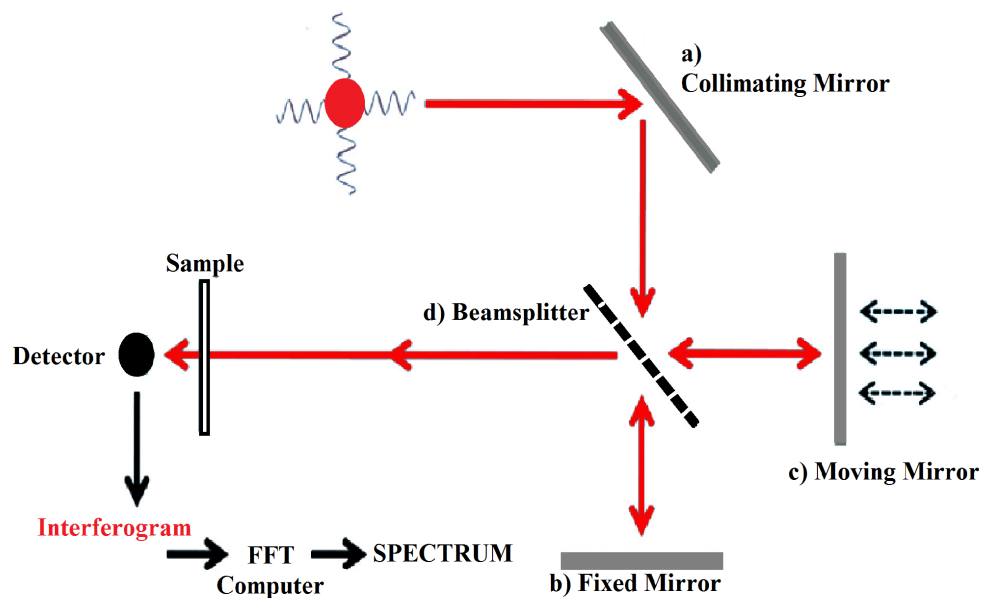Figure 4.7: Simplified diagram of a Fourier transform infrared spectrometer. Adapted image.[85]
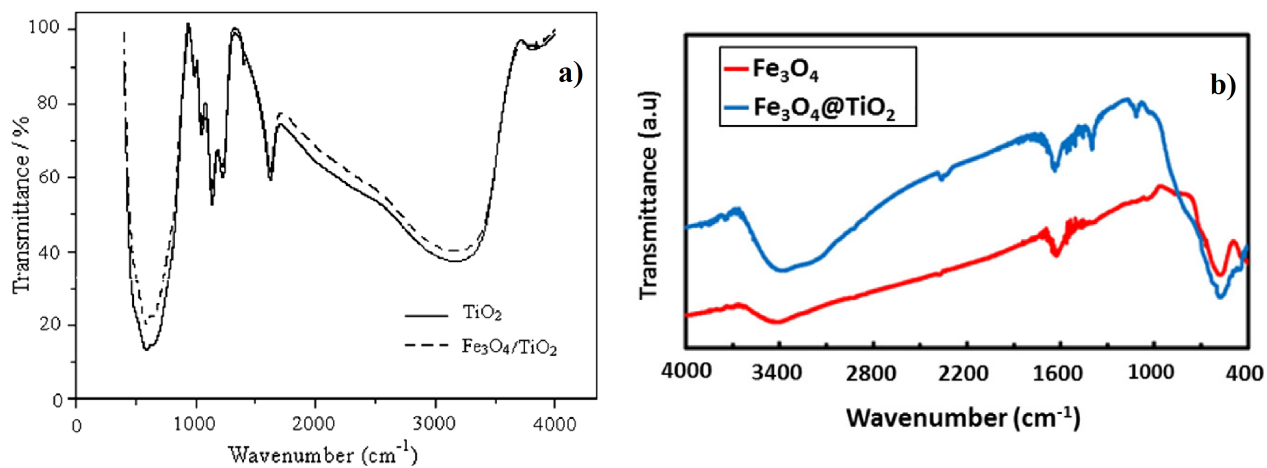
Figure 4.8: Example of FTIR spectra of TiO_2 and Fe_3O_4@TiO_2 Nanocomposte (a) and Fe_3O_4 NPs and Fe_3O_4@TiO_2 Nanocomposte (b).[73,108]

full spectrum as a function of wave number. The resulting graph is the FTIR spectrum that is searched in reference libraries for identification.[85] Figure 4.8 shows two examples of FTIR spectra for TiO_2, Fe_3O_4 NPs and $Fe_3O_4@TiO_2$ nanocomposite.

Figure 4.8 a) gives the FTIR spectra pattern of TiO_2 and $Fe_3O_4@TiO_2$ core-shell NP.[73] From this spectra it is possible to notice that FTIR spectra of TiO_2 and $Fe_3O_4@TiO_2$ core-shell NP are pretty similar, proving that a very good synthesis of TiO_2 has been achieved on the surface of Fe_3O_4 NPs in the core-shell type.[73] On the other hand Figure 4.8 b) shows the FTIR spectra of Fe_3O_4 NPs and $Fe_3O_4@TiO_2$ Nanocomposite to be in the range of 4000–400 cm^{-1}.[108] In this case, the results argue that there is a band stretch in the range of 500 - 700 cm^{-1}, in which the Ti-O-Ti stretching vibrations are located, due to this band is relatively broader due to the overlapping of Ti-O peak along with the Fe-O, demonstrating the attachment of TiO_2 on the surface of the Fe_3O_4 and the successful synthesis of $Fe_3O_4@TiO_2$ nanocomposite.[108] It is important to mention that in our work the FTIR results of the nanocomposites should have the information of both the magnetic nanoparticles as well as the TiO_2, since in this research project it is proposed to generate a hybrid material of TiO_2 decorated with Fe_3O_4 NPs.

Chapter 5

Methodology

5.1 Chemicals

Iron (III) chloride hexahydrate (ACS reagent 97%) and Iron (II) choride tetrahydrate (>99%) were purchased from Sigma Aldrich. Ammonium hydroxide (NH_4OH) was purchased from EMD milipore corporation. Titanium Dioxide (TiO_2) was purchased from MM representaciones. Glyphosate "Roundup 480, Agricola's herbicide" 480 g/L with 1L of additives, were purchased from Ecuaquimica. All chemicals were used as received without further modification, and they were of analytical reagent grade.

5.2 Synthesis of TiO_2 NPs by the Ultrasound Method

The synthesis of nanostructured TiO_2 was made by an ultrasound-assisted method, using titanium dioxide and sulfuric acid, following the previous studies of Nguyen Trung Duong et al.[109] They reports on the application of ultrasound to promote the chemical reaction between the micro particles of TiO_2 with sulfuric acid.[109] According to Hassanjani-Roshan et al.,[110] ultrasound intensity plays an important role in the morphology and dimensional properties of nanostructured TiO_2.[109,110] In addition Trung Duong et al.,[109] mention that the ultrasound intensity is used to control the dispersion of TiO_2 particles in sulfuric acid and collaborate by breaking the chemical bonds of TiO_2 to create new structures at a reaction temperature of 100 $°C$ in 1 h.[109,111] The performance of using ultrasonic waves in such reactions is to provide a highly complete mixture.[111] The experimental process is described below:

The synthesis of titanium dioxide nanoparticles was prepared using 20 g of Titanium Dioxide (TiO_2), that were added to 40 mL of sulphuric acid. The mixture was treated by the ultrasound method using a "Sonoplus ultrasound homogeniser mini 20" equipment as is shown in Figure 5.1 a). The benefit of performing ultrasound processes with these samples is to lead a chemical dynamic alteration to produce new precursors that are then used for new synthesis.[110,112] The specifications used in the ultrasound equipment were; a nominal ultrasonic output of 20 W, with
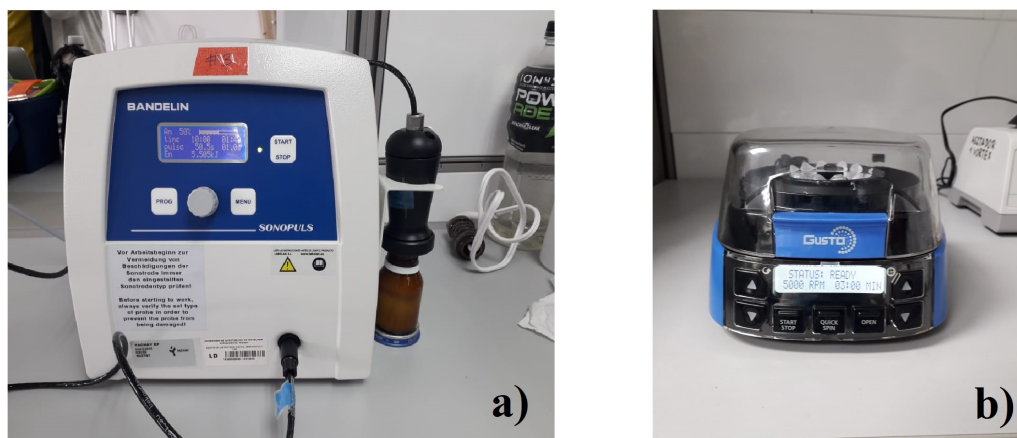
Figure 5.1: Synthesis of TiO$_2$ nanoparticles using ultrasonic method, a) ultrasonic TiO$_2$ treatment and b) separation of the sample using a centrifuge. [109]

a pulse level of 50.5 s and an amplitude of 50%.

Three ultrasound interactions of 10 min with a rest of 5 min between them, were performed to the sample. Then the sample was hydrolyzed with distilled water at 100 °C for 1 hour. [109] Consequently a sodium hydroxide solution was used to adjust the pH of the compound in a range of 8 to 11. [109] A separation process using "High-speed mini centrifuge, heathrow scientific-taste" and a careful process of washing with distilled water, were carried out to separate all by-products present in the sample Figure 5.1b). Then the sample was dried for 24 hours at 50 °C. Finally annealed process, to give a crystalline structure back to TiO$_2$, was performed using a muffle at 500 °C for two hours and air atmosphere. [109,111] The chemical reactions of nanostructured TiO_2 formation are detailed in the following equations: [109]

$$TiO_2 + 2H_2SO_4 \xrightarrow{ultrasonic\ energy + 100°C\ for\ 1h} H_2[TiO(SO_4)_2] + H_2O \tag{5.1}$$

$$H_2[TiO(SO_4)_2] \rightarrow TiOSO_4 + H_2SO_4 \tag{5.2}$$

$$TiOSO_4 + (n+1)H_2O \rightarrow TiO_2 \cdot nH_2O + H_2SO_4 \tag{5.3}$$

$$TiO_2 + nH_2O \rightarrow TiO_2 + nH_2O \tag{5.4}$$
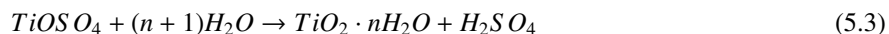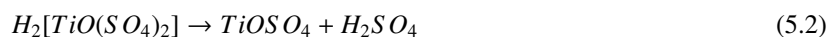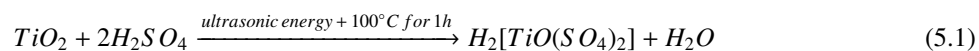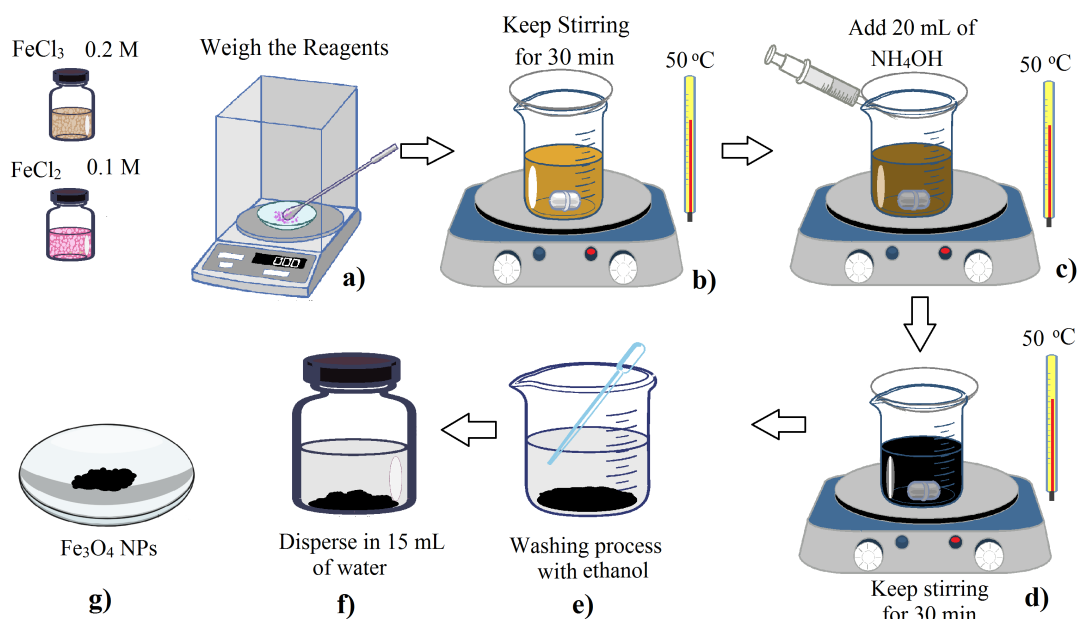
Figure 5.2: Experimental set up of Fe_3O_4 synthesis process.

5.3 Synthesis of Fe_3O_4 Nanoparticles

Figure 5.2 shows the synthesis of Fe_3O_4 Nps using the chemical co-precipitation method. [13] In general, this method involves the co-precipitation of aqueous salts of Fe^{2+} and Fe^{3+} with a molar ratio of 2:1, by the addition of NH_4OH as shown in Equation 5.5. [13,15,113] Specifically, 6.0 g of $FeCl_3.6H_2O$ and 3.0 g of $FeCl_2.4H_nO$ were weighed and dissolved in 100 mL of distilled water, as can be seen in figure 5.2 (a and b). The solution was stirred for 30 min at 50 $°C$. Then, 20 mL of NH_4OH was added into the solution, as it looks in figure 5.2 (c); consequently, Fe_3O_4 NPs are formed as a black precipitate. Finally the suspension was kept stirred for 30 min at 50 $°C$ in a simple reflux system as well as represented in the figure 5.2 (d).

$$FeCl_2 + 2FeCl_3 + 4NH_4OH \rightarrow Fe_3O_4 + 8HCl + 4NH_3 \tag{5.5}$$
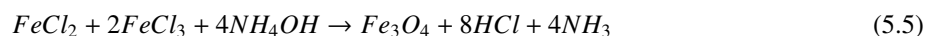
After cooling to room temperature the NPs were recovered using a magnet and then washed with distilled water and ethanol, as well as it is observed in figure 5.2 (e and f). The drying process of the sample was performed at 60 $°C$ for 30 min in order to have the powder as can be seen in figure 5.2 (g).
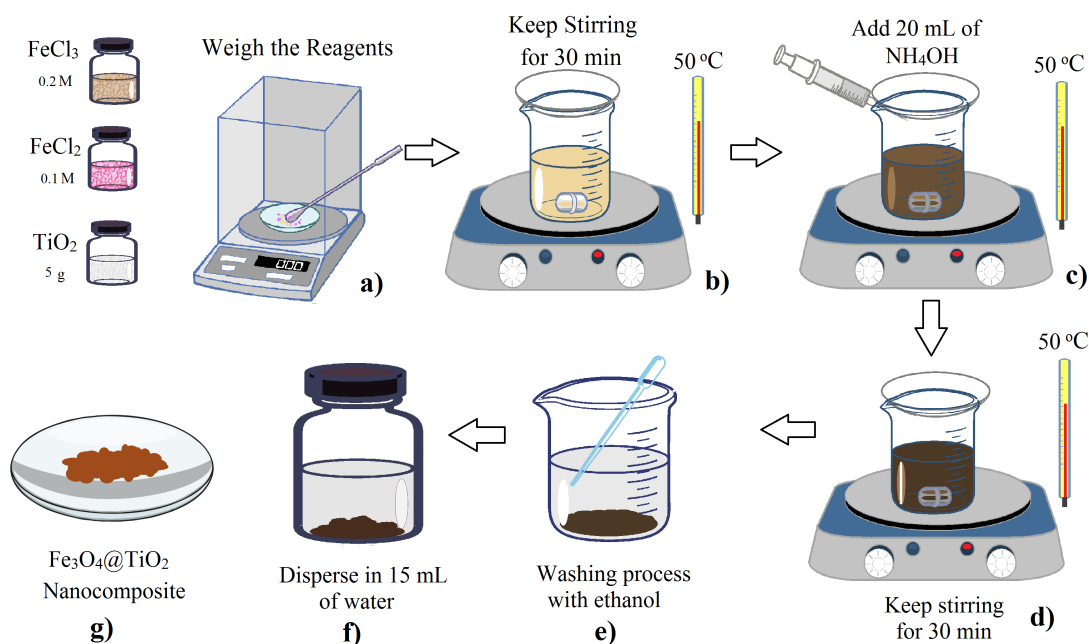
Figure 5.3: Experimental set up of synthesis Fe$_3$O$_4$@TiO$_2$ Nanocomposite.

5.4   Synthesis of Fe$_3$O$_4$@TiO$_2$ Nanocomposite

Regarding the synthesis of the nanocomposite, Fe$_3$O$_4$ nanoparticles were synthesized on TiO$_2$, using a chemical co-precipitation method.[13] In this work, was used two types of TiO$_2$: bulk commercial and the nanostructured synthesized one. Specifically, to prepare the nanocomposite we prepared a solution of 5.0 g of TiO$_2$ in 100 mL of distilled water with magnetic stirring, until to have a well dispersed solution. Then, 3.0 g of FeCl$_3$.6H$_2$O and 2.5 g of FeCl$_2$.4H$_2$O was added as can be seen in figure 5.3 (a). The solution was stirred for 30 min at 50 $^{\circ}C$, as it looks in figure 5.3 (b). Then, 20 mL of NH$_4$OH was added figure 5.3 (c). Consequently, Fe$_3$O$_4$@TiO$_2$ nanocomposite was formed as a gray precipitate. Finally the suspension was kept stirred for 30 min at 50 $^{\circ}$C in a simple reflux system as is shown in figure 5.3 (d). After cooling to room temperature, our nanocomposite was recovered using a magnet and then washed with distilled water and ethanol.as well as represented in the figure 5.2 (e and f). The drying process of the sample was performed at 60 $^{\circ}$C for 30 min in order to have the nanocomposite powder as can be seen in figure 5.2 (g).[13,15]

The synthesis of magnetic nanoparticles (Fe$_3$O$_4$) and magnetic nanocomposite (Fe$_3$O$_4$@TiO$_2$) were successfully prepared as shown in Figure 5.4. The nanoparticles and the nanocomposite are easily attracted by an external magnetic
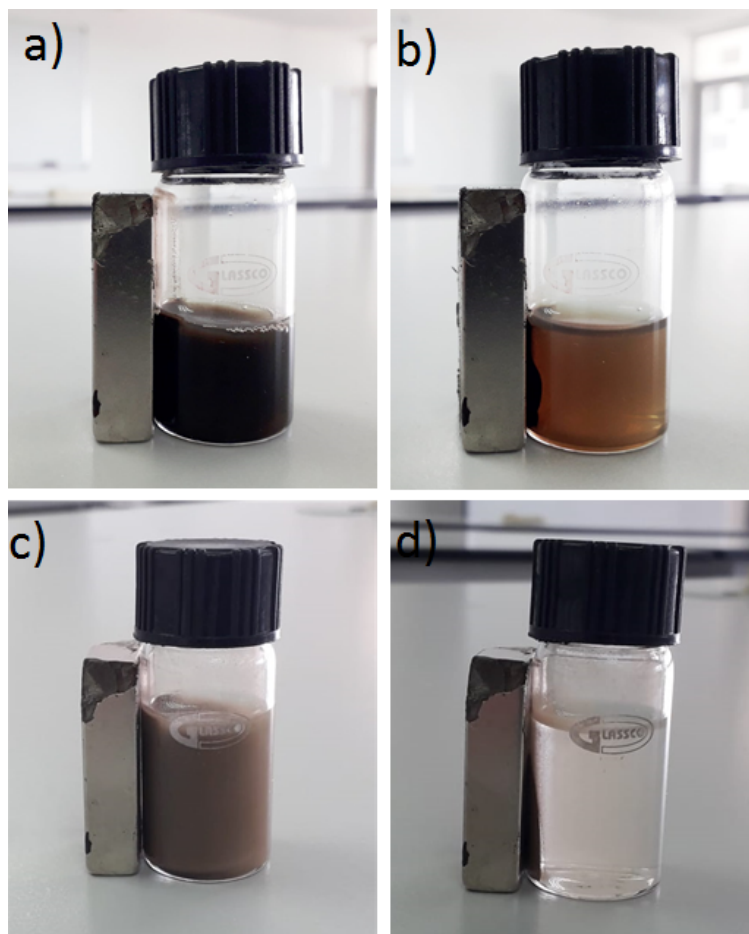
Figure 5.4: Magnetic response of a) and b) Magnetite nanoparticles (Fe_3O_4) c) and d) Magnetic nanocomposite of $TiO_2@Fe_3O_4$.

Figure 5.5: FTIR Spectrometer - Agilent Cary belonging to Yachay Tech University, Ecuador.

field, demonstrating the magnetic properties of the samples. After the drying process, the Fe_3O_4 nanoparticles and Fe_3O_4@TiO_2 nanocomposite presented a characteristic black and brown color respectively, due to the oxidation of Fe_3O_4 NPs surface, as is shown in Figure 5.4 b) for magnetic nanoparticles and d) for nanocomposite. This behaviour was previously reported by María Vanegas et al.[13,113]

5.5   Characterization Equipment

5.5.1   Fourier transform infrared spectroscopy

The FTIR spectra were obtained from powder-samples using Agilent Cary 630 FTIR Spectometer and the data collected with Agilent MicroLab Software. A full spectra data acquisitions was obtained at a wavenumber range of 400 - 4000. The data obtained were analyzed and plotted using Spectragryph and Origin-Pro software. A equipment photo is shown in Figure 5.5.
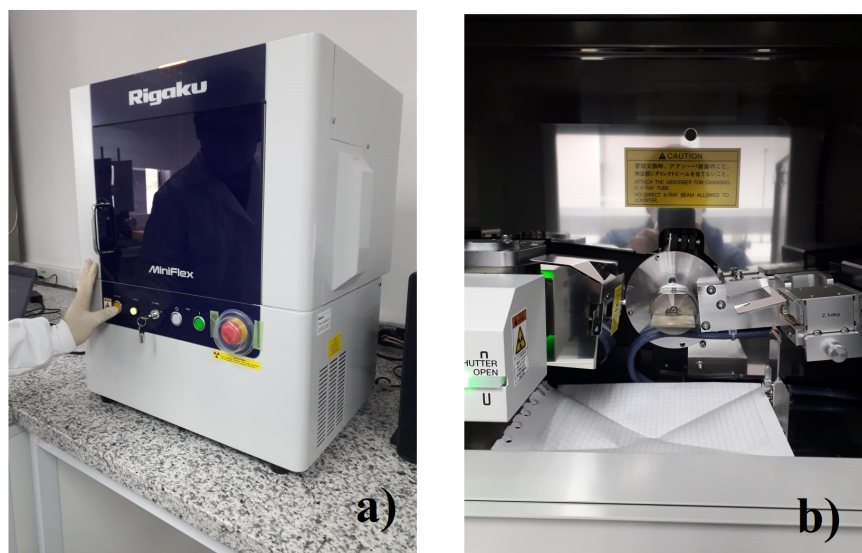
Figure 5.6: X-ray power diffractometer Miniflex-600 equipment belonging to Yachay Tech University, Ecuador. a) General photo of the equipment and b) internal part of the equipment

5.5.2 X-ray Diffraction

X-ray powder diffraction (XRD) patterns of the samples were recorded on a powder diffractometer @Miniflex-600, Rigaku trademark, with a D/tex Ultra2 detector equipment Figure 5.6. The X-ray generator was operated to 40kV and 15 mA, in a sealed tube CuK(alpha) radiation source. Additionally, for collecting data was employed a Theta/2θ in scan-axis, $0.005°$ step width in a scan range $3-90°$ in 2θ, and the D/tex Ultra2 detector in 1D scan mode. Finally, for it was used a Soller slit $1.25°$ receive and incident scattering, and high-length, receiving and incident slit 10.0 mm, 8.0 mm, and 13.0 mm, respectively. The miller index was determined using computational software QualX and PowCod 2017 data base. The crystallinity size was determined from XRD peaks using Scherer equation and the percentage of Anatase/rutile phase was determined using Spurr and Myers method.

5.5.3 Scanning Electron Microscopy

SEM micrographs were taken with a Scanning Electron Microscopy TESCAN MIRA 3 Schottky field belonging to Army Polytechnic School (ESPE), Quito - Ecuador. The Samples were prepared in a carbon substrate with a pure drop of each sample. A photo of the equipment is shown in Figure 5.7.

Figure 5.7:   Scanning Electron Microscope (SEM) belonging Army Polytechnic School (ESPE), Quito - Ecuador

5.6   Adsorption experiments

5.6.1   Calibration Curve

The calibration curve is the graphic representation that relates an instrumental signal as a function of the concentration of an analyte and defines the working interval in which the results to be reported have a known precision and accuracy that has been documented in validation of each method.[114] In this way, a calibration curve of commercial glyphosate was made in order to obtain the precision, limit of detection, limit of quantification and the sensitivity of the equipment that is being used. In order to obtain the detection limit, quantification limit and sensitivity of the equipment that is being used to quantify the glyphosate adsorption, a calibration curve was made using the Genova Nano Jenway Spectrophotometer Figure 5.8.

Commercial glyphosate with an initial concentration of 480 g/L and distilled water (10 mL) were used and the previously calculated volumes were carefully added according to Table 5.1. The absorbance measurements were taken by the Genova Nano Jenway spectrophotometer with the following specifications: wavelength range from 198 nm to 300 nm, the optical path was 0.5 um and 0.2 uL was used for measurements.[95] The results were analyzed using Origin computational program. The graph corresponding to this study is shown in Figure 5.9 and reflects a linear absorbance behavior as a function of glyphosate concentration. The absorbance values, that are plotted in the diagram, correspond to the wavelength of 200 nm, that's where the characteristic peak of glyphosate is located Figure 5.9 a).[77]
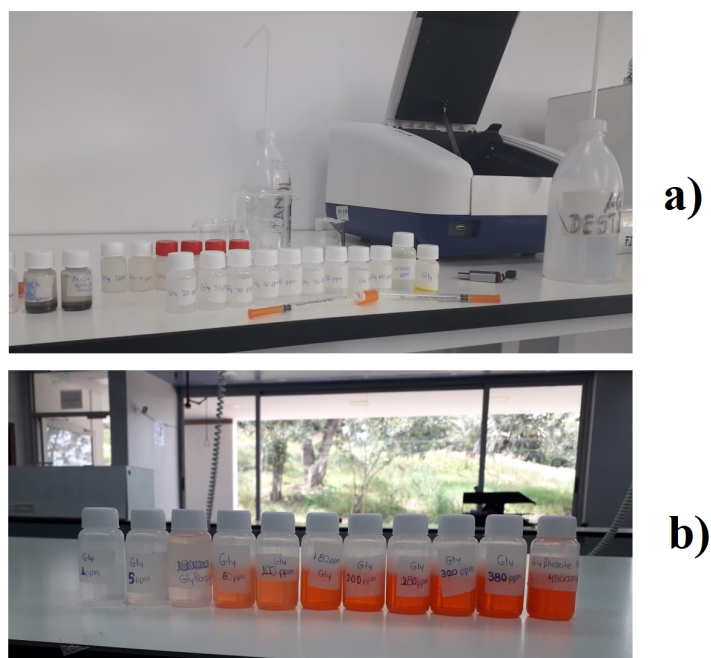
Figure 5.8: Experimental set-up of calibration curve of glyphosate at different concentrations

Concentration (g/L)	V. Glyphosate (mL)	V. Water (mL)	Absorbance (a.u.)
300	6.25	3.75	2.140
250	5.20	4.80	1.989
200	4.16	5.84	1.728
150	3.12	6.88	1.682
100	2.08	7.92	1.617
50	1.04	8.95	1.1568
10	0.2	9.8	0.8649
1	0.1	9.9	0.1239

Table 5.1: Calibration curve of commercial glyphosate at different concentrations
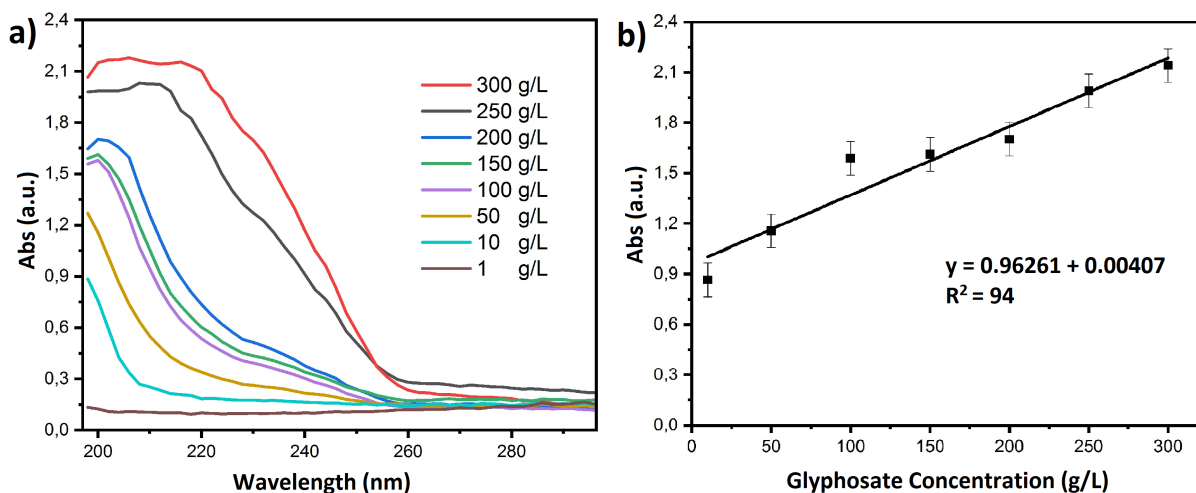
Figure 5.9: Calibration curve of commercial Glyphosate

With a view to obtain adequate accuracy and statistical reliability, the least squares method was used to find the calibration line that best fits the points obtained.[115,116] Where each point is defined by an independent variable, in this case the concentration, and a response variable in this case the level of absorbance.[115] The calibration line is defined by the following equation:

$$y = a + b * x \tag{5.6}$$

Where; y is the level of absorbance, b is the slope of the calibration curve, x is the concentration of the solution and a is the adjustment parameter of the calibration curve.[115]

The curve obtained with the experimental tests yields the correlation coefficient (R^2) equal to 0.94 as is shown in the Figure 5.9 b), which satisfies the parameters for the completion of the following measurements. With respect to the calibration curve there is a linear adjustment equal to: y = 0.96261 + 0.00407 x. Taking into account the results presented in the calibration curve it can be said that the detection limit and the quantification limit of the equipment, in order to represent the adsorption of the commercial glyphosate, should not be less than 1 g/L. In other words, the value to be taken into account to perform the adsorption experiments is greater than this value, since 1 g/L is the lowest value that can be determined using this equipment and these solutions. Regarding with equipment sensitivity it is prime to explain that our equipment has a low repeatability in the measurements. However the results was improved using a optical path equal to 0.5 um.

5.6.2 Adsorption of Glyphosate

Commercial glyphosate adsorption experiments were carried out to compare the adsorption capacity of TiO_2 bulk size, TiO_2 nano size, Fe_3O_4 NPs, nanocomposite $Fe_3O_4@TiO_2$ bulk size and nanocomposite $Fe_3O_4@TiO_2$ nano size. In this way, 6 samples of 10 mL of commercial glyphosate at 100 g/L were prepared. Then 0.5 g of each sample, mentioned above, were mixed with the glyphosate and placed under sun radiation. The purpose of exposing them under solar radiation is to improve the photocatalytic activity of the nanocomposite that could help for the glyphosate degradation. The The pH values of the samples were reported in Table 5.2.

Sample	pH
TiO_2 Bulk size	5
TiO_2 Nano size	6
Fe_3O_4	5
$Fe_3O_4@TiO_2$ Bulk size	5
$Fe_3O_4@TiO_2$ Nano size	4

Table 5.2: pH values of the samples.

5.6.3 Kinetic Adsorption Study

The kinetics describe the rate of adsorption of commercial glyphosate in the surface of the samples and determines the time in which the equilibrium is reached. The adsorption capacity Q_t (mg/g) and removal rate R (%) were used as indices that reflect the performance of the adsorbent. Calculation formulae of Q_t and R are as follows:

$$Q_t = \frac{V(C_i - C_e)}{m} \tag{5.7}$$

$$R = \frac{(C_i - C_e)}{C_i} x100\% \tag{5.8}$$

where Q_t is the adsorption response time (min), C_i and C_e are the initial glyphosate concentration and the glyphosate concentration at equilibrium (mg/L) respectively, V is the solution volume (L), and m is the mass of the adsorbent (g).

The adsorption process of commercial glyphosate on TiO_2 bulk size, TiO_2 nano size, Fe_3O_4 NPs, nanocomposite $Fe_3O_4@TiO_2$ bulk size and nanocomposite $Fe_3O_4@TiO_2$ nano size was simulated by the pseudo-first-order kinetic model and pseudo-second order kinetic. Different models can be expressed by the following equation:

Pseudo-first-order kinetic equation (PFO):

This model is widely applied to describe the behavior of adsorption processes. It has the following linearized form Equation 5.9:

$$ln(Q_e/(Q_e - Q_t)) = k_1 t \tag{5.9}$$

where Q_e = is the equilibrium adsorption capacity (mg/g); t = time(min) and k 1 = rate constant (1/min). Plotting $ln((Q_e - Q_t)/Q_e)$ vs. t gives a straight line that passes through the origin with a slope k1 for systems that obey this model.

Pseudo-second-order equation (PSO):

This model assumes that the uptake rate is second order with respect to the available surface sites. It has the following linearized form Equation 5.10:

$$\frac{t}{Q_t} = \frac{1}{k_2 Q_e^2} + \frac{t}{Q_e} \tag{5.10}$$

where k_2 is the pseudo-second-order (PSO) rate constant. Other symbols have the same meanings as in the PFO model.Plotting t/Q_t vs t gives a straight line for PSO- compliant kinetics. The slope is $1/Q_e$, and the intercept is $1/k_2 Q_e^2$. It is important to mention that the PFO and PSO models are the most used models in environmental adsorption kinetics studies and are useful for determining whether physical or chemical adsorption process. If the pseudo-first-order model provided a better fit result, then the adsorption is a physical process; while the pseudo-second-order model fits better, then it is chemical adsorption. [43]

Chapter 6

Results & Discussion

Nanomaterials characterisation discloses information on the physical, chemical and morphological properties of the samples, which are related to the removal efficiency of the glyphosate. This chapter describes the characterisation of the samples synthesized to provide information on: (a) its chemical composition; and (b) morphology and (d) particle size. For this: UV-vis spectroscopy, Fourier transform infrared spectroscopy (FTIR), X-ray diffraction (XRD), and scanning electron microscopy (SEM) were used. Subsequently, studies of the adsorption of commercial glyphosate were carried out to know the reaction kinetics in this process.

6.1   Characterization of materials

6.1.1   Fourier Transform Infrared Spectroscopy (FTIR)

The FTIR spectra of the commercial TiO_2 comparing with nanostructured synthesized one were shown in Figure 6.1 a) and b) respectively. From these spectra, the characteristic peak of TiO_2 were observed at about 500–700 cm^{-1} wavenumber, which is associated with the characteristic vibrational mode of anatase phase of TiO_2.[127–129] The extra peaks found in the spectrum of TiO_2 nano-size (Figure 6.1 b), can be attributed to the residues of the synthesis of this material. The peak at 3058 cm^{-1} indicates the presence of hydroxyl group (O–H). The absorption peak at 1625 cm^{-1} indicate the presence of hydroxyl group (–OH) from the crystal water adsorbed on the surface of TiO_2.[128,129] The absorption peaks around of 2320 cm^{-1} are attributed to the presence of carbon dioxide stretching vibration present in the air.[131] The peaks located at 2110 cm^{-1} and 1425 cm^{-1} indicate that the presence of C=C and C=N in-plane vibrations respectively. Finally, the band located around 1115 cm^{-1} is attributed to the C–O–C stretching vibrations according with what was reported by Zuoli He et al.[132] This band could be attributed to the bonds of carbonaceous organic materials that are present in the chemical composition of commercial titanium dioxide sample, even in TiO_2 nano size sample after sonication treatment.[132] From these results it is possible to argue that the samples correspond to TiO_2.
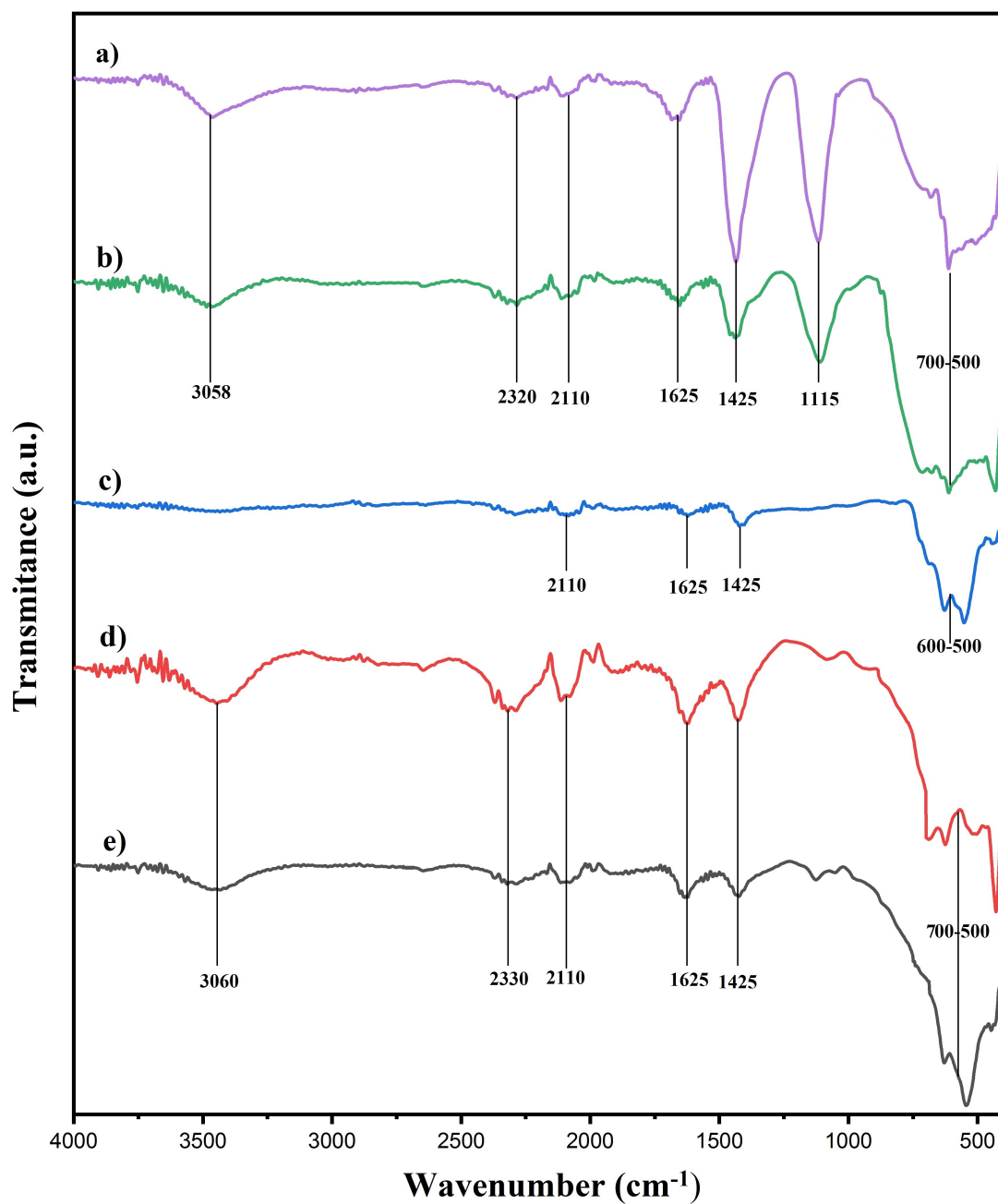
Figure 6.1: FTIR spectra of a) TiO_2 bulk size, b)TiO_2 nano size, c) Fe_3O_4 NPs, d) Fe_3O_4@TiO_2 bulk size and e) Fe_3O_4@TiO_2 nano size

On the other hand, FTIR spectrum obtained from magnetite nanoparticles is presented in Figure 6.1 c). The two intense peaks observed between 500 cm^{-1} and 600 cm^{-1} are attributed to the stretching vibration mode associated to the metal-oxygen Fe–O bonds in the crystalline lattice of Fe_3O_4 NPs. [133] They are characteristically pronounced for all spinel structures and for ferrites in particular. [134] The peaks at 1625 cm^{-1} are due to the hydroxyl groups of molecular water, is the H-O-H bending of the coordinated water. [108] Also Fe_3O_4 spectrum show a broad band at 2110 cm^{-1} and 1425 cm^{-1}, which are attributed to the asymmetric and symmetric stretching vibrations of C≡C and C-N in-plane. [131]

With respect to the nanocomposites (Fe_3O_4@TiO_2), the FTIR spectrum are shown in Figure 6.1; d) for the bulk-size and e) for the nano-size. Both Fe_3O_4@TiO_2 nanocomposites possess more signals of TiO_2 than Fe_3O_4. The spectrum show a broad band at 3060 cm^{-1} in both cases, which are attributed to the surface hydroxyl group (O-H). [131] The peak at around 2330 cm^{-1} may originate from the carbon dioxide in the air. [131] The peaks at 1655 cm^{-1} are due to the hydroxyl groups of molecular water that was adsorbed on the surface of Fe_3O_4@TiO_2 nanoparticles. [128,129] Peaks observed at 1210 cm^{-1} and 1425 cm^{-1} are assign to C≡C and C-H stretching respectively. The peaks in the range of 500 cm^{-1} to 700 cm^{-1} might be attributed to the presence of stretching vibrations of Ti-O and Fe-O-Ti bonds. [127] It is important to mention that in the spectrum that corresponds to Fe_3O_4@TiO_2 bulk-size sample (Figure 6.1 d), it is clear to see the shift of the characteristic peaks of the magnetite towards the left around 700 cm^{-1}. This means that, given the presence of the characteristic peaks of the samples of TiO_2 and Fe_3O_4 in this region, there is a formation of a bond between these two materials. It should be mentioned that due to the synthesis technique that we use for nanocomposites (TiO_2 decorated with Fe_3O_4 NPs) these bonds are physical since they are due to the interaction of the magnetite with the surface of the titanium dioxide. In the same way, although not so evident, this interaction can be seen in the spectrum corresponding to Fe_3O_4@TiO_2 nano-size sample (Figure 6.1 e). According to Saeid Salamat, [131] this peaks relatively broader due to the overlapping of Ti-O peak along with the Fe-O peak mentioned above, proving the attachment of TiO_2 on the surface of the Fe_3O_4 and the successful synthesis of Fe_3O_4@TiO_2. [131] It is should be to clarify that the peak located around 1115 cm^{-1} in the TiO_2 precursor samples (Figure 6.1 a and b) decreases considerably after the synthesis of magnetic nanoparticles on them (Figure 6.1 d and e). This can be attributed to the fact that the materials that were used in the synthesis of Fe_3O_4 NPs, such as ammonium hydroxide, eliminated the carbonaceous organic particles present in the Titanium Dioxide chemical composition.

6.1.2   X-ray diffraction (XRD)

XRD patterns are shown in Figure 6.2. The diffraction peaks and miller indices were studied using "QualX" software (it is a computer program capable of identifying crystalline phases using powder diffraction data) and the "PowCod 2007" database. For the precursor sample of TiO_2 bulk-size, the diffraction peaks placed in Figure 6.2 a), show high sharpness and intensity for its two crystalline phases. With regard to the anatase structure phase, the diffraction peaks appear at angles and miller indices of 2θ = 25.3° (101), 37.8° (004), 48.0° (200), 55.0° (211), 62.6° (204), 75.0° (215) and 149.9° (424). And for the rutile structure phase the refractive peaks appear for angles and miller indices of 2θ = 27.4° (110), 36.0° (101), 41.2° (111), 54.3° (211), 56.6° (220) and 69.0° (301). On the other hand, in the case

of the TiO_2 nano-size sample showing in Figure 6.2 b), it is possible to observe the reflections of anatase crystalline structure with angles and miller indices at $2\theta = 25.34°$ (101), 37.74° (004), 48.04° (200), 55.04° (211), 62.64° (204) and 75.04° (215). And for the rutile phase the refractive peaks appear for the angles and miller indices at 20 = 27.44° (110), 36.04° (101), 41.24° (111), 54.34° (211), 56.64° (220) and 69.04° (301). For both the refractive angles and miller indices are the same, since it effectively corresponds to TiO_2 samples, and this results are reaffirmed as reported by Ruby Chauhan et al. [135]

The XRD pattern of Fe_3O_4 NPs (Figure 6.2 c).) demonstrates sharp and intense diffraction peaks, since each plane of the NPs reflects the incident X-ray at certain scattering angle 2θ. Each peak was found at around 2θ is corresponding to one lattice plane of Fe_3O_4 as follow; 18.3° (102), 30.0° (200), 30.14° (020), 30.146° (114), 35.45° (212), 35.47° (016), 35.5° (106), 37.1° (024), 43.0° (220), 56.9° (322), 57.0° (232), 32.67° (228), and 62.66° (040). Whereas the results of X-ray diffraction obtained for nanostructured hybrid materials are presented in Figure 6.2 d) for $Fe_3O_4@TiO_2$ bulk size and e) for $Fe_3O_4@TiO_2$ nano size. These peaks demonstrate that Fe_3O_4 NPs and TiO_2 (in their anatase and rutile phases) are present in the XRD diffractograms, which are represented by a blue square, red circle and black star respectively. In addition, it can be noticed that the intensity of Fe_3O_4 NPs peak decreases with TiO_2. This reduction may due to the effect of thickness of TiO_2 than Fe_3O_4 nanoparticles. [126]

The quantification of phase proportions of TiO_2 is usually carried out using XRD. Such analyses are often done using the method reported by Spurr and Myers, [136] which utilizes the ratio of the anatase (101) peak at 2θ equal to 25·30° to rutile (110) peak at 2θ equal to 27·43°. The ratio of the intensities of these peaks, I_{101}/I_{110}, is used in an empirically determined formula (Equation 6.1) to give the weight fractions of anatase and rutile phases. [109]

$$\%A = \frac{100}{1 + 1.265\frac{IR}{IA}} \tag{6.1}$$

where A is the percentage of anathase phase present in the sample and (IR/IA) is the ratio of the intensity of the strongest anatase reflection to the intensity of the strongest rutile reflection. [136]

Given the results in Table 6.1, it can be confirmed that both TiO_2, bulk precursor and nano synthesized samples, present characteristics of the anatase phase than a rutile phase. In addition, it is important to clarify that the temperature used to annealed the sample for give again the crystalline structure to TiO_2 treated, was 500°C under air atmosphere, was the optimal temperature to give an anatase/rutile phase mixture in a proportion of 74.6% to 25.4%. These results are consistent with literature. [137] Viana et al., [138] reported that the crystallization values for annealing titanium dioxide nanoparticles at a temperature in the range of 500°C to 600°C achieve an anatase/rutile phase transition. [138]

The theoretical particle size calculation of the samples was carried out using the Scherrer-Debye formula. This formula correlates the particle size through the crystal broadening observed in the X-ray diffractograms. Then, in order to calculate the average particle size in all nanomaterials, the following Equation 6.2 was applied. [137,139]
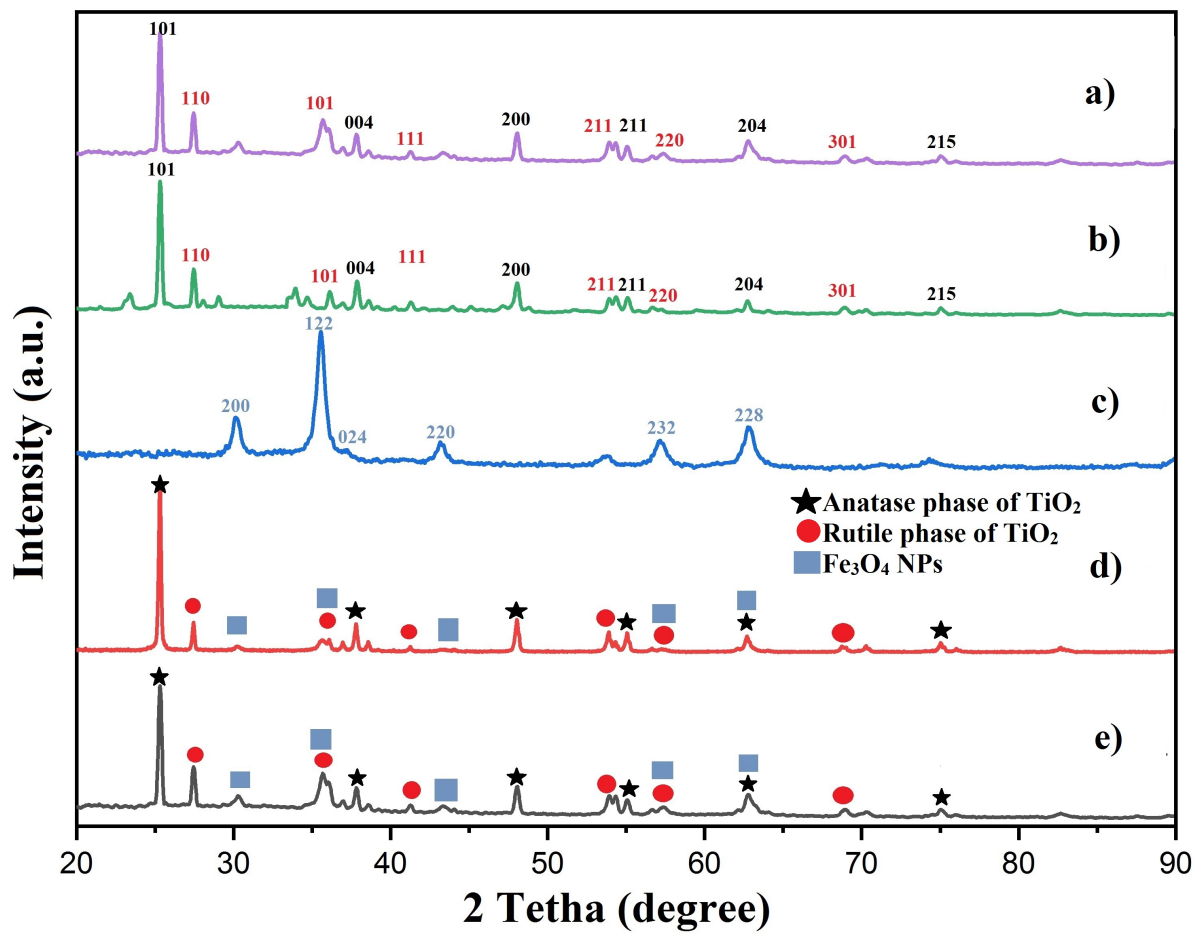
Figure 6.2: XRD patterns of a) TiO_2 bulk size, b)TiO_2 nano size, c) Fe_3O_4 NPs, d) Fe_3O_4@TiO_2 bulk size and e) Fe_3O_4@TiO_2 nano size.

Sample	Anatase phase (%)	Rutile phase (%)
TiO_2 Bulk size	82	18
TiO_2 Nano size	75	25

Table 6.1: Anatase/Rutile percentages of titanium dioxide in the initial sample and after nanostructured synthesis

$$D = \frac{K\lambda}{\beta cos(\theta)} \hspace{4cm} (6.2)$$

Where D is the mean particle size (nm), K is crystallite shape factor (a good approximation is 0.9), λ is the X-ray wavelength in this case CuK(alpha) equal to 0.15406 nm, β is the full width at half the maximum (FWHM) in radians of the X-ray diffraction peak and θ is the Braggs' angle (deg). [137,139]

Table 6.2 shows the average particle size of all samples. For the calculation of the FWHM, the high intensity peak was used and analyzed using origin software. For example, in the case of TiO_2, the peak with high intensity is located at an angle and miller index of $2\theta = 25.3$ (101) and for Fe_3O_4 NPs is located at $2\theta = 35.45°$ (212). Thus, the results show that it is possible to reduce the particle size of TiO_2 from 40 nm to 31 nm compared to the precursor sample using the ultrasound-assisted method described above. [109] On the other hand, the particle size of Fe_3O_4 NPs averages 10 nm. With respect to results for hybrid nanocomposites Table 6.2, in the two TiO_2 presentations, show that after the synthesis our nanocomposites ($Fe_3O_4@TiO_2$) don't have big changes in particle size. This is coherent due to the Fe_3O_4 NPs were synthesized on the surface of TiO_2 and not in the opposite way.

Sample	D TiO_2 (nm)	D Fe_3O_4 (nm)
TiO_2 Bulk size	40	-
TiO_2 Nano size	31	-
Fe_3O_4	-	10
$Fe_3O_4@TiO_2$ Bulk size	42	6
$Fe_3O_4@TiO_2$ Nano size	30	7

Table 6.2: Particle size calculated for the different synthesized samples using the Scherrer equation.

6.1.3 EDS/Elemental Mapping

A elemental mapping using EDS was done to hybrid nanomaterials as is show in Figure 6.3. The results indicate a segregated elemental distribution in the red and green colored regions, which correspond to the areas in which the Fe and Ti elements are detected respectively Figure 6.3 a) and b). This fact agrees with what was raised, since in the synthesis strategy, it is expected that the phases will be coupled with each other by simple mixing, once the iron nanoparticles have already formed on the surface of the TiO_2. The union of the phases has been effectively carried out, although with a non-homogeneous coupling, since there are a large number of magnetic nanoparticles surrounding the region studied Figure 6.3 c). However, it is possible to observe red points that correspond to Fe on the green marked surface corresponding to Ti, generating a magnetic hybrid material. [15]
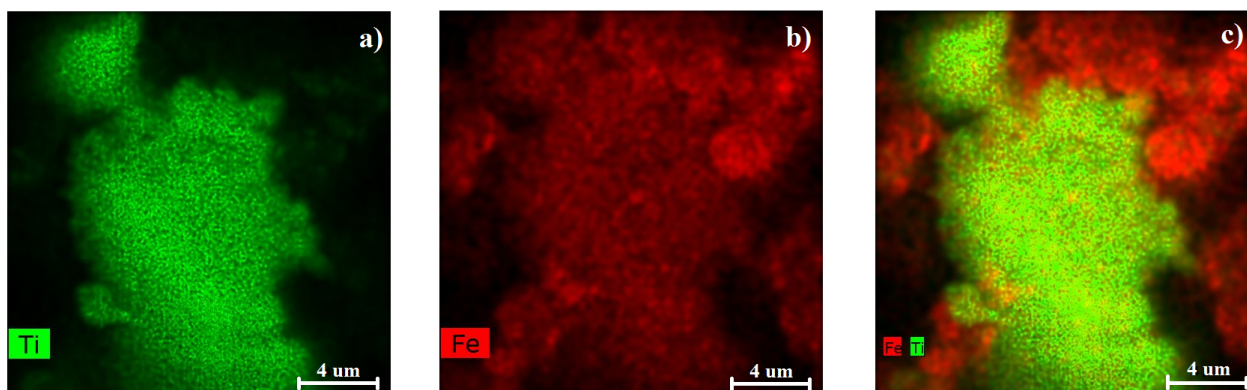
Figure 6.3: EDS/elemental mapping of Fe_3O_4@TiO_2 nanocomposite.

6.1.4   Scanning Electron Microscopy (SEM)

Figure 6.4 a) shows the SEM micrograph of the magnetic nanoparticles (Fe_3O_4). This micrograph reveals that the sample has a broad uniform distribution of homogeneous-sized spherical nanoparticles.[124] In addition, it can be observed that nanoparticles tend to be easily added with each other, causing the formation of clusters, this may be due to the small size and magnetic properties of these nanoparticles, these results are confirmed by Tianjie Hong, et al.[122,123,125] These particle agglomerations are formed during the sample drying process, since it is where nanoparticle agglomeration/aggregation is promoted, especially with magnetite nanoparticles due to dipole interactions.[140] The nanoparticles size was measured using the ImageJ program, which consists of plotting the diameter of each particles to obtain an average and adjusted to a histogram study, where the particle size of the nanoparticles obtained is shown under a given scale. In this way, the histogram results in Figure 6.4 b) show that the size of the Fe_3O_4 NPs has an average diameter of 40 ± 20 nm.

Regarding to nanostructured nanocomposite Fe_3O_4@TiO_2, the magnetic nanoparticles that are formed on the TiO_2 surface by the chemical co-precipitation method are shown in Figure 6.4 c). SEM micrograph shows that the nanocomposite was formed of large particles of TiO_2 of 100 ± 20 which are agglomerated.[70,111,140] Also in a general way, thanks to the contrast of micrography, the coupling of the two materials in the form of circular nanoparticle clusters on the surface of another material can be distinguished. This is possible to differentiate, due to the brightness contrast is given by the elements present and their different atomic number: the heavier the element, the brighter it will appear in the micrograph.[72,73,141] Therefore, iron has a higher atomic number than titanium, making the iron nanoparticles appear whitish and brighter in the micrograph.[72,141]

In summary, all the characterizations techniques that have been performed, confirms that TiO_2, Fe_3O_4 NPs and the nanocomposites have been successfully obtained. The UV-vis results demonstrate the presence of the charac-

Figure 6.4: SEM micrographs and average particle size distribution of (a and b) Fe_3O_4 NPs, (c and d) $Fe_3O_4@TiO_2$ nanocomposite.

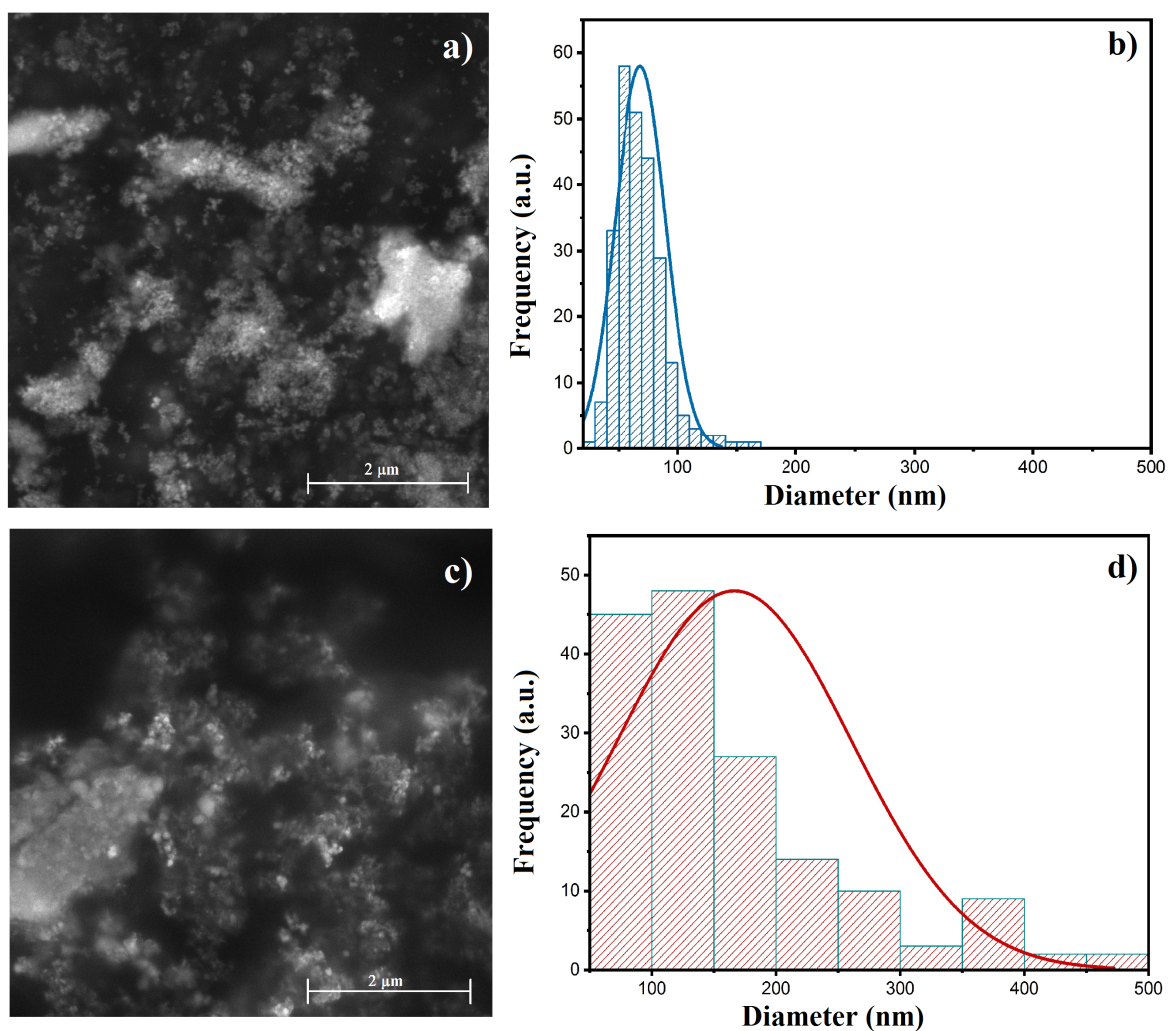teristic peaks of TiO_2 and Fe_3O_4 NPs found in the regions established by the literature. The XRD patters confirm the presence of Fe_3O_4 NPs and TiO_2 with a higher percentage of the anatase than rutile crystalline phase. SEM and EDS elemental mapping micrographs confirm the presence of both materials in its chemical composition and reveals the aggregation of iron nanoparticles. The particle size analysis of the nanocomposite by XRD that was 42 ± 10 nm differ from the SEM that was 100 ± 20 nm. This is because the agglomeration/aggregation is done due to the magnetic properties that the sample present.

6.2   Adsorption Process

In this section the equilibrium adsorption studies were carried out to determine the maximum effective adsorption capacity of commercial glyphosate using TiO_2 bulk size, TiO_2 nano size, $Fe_3O_4@TiO_2$ bulk size, $Fe_3O_4@TiO_2$ nano size and Fe_3O_4 NPs. All experiments were done with a adsorbent sample dosage of 0.5 g and 10 mL of 100 g/L of commercial glyphosate under solar radiation. The results obtained from the adsorption curves and their kinetics are presented and discussed for each sample as stated in the following Figures 6.6 - 6.9. The theoretical values retrieved from the curves are summarized in Table 6.3.

Figure 6.5 describe the results obtained in the commercial glyphosate adsorption process on the TiO_2 bulk-size surface. Item a) Figure 6.5, shows the relationship of absorbance as a function of time at a wavelength of 200 nm, where it can be seen that the quantified absorbance decreases as a function of the elapsed time of the reaction. It is clear to notice that the maximum adsorption value was reached in 30 min. The percentage of glyphosate removed using TiO_2 bulk-size sample was calculated employing Equation 5.8 described in Chapter 5, and presented in item b) Figure 6.5. The results said that an amount of 25% of commercial glyphosate was removed from the solution. Fitting results of adsorption data based on he pseudo-first-order kinetic model and pseudo-second-order kinetic model are shown in Figure 6.5 c) and d) respectively. The parameters are listed in Table 6.3. With this results it can be say that commercial glyphosate adsorption on TiO_2 bulk-size conforms the pseudo-second-order kinetic model with a correlation coefficient (R^2 = 0.98) which indicates that this adsorption system is not a first order reaction and that the pseudo-second-order kinetic model, based on the assumption that the rate limiting step may be chemical sorption or chemisorption involving valency forces through sharing or exchange of electrons between TiO_2 bulk-size and commercial glyphosate, provides the best correlation of the data. [47,142] The theoretical value of adsorption capacity (Q_t), was calculated using Equation 5.7 Chapter 5, and is placed in table 6.3. Q_t results reflect that an amount of commercial glyphosate of 11.31 mg/g was removed.

In contrast with the previous results, glyphosate adsorption curves using TiO_2 nano-size sample are shown in Figure 6.6. The results show a consistent adsorption kinetics, due to the initial concentration of commercial glyphosate decreases with time, as can be seen in Figure 6.6 a). Unexpectedly, our results diverge with the characteristics of the sample, since a greater adsorption was expected using this sample in comparison with its precursor one (TiO_2 bulk-size). This may be due to several aspects that could be related to material characteristics. Perhaps the chemical
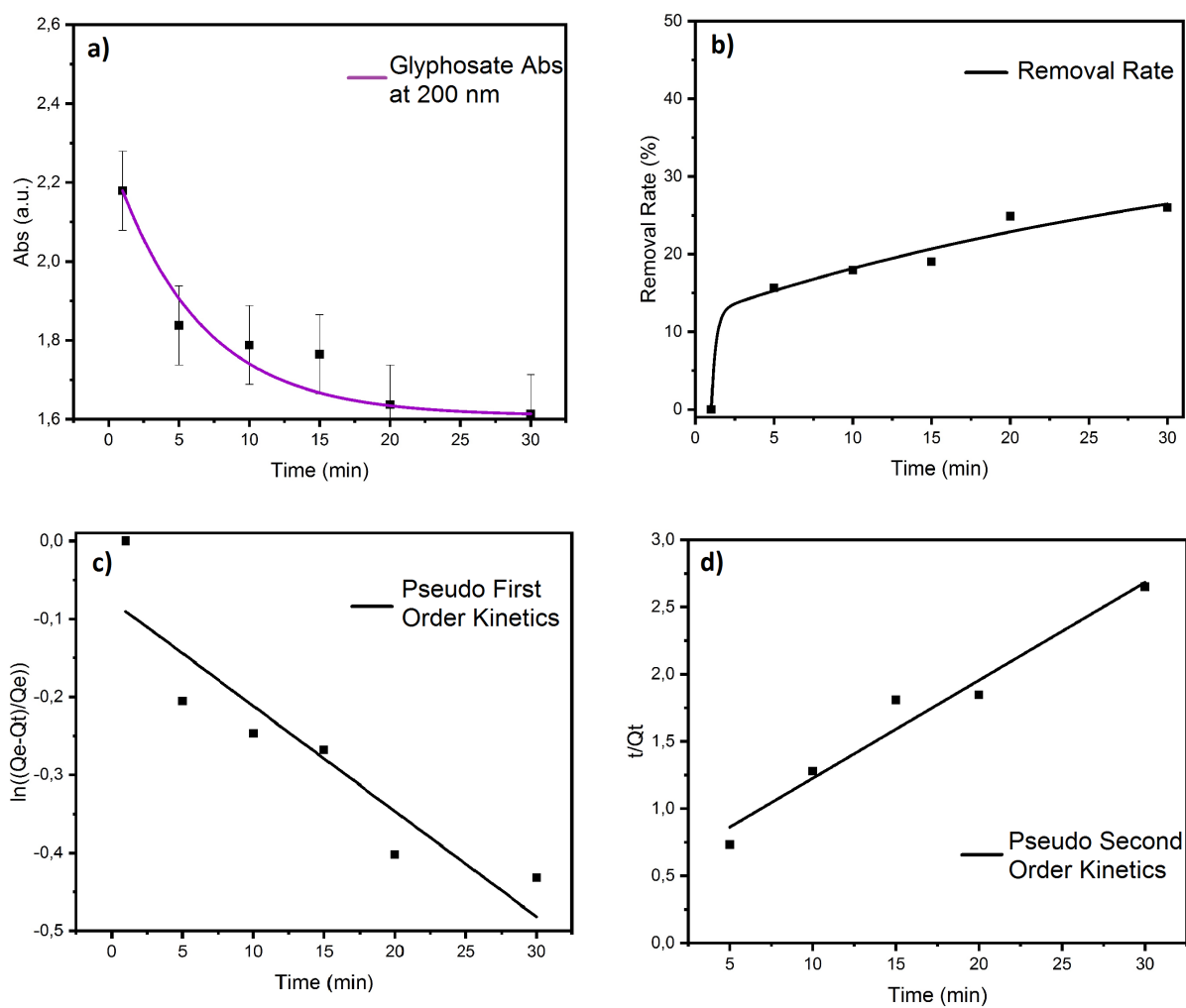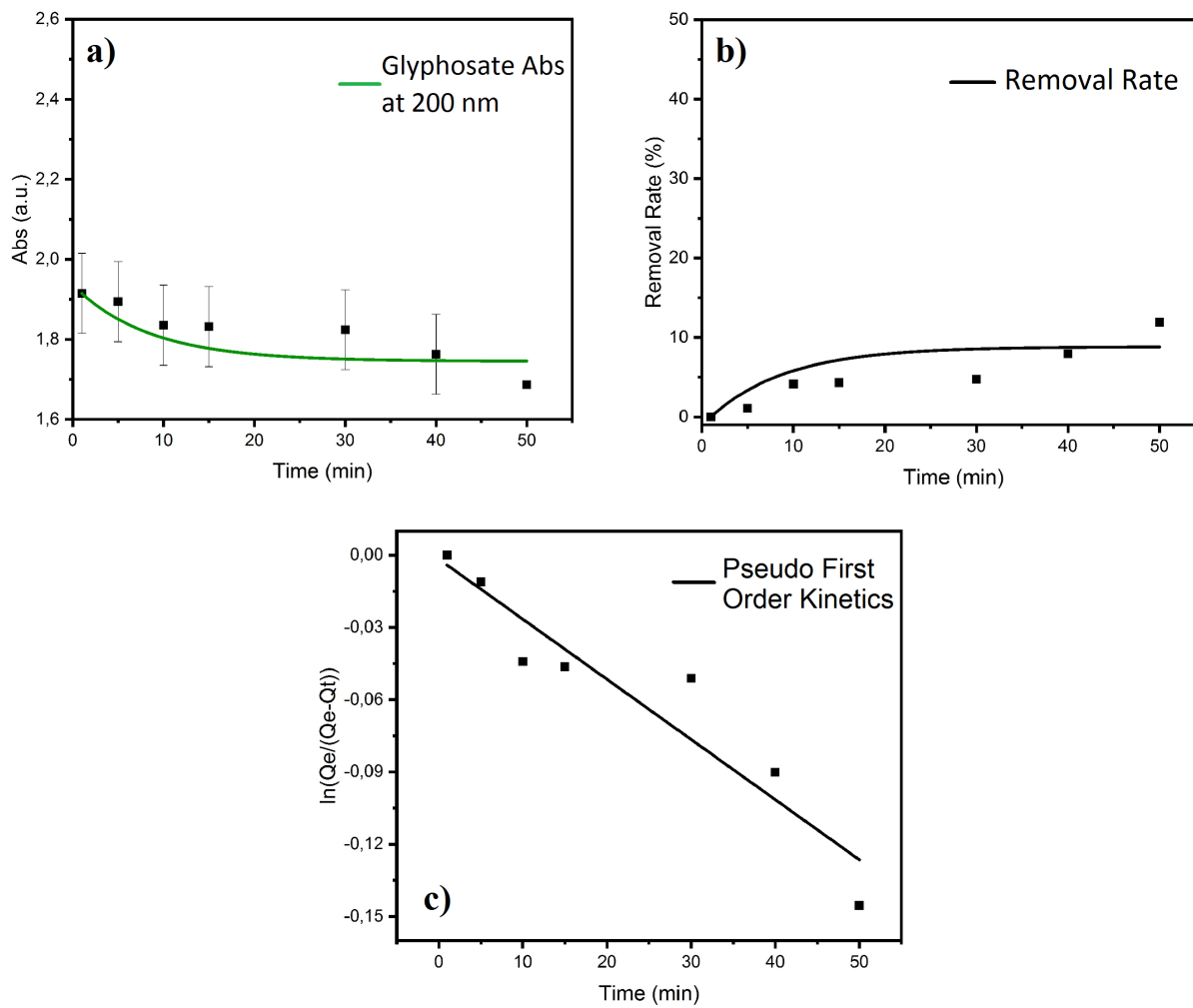
Figure 6.5: Adsorption behavior and kinetics models of glyphosate with TiO_2 bulk size.

Figure 6.6: Adsorption behavior and kinetics models of glyphosate with TiO_2 nano size

Sample	Q_t (mg/g)	R (%)	Pseudo First Order Kinetic		Pseudo Second Order Kinetic	
			k_1 (min^{-1})	R^2	k_2 (g/(mg min))	R^2
TiO_2 Bulk Size	11.31	26	-9.84x10^{-3}	0.94	1.93x10^{-3}	0.98
TiO_2 Nano Size	4.56	11	-2.49x10^{-3}	0.94	9.45x10^{-5}	0.41
Nanocomposite Bulk Size	6.96	16	-3.52x10^{-3}	0.69	1.08 x10^{-3}	0.91
Nanocomposite Nano Size	3.54	9	-2.1x10^{-3}	0.94	1.66 x10^{-4}	0.96

Table 6.3: Parameters of adsorption dynamics model.

process to reduce the particle size of TiO$_2$, using ultrasound assisted method and sulfuric acid, could have affected the catalytic properties of the sample. On account of high ultrasound interactions to break the chemical bonds in titanium dioxide particles, cause an irreversible chemical alteration to the sample even after the annealed process.[109] Furthermore, this low adsorption capacity of commercial glyphosate on TiO$_2$ nano-size can be attributed to the pH of the sample (Table5.2). Reported studies,[11] affirm that the removal efficiency of glyphosate decrease significantly when the pH increase, implying that acidic condition is more favorable to the adsorption process.[11] According with Yajuan Li, et al.[142] report that good adsorption capacity enhance when the pH was between 3 and 5.[142] They explain that the pH effect in adsorption process could be attributed to the electrical properties of adsorbent and pollutants, because in order to have a good adsorption capacity both glyphosate and the adsorbent must to be in strong electrostatic attraction.[142] Other studies,[143] argue that at pH of 3, the Ti surface will be positively charged, while the phosphate group of glyphosate will be negatively charged leading to the expectation that the compound will adsorb the surface of Ti. In contrast, at higher pH values, the absorbent surface as well as glyphosate will be negatively charged, and hence adsorption would not be expected.[143] It must be pointed out that, even when, sulfuric acid (H_2SO_4) is used for the synthesis of TiO$_2$ nano-size, the pH of the sample was adjusted to 10 using sodium hydroxide (NaOH).[109] Making that the pH of TiO$_2$ nano-size sample has a higher value (pH=6), than the precursor sample TiO$_2$ bulk -size (pH=5), even after the calcination process due to the boiling point of NaOH (1.388 °C) is higher than that of H_2SO_4(337 °C). Another reason for the low absorption may be related to the solubility of the adsorbent on the adsorbate, in other words the solubility of the TiO$_2$ nano-size sample in the glyphosate solution, since during the adsorption experiments with this sample (TiO$_2$ nano-size) the immediate formation of precipitate occurred in the first few minutes compared to the precursor sample (TiO$_2$ bulk-size) which had a very good dispersion of material in the solution. This means that there was not enough contact of the nano-sized titanium dioxide nanoparticles (synthesized by the ultrasound method) with the glyphosate, thus avoiding its adsorption.

However, an 11% adsorption of commercial glyphosate was achieved using TiO$_2$ nano-size, as can be seen in figure 6.6 b). The maximum adsorption quantity Q$_t$ was 4.56 mg/g. The fitting results of adsorption data based on pseudo-first-order kinetic model and pseudo-second-order kinetic model, the results suggest that commercial glyphosate adsorption on TiO$_2$ nano-size conforms to pseudo-first-order kinetic model with a higher correlation coefficient (R^2 = 0.94) Figure 6.6 c). This indicates that physisorption is the rate controlling step for this adsorption
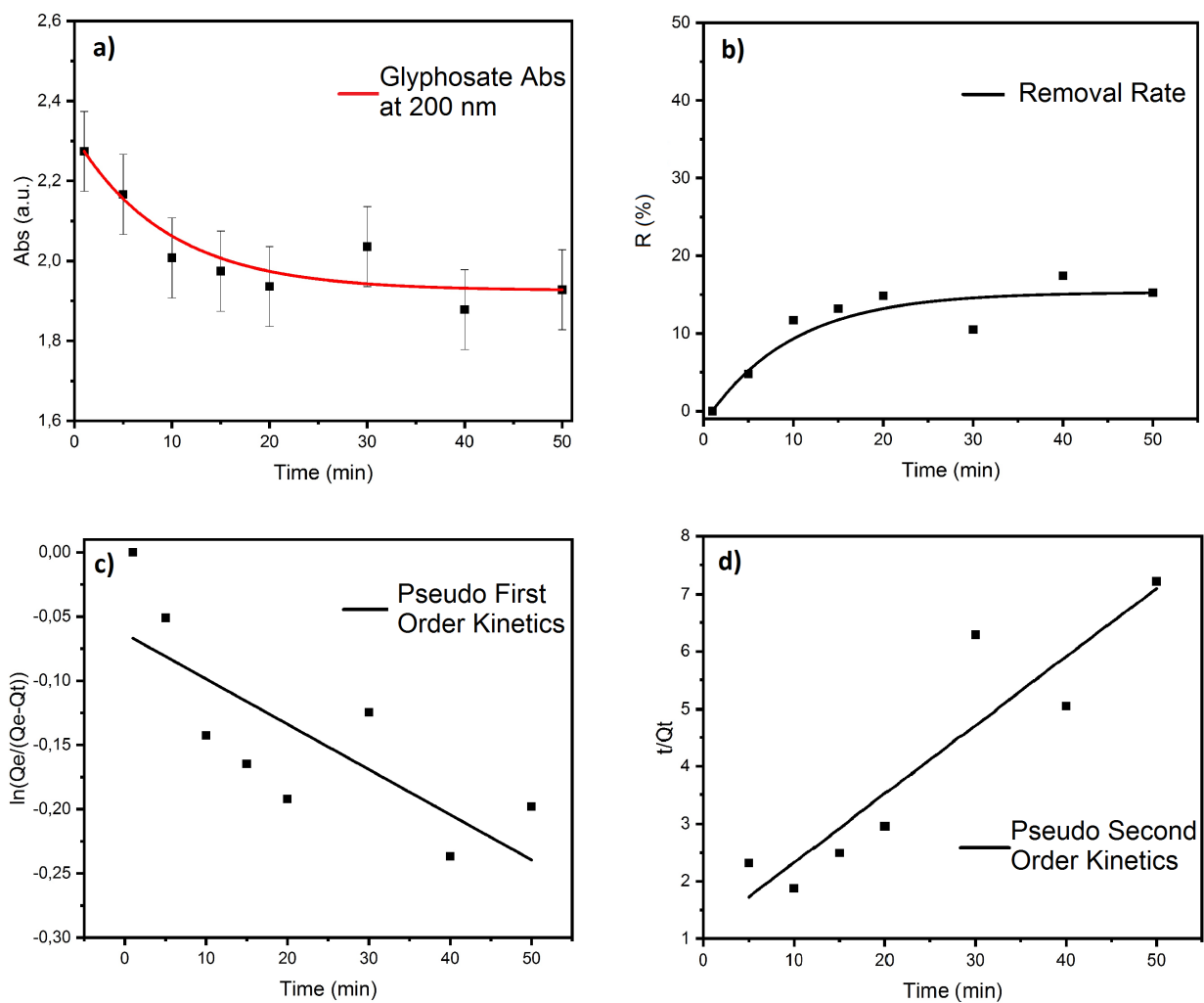
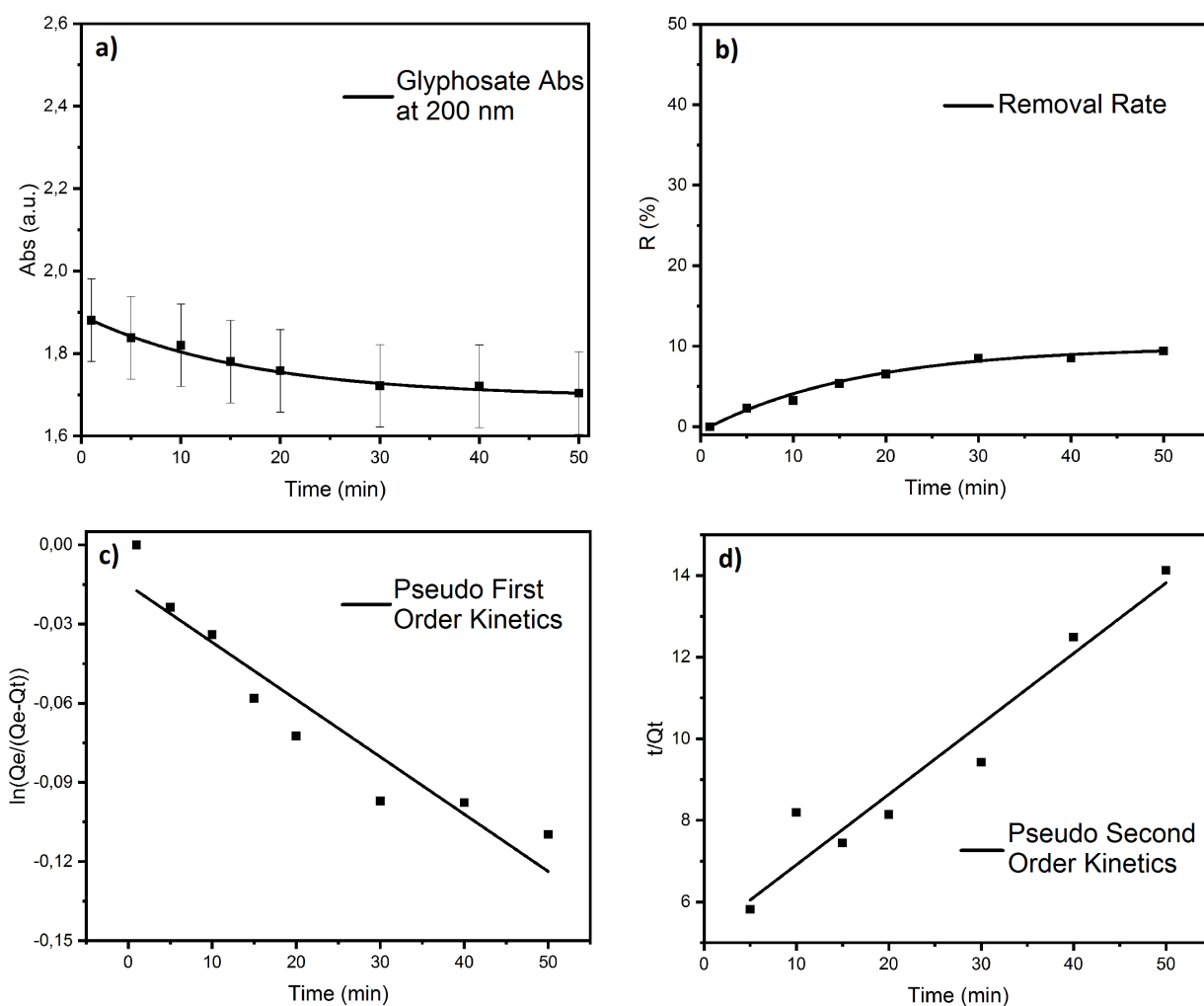Figure 6.7: Adsorption behavior and kinetics models of glyphosate with nanocomposite $Fe_3O_4@TiO_2$ bulk size

Figure 6.8: Adsorption behavior and kinetics models of glyphosate with nanocomposite $Fe_3O_4@TiO_2$ nano size

process and its given by the weak interactions like Van der Waals forces.[35]

The adsorption results for commercial glyphosate using the nanocomposites Fe_3O_4@TiO_2 bulk-size and Fe_3O_4@TiO_2 nano-size are presented in Figure 6.7 and Figure 6.8 respectively. The results contrast with the previous results obtained with the precursor samples of TiO_2 bulk-size and TiO_2 nano-size. In the first case (nanocomposite bulk-size), the maximum glyphosate adsorption value was achieved at 50 min, while for the precursor sample was 30 min Figure 6.7 a). In addition, the percentage value of removal rate for commercial glyphosate decrease to 16% compared to the previous one which was 26% according to Figure 6.7. In the second case, the maximum adsorption of glyphosate can be achieved in the same time of 50 min, but likewise the amount of glyphosate removed decreases from 11% to 9% Figure 6.8 b). These results could be attributed to the presence of the iron oxide nanoparticles, because the interaction of Fe ions with glyphosate cause a formation of a new complex in the solution, causing a low electrostatic attraction between Fe_3O_4@TiO_2 and commercial glyphosate.[145] However, the advantage that the nanocomposites have compared to the precursor samples is their easy recovery by applying an external magnetic field. Its is important to mention that preliminary experiments showed that the application of an external magnetic field is enough to recover all the adsorbent material from the solution, thus concluding a great nanoengineering process. In fact, it can be stated that after the samples (Fe_3O_4@TiO_2), fulfill their adsorption action within 50 min, the nanocomposite can be easily recovered from the contaminated water using a magnet in order to avoid desorption process.

Regarding the adsorption kinetics models, both samples present good fit for pseudo-second-order model with a higher correlation coefficient ($R^2 = 0.91$ for Fe_3O_4@TiO_2 bulk size and $R^2 = 0.96$ for Fe_3O_4@TiO_2 nano size) which indicates that chemisorption is the rate controlling step for these adsorption.[142]. This provides a stronger bond as it involves the transfer or sharing of electrons between the commercial glyphosate and Fe_3O_4@TiO_2 nanocomposites.[43] It is important to mention that for all samples the values of k1 and k2 (Table 6.3) constants are in accordance with the reported by Tan k. et al.,[43] which affirm that the rate constant k1 is a function of the process conditions due to decrease with increasing initial bulk concentration.[43]

Adsorption/Desorption Process

Figure 6.9 shows the adsorption process and its subsequent desorption process of the commercial glyphosate using TiO_2 bulk size a), TiO_2 nano size b), Fe_3O_4@TiO_2 bulk size c), Fe_3O_4@TiO_2 nano-size d) and Fe_3O_4 NPs e) as a function of the time. In general, the experiments seem to be conducted in three stages; an initial one in which commercial glyphosate is adsorbed on the surface of the sample, the second one related with the desorption process, and finally an equilibrium stage. Specifically, the kinetics of the adsorption process begins with the diffusion of the glyphosate molecules on the surface of the samples.[43,45] During the first minutes of the reaction at the initial stage of the adsorption process, higher rates of adsorption take place; this may be due to the availability of more adsorption sites and the fact that the glyphosate molecules exchange easily on the surface of the samples. On the other hand, the desorption process occurs when the glyphosate is released from the sample to the solution.[45] The desorption process observed contradict with the literature, due to an equilibrium stage was expected after the adsorption process. This could be attributed to the chemical composition of commercial glyphosate that is being use.
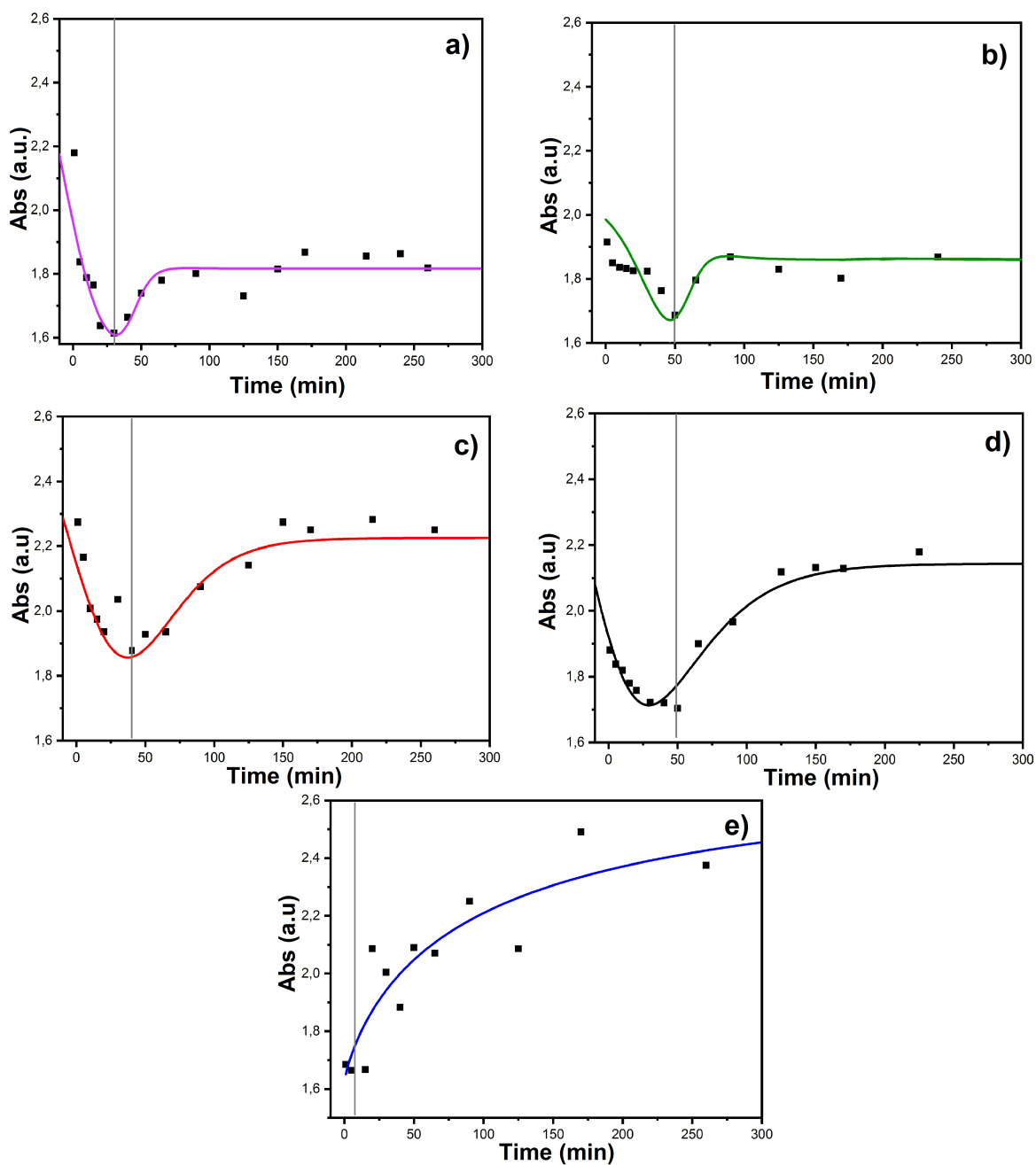
Figure 6.9: Adsorption/Desorption behavior of glyphosate during the time of a) TiO_2 bulk size, b)TiO_2 nano size, c) $Fe_3O_4@TiO_2$ bulk size, d) $Fe_3O_4@TiO_2$ nano size and e) Fe_3O_4 NPs.

Commonly commercial agricultural formulations have different amounts of glyphosate concentration ranging from 1% to 41%. And also this formulations contain an isopropylamine glyphosate salt, surfactants, and several minor components including defoaming agents and inorganic ions.[18] Therefore adsorption of commercial glyphosate in aqueous solutions is difficult, since the contribution of surfactants, additives and adjuvants that help increase its power.

It should be note that the adsorption/desorption results of commercial glyphosate using the nanocomposites, based $Fe_3O_4@TiO_2$ bulk-size item c) and $Fe_3O_4@TiO_2$ nano-size item d) in Figure 6.9, have an additional behavior in their desorption process. It can be seen that there is a higher desorption rate of commercial glyphosate after reaching the maximum adsorption value. This behavior is attributed to the presence of the magnetic nanoparticles in their composition, due to the results obtained using only Fe_3O_4 NPs (Figure 6.9 e), show an evident desorption process of commercial glyphosate as a function of time. There has been reported,[145] that the interaction between the glyphosate and Fe_3O_4 NPs forms a glyphosate/metal complex Figure 6.10. Glyphosate, like many other phosphonic acids, acts as a chelating agent and forms stable complexes with divalent and trivalent metallic cations as iron. According with Mark L. Bernards[146] he reports that the chemical structure of glyphosate includes a negatively charged molecule that will bind to positively charged metals for example iron, when they are dissolved in a water-based solution. In a typical solution, glyphosate has a -2 charge,[146] with this negative charge, it is strongly attracted to positively charged molecules.When glyphosate binds to a metal, much of the glyphosate-metal complex remains on the samples surface.

FTIR characterization analysis of Glyphosate@Fe_3O_4

The formation of glyphosate/metal complex, due to the interaction between the glyphosate and Fe_3O_4 NPs, was elucidated well on basis of the FTIR analysis. Figure 6.11 showed a comparison of FTIR spectra of glyphosate and glyphosate@Fe_3O_4 NPs samples. The typical spectrum of commercial glyphosate Figure 6.11 (purple line), is confirmed by the presence of the peaks of amine group at 1620 cm^{-1}, carboxylic group at 1400 cm^{-1} and phosphate group at 1080 cm^{-1} - 913 cm^{-1}.[147,148] The peaks located at the range of 400 to 840 cm^{-1} correspond to the nitro compound and disulfide groups, and are attributed to the other relevant additives or surfactants used in its commercial formulation.[147] The sharp band and intense peak at 3320 cm^{-1}, is attributed to the presence of hydroxil group (-OH) in the sample.[147,148] The three peaks at 2215 cm^{-1}, 1322 cm^{-1} and 1165 cm^{-1} is assigned to the stretching vibration to the C=C, C-O and P=O bonds, respectively.[147–149]

On the other hand the peaks positioned in the spectrum of glyphosate + Fe_3O_4 NPs sample Figure 6.11 (orange line), are in relation with the previous one. However, it is important to mention that the main difference between the spectrum is that new peaks reappeared in the phosphate region at 979 cm^{-1}. According to Ramarakhiani et al.,[147] this finding conformed that a direct interaction for complex formation occurred through phosphate groups present at glyphosate molecule and metal ions, in this case the Fe ions.[147] Furthermore it is clear to see, in comparison, that the characteristic peaks corresponding to the phosphate group located at 1080 cm^{-1}, 1165 cm^{-1} and 913 cm^{-1} of the sample containing only glyphosate Figure 6.11 (purple line), decrease in intensity and disappear in the glyphosate + Fe_3O_4 NPs sample Figure 6.11 (orange line). This is clearly attributed to the formation of the complex in these
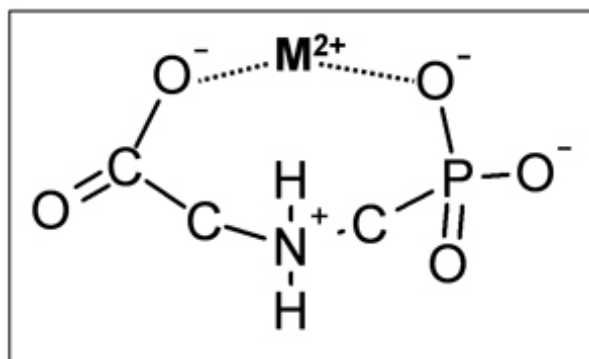
Figure 6.10: Glyphosate bound to a metal ion. M^{2+} represents the iron - glyphosate binds.
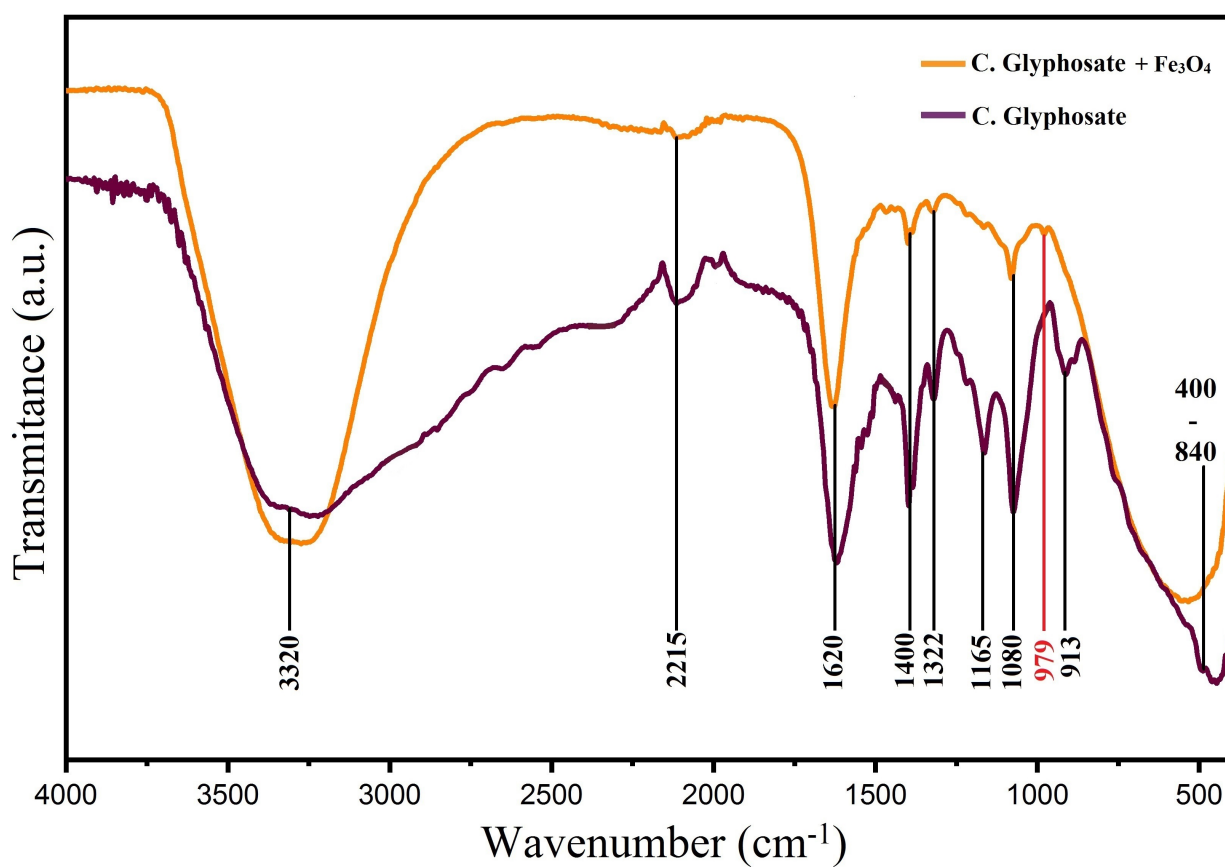

Figure 6.11: FTIR results of Glyphosate and Glyphosate bound to Fe_3O_4 nanoparticles.

phosphate groups and affirming what is stated in Figure 6.10. Thus, commercial glyphosate was not adsorbed on magnetite or nanocomposites based magnetite, by the complexation of glyphosate in the phosphate group, rather, the desorption phenomenon could have occurred as a result of the magnetic decomposition to an iron oxide, due to the acidic medium in which it was worked. Or also this is because, amine, phosphate and carboxylate groups are present in glyphosate structure.[147] Because, glyphosate when this is in aqueous solution is present as zwitterionic molecule and has capability to form chelating ring and cross structural complex with various metal ions and surfaces.[147] Therefore, in our case, the complexes formed in the interaction of commercially glyphosate/Fe could be the cause of the absorbance increase and therefore the glyphosate desorption. However, the advantages to synthesized magnetic nanocomposites based Fe_3O_4@TiO_2, are their easy separation and recovery before to glyphosate/Fe complexes are formed and desorption process starts.

Summary and Recommendations

So far, it has been show that a adsorption of commercial glyphosate (100 g/L), can be obtained using TiO_2 bulk size a), TiO_2 nano size b), Fe_3O_4@TiO_2 bulk size c), Fe_3O_4@TiO_2 nano-size d) and Fe_3O_4 NPs Figure 6.12. A highest efficiency of 26% was achieved in the adsorption experiment of commercial glyphosate using TiO_2 bulk size. Regarding the adsorption experiment by TiO_2 nano-size, the effect of the pH, cause a decrease in the adsorption efficiency, obtaining an 11% of removal rate. The pH values are extremely important, because the samples must to be in electrostatic attraction between the adsorbent and adsorbate, in order to increase the adsorption process.[142] The adsorption results by Fe_3O_4@TiO_2 nanocomposites show a decrease in adsorption efficiency from 26% to 16% for bulk-size nanocomposite and 11% to 9% for nano-size nanocomposite in comparison to their precursor samples, due to the presence of Fe_3O_4 NPs. The commercial glyphosate adsorption/desorption mechanism with Fe_3O_4 mainly include a formation of glyphosate/metal complex, which increases the absorbance values inducing a desorption process of glyphosate complex. Although the results of glyphosate absorption with nanocomposite are not good, the advantages to synthesize a nanocomposite based on Fe_3O_4@TiO_2 for the adsorption of commercial glyphosate are the easy separation and recovery after 50 min, before to desorption process starts. The commercial glyphosate kinetics results by TiO_2 bulk-size, Fe_3O_4@TiO_2 bulk-size and Fe_3O_4@TiO_2 nano-size conformed to pseudo-second-order kinetic model, being controlled by chemisorption process. Meanwhile, the adsorption results by TiO_2 nano-size conform to pseudo-first-order kinetic model, being a physisorption predominate in this reaction due to several factors like: pH and porous size.

In order to improve the results using the nanocomposites as adsorbents, it is suggested to adjust the pH to a value of 3 and increase the adsorbent loading. In addition, synthesizing a nanocomposite based on Fe_3O_4@TiO_2 in a core-shell design, with a center of magnetic NPs, could avoid the formation chemical complexes of Fe/glyphosate and avoid the desorption process. On the other hand, taking into account that TiO_2 is a photosynthetic semiconductor, it is recommended to design a strong UV light reactor enough to degrade commercial glyphosate using photocatalysis.
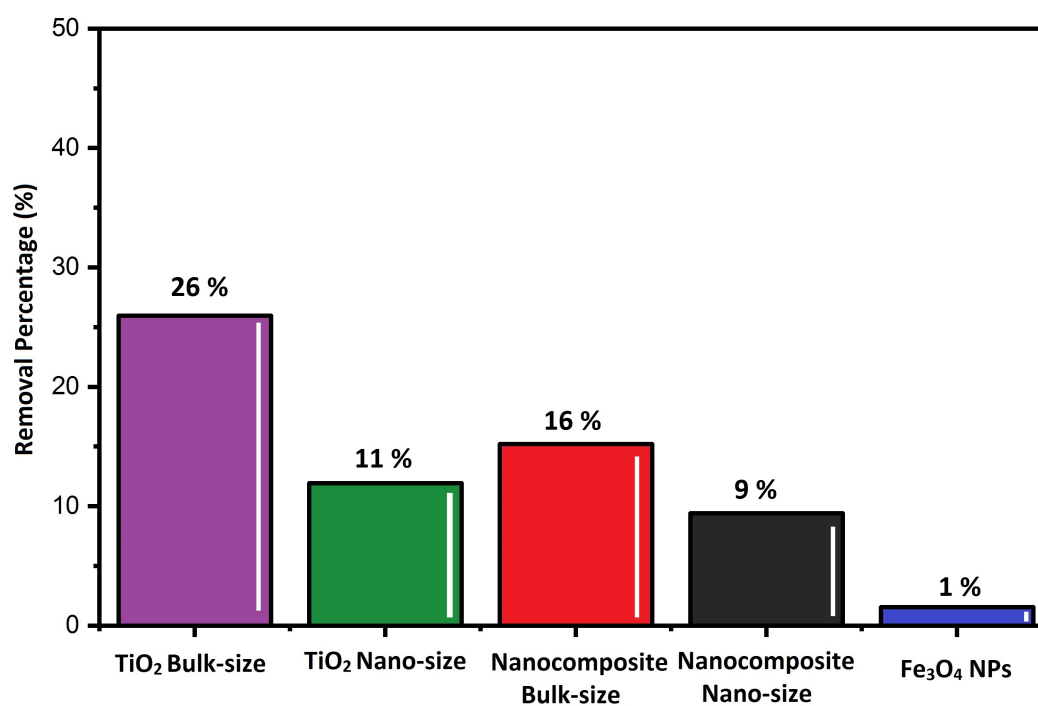
Figure 6.12: Removal rate results of commercial glyphosate adsorption.

Chapter 7

Conclusions & Outlook

Fe_3O_4@TiO_2 nanocomposite was successfully synthesized by using the chemical co-precipitation method and used in adsorption of commercial glyphosate. The FTIR results demonstrate the presence of the characteristic peaks of TiO_2 and Fe_3O_4 NPs. XRD patters confirm the structure of Fe_3O_4 NPs and TiO_2 with a higher percentage of the anatase crystalline phase than the rutile one and an average particle size of 42 ± 10 nm. SEM and EDS elemental mapping micrographs confirm the presence of both materials in its chemical composition and reveal the aggregation of the nanoparticles with an average particle size of 100 ± 20 nm. The maximum values of the removal rate (R) were reached by the samples: TiO_2 bulk-size and Fe_3O_4@TiO_2 bulk-size (26% and 16% respectively). The commercial glyphosate adsorption results of the samples with TiO_2 bulk-size, Fe_3O_4@TiO_2 bulk-size and Fe_3O_4@TiO_2 nano-size correspond to a pseudo-second-order kinetic model, being controlled by the chemisorption process. Meanwhile, the adsorption results by TiO_2 nano-size conform to the pseudo-first-order kinetic model, being the physisorption process predominate in this reaction. The behavior of commercial glyphosate with Fe_3O_4 NPs mainly includes a formation of a glyphosate/metal complex inducing a desorption process. Indeed, it has been demonstrated that the adsorption of commercial glyphosate can be obtained using Fe_3O_4@TiO_2 nanocomposite. The nanocomposite has advantages over the conventional samples as the easy separation and recovery of the nanocomposite after 50 min, before to desorption process starts, demonstrating a significant potential in the removal of commercial glyphosate from aqueous solution for wastewater treatment engineering.

Bibliography

[1] Lidong Cao, Dukang Ma, Zhaolu Zhou, Chunli Xu, Chong Cao, Pengyue Zhao and Qiliang Huang. Efficient photocatalytic degradation of herbicide glyphosate in water by magnetically separable and recyclable BiOBr/Fe$_3$O$_4$ nanocomposites under visible light irradiation. *Chemical Engineering Journal*, 368, 212-222, 2019, Doi:10.1016/j.cej.2019.02.100

[2] Yong Chen, Feng Wu, Yixin Lin, Nansheng Deng, Nikolai Bazhin and Evgeni Glebov. Photodegradation of glyphosate in the ferrioxalate system. *Journal of Hazardous Materials*, 148 (1-2): 360-365, 2007, Doi: 10.1016/j.jhazmat.2007.02.0044

[3] Robert Annett, Hamid R. Habibi and Alice Hontela. Impact of glyphosate and glyphosate-based herbicides on the freshwater environment. *Journal of Applied Toxicology*, 34(5), 458–479, 2014, Doi: 10.1002/ja.2997

[4] Jörgen Jönsson, Rob Camm and Tom Hall. Removal and degradation of glyphosate in water treatment: a review. *Journal of Water Supply: Research and Technology AQUA*, 62(7), 395–408, 2013, Doi: 10.2166/aqua.2013.080

[5] Henry W. Talbot, Layne M. Johnson and Douglas M. Munnecke. Glyphosate utilization by Pseudomonas sp. and Alcaligenes sp. isolated from environmental sources. *Current Microbiology*, 10(5), 255-259, 1984, Doi: 10.1007/bf01577137

[6] Peerawas Kongsong, Lek Sikong, Sutham Niyomwas and Vishnu Rachpech. Photocatalytic degradation of glyphosate in water by N-doped SnO$_2$/TiO_2 thin-film-coated glass fibers. *Photochemistry and photobiology*, 90(6), 1243–1250, 2014, Doi: 10.1111/php.12338

[7] Idrovo, A. Javier. De la erradicación de cultivos ilícitos a la erradicación del glifosato en Colombia. *Revista de la Universidad Industrial de Santander. Salud*, 47(2), 113–114, 2015.

[8] A. Sviridov, T. Shushkova, I. Ermakova, E. Ivanova, D. O. Epiktetov, A. Leontievsky. Microbial degradationof glyphosate herbicides. *Applied Biochemistry and Microbiology*, 51, 188–195, 2015, Doi: 10.1134/S0003683815020209

[9] Navid Hosseini and Mohammad Reza Toosi. Combined adsorption process and photocatalytic degradation of some commercialherbicides over N-doped TiO$_2$ particles supported on recyclable magnetic

hexagonal mesoporous silica. *Separation Science and Technology*, 54(11), 1697–1709, 2019, Doi: 10.1080/01496395.2018.1539105

[10] Vinod Kumar Gupta, Tanju Eren, Necip Atar, Mehmet Lütfi Yola, Cemal Parlak and Hassan Karimi-Maleh. $CoFe_2O_4@TiO_2$ decoratedreduced graphene oxide nanocomposite for photocatalytic degradation of chlorpyrifos. *Journal of Molecular Liquids*, 208, 122–129, 2015, Doi: 10.1016/j.molliq.2015.04.032

[11] Y.S. Hu, Y.Q. Zhao and B. Sorohan. Removal of glyphosate from aqueous environment by adsorption using water industrial residual. *Desalination*, 271(1-3), 150–156, Doi: 10.1016/j.desal.2010.12.014

[12] Shayan Miar Alipour, Donia Friedmann, Jason Scott and Rose Amal. TiO_2/porous adsorbents: Recent advances and novel applications. *Journal of hazardous materials* 341, 404–423, 2018, Doi: 10.1016/j.jhazmat.2017.07.070

[13] Sawsan Dagher, Ahmed Soliman, Aiman Ziout, Nacir Tit, Ali Hilal-Alnaqbi, Saud Khashan, Fadi Alnaimat and Jaber Abu Qudeiri. Photocatalytic removal of methylene blue using titania-and silica-coated magnetic nanoparticles. *Materials Research Express*, 5(6), 065518, 2018, Doi: 10.1088/2053-1591/aacad4

[14] Chen Jian, Zhi Hu and Nan X. Wang. Photocatalytic mineralization of glyphosate in a small-scale plug flow simulation reactor by UV/TiO$_2$. *Journal of Environmental Science and Health, Part B*, 47(6), 579–588, 2012, Doi: 10.1080/03601234.2012.665751

[15] Marco Lucas, Pedro B. Tavares, Jose A. Peres, Joaquim L. Faria, Mariana Rocha, Clara Pereira and Cristina Freire. Photocatalytic degradation of Reactive Black 5 with TiO$_2$-coated magnetic nanoparticles. *Catalysistoday* 209, 116–121, 2015, Doi: 10.1016/j.cattod.2012.10.024

[16] Saeid Salamat, Habibollah Younesi and Nader Bahramifar. Synthesis of magnetic core–shell Fe$_3$O$_4@TiO_2$ nanoparticlesfrom electric arc furnace dust for photocatalytic degradation of steel mill wastewater. *RSC Advances* 7(31), 19391–19405, 2017, Doi: 10.1039/c7ra01238a

[17] Andrea Villalba. Resistencia a herbicidas. Glifosato. *Ciencia,docenciaytecnología* 20, 169–186, 2009.

[18] Sally M. Bradberry, Alex T. Proudfoot and J. Allister Vale. Glyphosate poisoning. *Toxicological reviews*, 23(3), 159–167, 2004, Doi: 10.2165/00139709-200423030-00003

[19] Stephen O Duke and Stephen B Powles. Glyphosate: a once-in-a-century herbicide. *Pest Management Science: formerly Pesticide Science*, 64(4), 319–325, 2008, Doi: 10.1002/ps.1518

[20] Cluadia Monroy, Andrea Cortés, Diana Sicard and Helena de Restrepo. Citotoxicidad y genotoxicidad en célulashumanas expuestas in vitro a glifosato. *Biomédica, Revista del Instituto de Salud*, 25(3), 335–345, 2005, Doi: 10.7705/biomedica.v25i3.1358

[21] Carolina Campuzano, Luisa Feijoó, Karen Manzur, María Palacio, Julián Rendón, and Juan Zapata. Efectos de laintoxicación por glifosato en la población agrícola: revisión de tema. *CES Salud Pública*, 8(1), 121–133, 2017.

[22] Texto Unificado de Legislacion secundaria de medio ambiente. 2017, Revised on July 10 - 2020 from: https://www.ambiente.gob.ec/wp-content/uploads/downloads/2018/05/TULSMA.pdf

[23] Secundario, Texto Unificado de la Ley ambiental. *Norma de Calidad Ambiental y de Desacarga de efluentes: Recurso Agua*, Libro VI Anexo1. Anexo4, 2000. Revised on April 10 - 2020 from: https://www.ambiente.gob.ec/wp-content/uploads/downloads/2018/05/TULSMA.pdf

[24] Peñaherrera Colina. Situación actual sobre el uso del glifosato en Ecuador. *Viabilidad del glifosato en sistemas productivos sustentables* 2013, Revised on April 10 - 2020 from: http://www.ainfo.inia.uy/digital/bitstream/item/7629/1/18429080413103109.pdfpage=154

[25] Isabel Oller, S. Malato, Jose Sánchez. Combination of advanced oxidation processes and biological treatments-for wastewater decontamination—a review. *Science of The Total Environment*, 409(20), 4141–4166, 2011, Doi: 10.1016/j.scitotenv.2010.08.061

[26] Maria Klavarioti, Dionissios Mantzavinos, Despo Kassinos. Removal of residual pharmaceuticals from aqueous systems byadvanced oxidation processes. *Environment International*, 35(2), 402–417, 2009, Doi: 10.1016/j.envint.2008.07.009

[27] Sarai Bes, Adrian Silva, and Christophe Bengoa. Manual tecnico sobre procesos de oxidacion avanzada aplicados al tratamientode aguas residuales industriales. *España: CYTED*, 2018

[28] Roberto Andreozzi, Vincenzo Caprio, Amedeo Insola, Raffaele Marotta. Advanced oxidation processes (AOP) for water purificationand recovery. *Catalysis today*, 53(1), 51–59, 1999, Doi:10.1016/S0920-5861(99)00102-9

[29] Chen, H.-Y. Why the Reactive Oxygen Species of the Fenton Reaction Switches from Oxoiron(IV) Species to Hydroxyl Radical in Phosphate Buffer Solutions? A Computational Rationale. *ACS Omega*, 4, 9, 14105–14113, 2019, Doi:10.1021/acsomega.9b02023

[30] Juan Carlos Colmenares and Rafael Luque. Heterogeneous photocatalytic nanomaterials: prospects and challenges in selective transformations of biomass-derived compounds. *Chemical Society Reviews*, 43(3), 765-778, 2016, Doi: 10.1039/C3CS60262A

[31] Marye Anne Fox. Organic heterogeneous photocatalysis: chemical conversions sensitized by irradiated semiconduc-tors. *Accounts of Chemical Research*, 16(9), 314–321, 1983, Doi: 10.1021/ar00093a001

[32] Alex Ihadon, Paul Fitzpatrick. Heterogeneous photocatalysis: recent advances and applications. *Catalysts*, 3(1), 189–218, 2013, Doi: 10.3390/catal3010189

[33] Marta Litter. Heterogeneous photocatalysis: transition metal ions in photocatalytic systems. *Applied Catalysis B: Environmental*, 23(2-3), 89–114, 1999, Doi: 10.1016/S0926-3373(99)00069-7

[34] Soledad Esteban Santos. Catálisis en química orgánica. *Editorial UNED*, 2017.

[35] Jacques P. Fraissard, Curt W. Conner. Physical adsorption: experiment, theory, and applications. *Springer Science Business Media*, 491, 1997.

[36] I. Tuñón, E. Ortí, C. Gómez, J. Pascual-Ahui, and I Monzó. Superficies sólidas: adsorción y catálisis heterogénea. Revised on 22 July 22 - 2020 from: $https://www.uv.es/tunon/pdf\_doc/Superficies\_Solidas_A.pdf$

[37] Shouheng Sun and Hao Zeng. Size-controlled synthesis of magnetite nanoparticles. *Journal of the American Chemical Society*, 124(28), 8204–8205, 2002, Doi: 10.1021/ja026501x

[38] Zeid A. ALOthman. A review: fundamental aspects of silicate mesoporous materials. *Materials*, 5(12), 2874–2902, 2012, Doi: 10.3390/ma5122874

[39] Perla B. Balbuena and Keith E. Gubbins. Theoretical interpretation of adsorption behavior of simple fluids in slit pores. *Langmuir*, 9(7), 1801–1814, 1993, Doi: 10.1021/la00031a031

[40] Mays Alhamami, Huu Doan and Chil-Hung Cheng. A review on breathing behaviors of metal-organic-frameworks(MOFs) for gas adsorption. *Materials*, 7(4), 3198–3250, 2014, Doi:10.3390/ma7043198

[41] Lu Lv, G. Tsoi and S. Zhao. Uptake equilibria and mechanisms of heavy metal ions on microporous titanosilicate ETS-10. *Industrial engineering chemistry research*, 43(24), 7900–7906, 2004, Doi:10.1021/ie0498044

[42] Ruthven Douglas M. Principles of adsorption and adsorption processes. John Wiley Sons, 1984.

[43] K. L. Tan, B. Hameed. Insight into the adsorption kinetics models for the removal of contaminants from aqueoussolutions. *Journal of the Taiwan Institute of Chemical Engineers*, 74, 25–48, 2017, Doi: 10.1016/j.jtice.2017.01.024

[44] Ilje Pikaar, Albert A. Koelmans and Paul C. M. van Noort. Sorption of organic compounds to activated carbons. Evaluationof isotherm models. *Chemosphere*, 65(11), 2343–2351, 2006, Doi:10.1016/j.chemosphere.2006.05.005

[45] Edzwald, James K. Water Quality and Treatment A Handbook on Drinking Water. *McGrawHill*, 2010.

[46] Chaim Aharoni and Donald L. Sparks. Kinetics of soil chemical reactions—a theoretical treatment. *Rates of soil chemical processes*, 27, 1–18, 1991, Doi: 10.2136/sssaspecpub27.c1

[47] Y. S. Ho, G. McKay. Pseudo-second order model for sorption processes. *Process biochemistry*, 34(5),451–465, 1999, Doi: 10.1016/S0032-9592(98)00112-5

[48] A. K. Haghi, Sabu Thomas, Moein MehdiPour MirMahaleh, Saeedeh Rafiei, Shima Maghsoodlou, Arezo Afzali. Foundations of nanotechnology, Three Volume Set. *CRC Press*, 2015.

[49] Bharat Bhushan. Springer hand book of nanotechnology. *Springer*, 2017.

[50] Buzea, Cristina, Ivan I. Pacheco, and Kevin Robbie. Nanomaterials and nanoparticles: sources and toxicity. *Biointerphases*, 2(4), MR17–MR71, 2007, Doi: 10.1116/1.2815690

[51] Jo Anne Shatkin. Nanotechnology: health and environmental risks. *Crc Press*, 2012.

[52] Roger Whatmore. Nanotechnology—what is it? Should we be worried?. *Occupational Medicine*, 56(5), 295–299, 2006, Doi:10.1093/occmed/kql050

[53] Toumey, C. Plenty of room, plenty of history. *Nature nanotechnology*, 4(12), 783–784, 2009, 2009, Doi:10.1038/nnano.2009.357

[54] Attarad Ali, Hira Zafar, Muhammad Zia, Ihsan ul Haq, Abdul Rehman Phull, Joham Sarfraz Ali and Altaf Hussain. Synthesis, characterization,applications, and challenges of iron oxide nanoparticles. *Nanotechnology, science and applications*, 9, 49-67, 2016, Doi: 10.2147/NSA.S99986

[55] Ibrahim Khan, Khalid Saeed and Idrees Khan. Nanoparticles: Properties, applications and toxicities. *Arabian Journal of Chemistry*, 12(7), 908–931, 2019, Doi: 10.1016/j.arabjc.2017.05.011

[56] Siyam M. Ansar, Fathima S. Ameer, Wenfang Hu, Shengli Zou, Charles U. Pittman, and Dongmao Zhang. Removal of molecular adsorbateson gold nanoparticles using sodium borohydride in water. *Nanoletters*, 13(3), 1226–1229, 2013, Doi: 10.1021/nl304703w

[57] Fritz Allhoff, Patric Lin, Daniel Moore. What is nanotechnology and why does it matter?: from science to ethics. *JohnWiley Sons*, 2009.

[58] V. Pokropivny, V. Skorokhod. Classification of nanostructures by dimensionality and concept of surface formsengineering in nanomaterial science. *Materials Science and Engineering:C*, 27(5-8), 990–993, 2007, Doi:10.1016/j.msec.2006.09.023

[59] Won-Kyung Shin, Jinhyun Cho, Aravindaraj G. Kannan, Yoon-Sung Lee and Dong-Won Kim. Cross-linked composite gel polymer elec-trolyte using mesoporous methacrylate-functionalized SiO_2 nanoparticles for lithium-ion polymer batteries. *Scientific reports*, 6(1), 26332, 2016, Doi: 10.1038/srep2632

[60] Tuan Sang Tran, Seung Jun Park, Sung Sic Yoo, Tae-Rin Lee and TaeYoung Kim. High shear-induced exfoliation of graphite into highquality graphene by Taylor–Couette flow. *RSC advances*, 6(15), 12003–12008, 2016, Doi: 10.1039/C5RA22273G

[61] Siddhant Jain and Mohan Singh Mehata. Medicinal plant leaf extract and pure flavonoid mediated green synthesis of silvernanoparticles and their enhanced antibacterial property. *Scientific reports*, 7(1), 1–13, 2017, Doi:10.1038/s41595-017-15724-8

[62] Ling Zhang, Rong He and Hong-Chen Gu. Oleic acid coating on the monodisperse magnetite nanoparticles. *Applied Surface Science*, 253(5), 2611–2617, 2006, Doi: 10.1016/j.apsusc.2006.05.023

[63] Ting Guo, Mei Lin , Junxing Huang, Chenglin Zhou, Weizhong Tian, Hong Yu, Xingmao Jiang , Jun Ye , Yujuan Shi, Yanhong Xiao, Xuefeng Bian, and Xiaoqian Feng. The recent advances of magnetic nanoparticles in medicine. *JournalofNanomaterials*, 1-8, 2018, Doi: 10.1155/2018/7805147

[64] Martin Friák, Arno Schindlmayr and Matthias Scheffler. Ab initio study of half-metal to metal transition in magnetite. *New journal of physics*, 9(1), 5-5, 2007, Doi: 10.1088/1367-2630/9/1/005

[65] AnA. L. Andrade, D. M. Souza, M. C. Pereira, J. D. Fabris and R. Z. Domingues. Synthesis and characterization of magneticnanoparticles coated with silica through a sol-gel approach. *Cerâmica*, 55(336), 420–424, 2009, Doi: 10.1590/S0366-69132009000400013

[66] Juliana de Freitasa, Rogerio Mendes, Isabella Garcia, Taciane da Costab, Maria Nogueira, Miguel Júniorb and Rodrigo Costa. Magnetic nanoparticles obtained by homogeneous coprecipitation sonochemically assisted. *Materials Research*, 18(2), 220–224, 2015, Doi: 10.1590/1516-1439.366114

[67] Sarah Briceño, Werner Brämer-Escamilla, Pedro Silva, Gerzon Delgad, Eric Plaza, Jordana Palacios and Edgard Cañizales. Effects ofsynthesis variables on the magnetic properties of $CoFe_2O_4$ nanoparticles. *Journal of Magnetism and Magnetic Materials*, 324(18), 2926–2931, 2012, Doi:10.1016/j.jmmm.2012.04.051

[68] Pierre Dresco, Vladimir Zaitsev, Richard Gambino, and Benjamin Chu. Preparation and properties of magnetite and polymer magnetite nanoparticles. *Langmuir*, 15(6), 1945–1951, 1999, Doi: 10.1021/la980971g

[69] Enisa Omanović-Mikličanin, Almir Badnjević, Anera Kazlagić, Muhamed Hajlovac. Nanocomposites: a brief review. *Health and Technology*. 1-9, 2019, Doi:10.1007/s12553-019-00380-x

[70] Virginia Noval and Jose Carriazo. $Fe_3O_4 - TiO_2$ and $Fe_3O_4 - SiO_2$ Core-shell Powders Synthesized from Industrially Processed Magnetite (Fe_3O_4) Microparticles. *Materials Research*, 22(3), 2019, Doi: 10.1590/1980-5373-mr-2018-0660

[71] S. Rana, R. S. Srivastava, M. M. Sorensson and R. D. K. Misra. Synthesis and characterization of nanoparticles withmagnetic core and photocatalytic shell: anatase TiO_2-$NiFe_2O_4$ system. *Materials Science and Engineering:B*, 119(2), 144–151, 2005, Doi: 10.1016/j.mseb.2005.02.043

[72] Rajesh Chalasani and Sukumaran Vasudevan. Cyclodextrin-functionalized $Fe_3O_4@TiO_2$: reusable, magnetic nanoparticlesfor photocatalytic degradation of endocrine-disrupting chemicals in water supplies. *ACS Nano*, 7(5), 4093–4104, 2013, Doi: 10.1021/nn400287k

[73] Qinghang He, Zhenxi Zhang, Jianwen Xiong, Yuying Xiong, and Hua Xiao. A novel biomaterial—Fe_3O_4 : TiO_2 core-shell nano particlewith magnetic performance and high visible light photocatalytic activity. *Optical Materials*, 31(2), 380–384, 2008, Doi: 10.1016/j.optmat.2008.05.011

[74] Tiejun Xin, Mingliang Ma, Hepeng Zhang, Junwei Gu, Shuangjie Wan,g Mengjiao Liu and Qiuyu Zhang. A facile approach for the synthesis of magnetic separable $Fe_3O_4@TiO_2$, core–shell nanocomposites as highly recyclable photocatalysts. *Applied Surface Science*, 288, 51–59, 2014, Doi:10.1016/j.apsusc.2013.09.108

[75] Nam Tran, Patrick Drogui, Tuan Linh Doan, Thanh Son Le and Hoai Chau Nguyen. Electrochemical degradation and mineralization ofglyphosate herbicide. *Environmental technology*, 38(23), 2939–2948, 2017, Doi: 10.1080/09593330.2017.1284268

[76] Rui Huo, Xue-Ling Yang, You-Qin Liu and Yue-Hua Xu. Visible-light photocatalytic degradation of glyphosate over BiVO$_4$ prepared by different co-precipitation methods. *Materials Research Bulletin*, 88, 56–61, 2017, Doi: 10.1016/j.materresbull.2016.12.012

[77] Eduardo Vidal, Antonio Negro, Alberto Cassano and Cristina Zalazar. Simplified reaction kinetics, models and experiments forglyphosate degradation in water by the UV/H$_2$O$_2$ process. *Photochemical Photobiological Sciences*, 14(2), 366–377, 2015, Doi:10.1039/c4pp00248b

[78] Shadia J. Ikhmayies. Characterization of nanomaterials. *JOM*, 66(1), 28–29, 2014, Doi: 10.1007/s11837-013-0826

[79] Anshida Mayeen, Leyana K. Shaji, Anju K. Nair and Nandakumar Kalarikkal. Characterization of Nano-materials: Chapter 12 - Morphological Characterization of Nanomaterials. *Elsevier*, pp335–364, 2018, Doi: 10.1016/B978-0-08-101973-3.00012-2

[80] Brian M. Tissue. Ultraviolet and visible absorption spectroscopy. *Characterization of Materials*, 1–13, 2002, Doi: 10.1002/0471266965.com059.pub2

[81] Michael H. Penner. Ultraviolet, Visible, and Fluorescence Spectroscopy, *Springer*, pp 387–405, 2010, Doi: 10.1007/978-1-4419-1478-1_22

[82] Akash, Muhammad Sajid Hamid, and Kanwal Rehman. Essentials of Pharmaceutical Analysis. *Springer*, 2020.

[83] Ismail, A. A., van de Voort, F. R., Sedman, J. Chapter 4 Fourier transform infrared spectroscopy: Principles and applications. Instrumental Methods in Food Analysis, 93–139, 1997, Doi:10.1016/s0167-9244(97)80013-3

[84] Wellner, N. Fourier transform infrared (FTIR) and Raman microscopy: principles and applications to food microstructures. Food Microstructures, 163–191, 2013. Doi:10.1533/9780857098894.1.163

[85] Smith, B. How an FTIR works. Fundamentals of Fourier Transform Infrared Spectroscopy, 2011, 19–54.

[86] Titus, D., James Jebaseelan Samuel, E., Roopan, S. M. Nanoparticle characterization techniques. Green Synthesis, Characterization and Applications of Nanoparticles, 303–319, 2019. Doi:10.1016/b978-0-08-102579-6.00012-5

[87] Heidari, A.; Gobato, R. Ultraviolet Photoelectron Spectroscopy (UPS) and Ultraviolet–Visible (UV–Vis)Spectroscopy Comparative Study on Malignant and Benign Human Cancer Cells and Tissues with the Passageof Time under Synchrotron Radiation. *Parana Journal of Science and Education*, 4(6), 18–33, 2014.

[88] Chen Xu, Ye Song, Linfeng Lu, Chuanwei Cheng, Dongfang Liu, Xiaohong Fang, Xiaoyuan Chen, Xufei Zhu and Dongdong Li. Electrochemically hydrogenated TiO$_2$ nanotubes with improved photoelectrochemical water splitting performance. *Springer*, 8(1), 49–62, 2013, Doi: 10.1186/1556-276x-

[89] Harriet P. Moeur, Andrew Zanella, and Thomas Poon. An Introduction to UV-Vis Spectroscopy Using Sun-screens. *Journal of Chemical Education*, 83(5), 769, 2006, Doi:10.1021/ed083p769

[90] Kawther El-Gendy, Eman Mosallam, Nabila Ahmed, Nagat Aly. Determination of glyphosate residues in Egyptian soil samples. *Analytical Biochemistry*, 557, 1–6, 2018, Doi:10.1016/j.ab.2018.07.004

[91] McConnell, J. Scott, Rose M. McConnell, and Lloyd R. Hossner. Ultraviolet spectra of acetic acid, glycine, and glyphosate. *Journal of the Arkansas Academy of Science* 47.1 (1993): 73-76.

[92] Mauricio Rodríguez Páez. Y. Ochoa-Muñoz, J. E. Rodriguez-Páez. (2018) Uso de Nanoparticulas de ZnO (ZnO NPs) en la Remoción del Herbicida Glifosato. *Departamento de Física/FACNED. Universidad del Cauca. Popayán – Colombia* Retrieved: 27 march 2021, from:https://expeditiorepositorio.utadeo.edu.co/bitstream/handle/20.500.12010/8239/Trabajo%20de%20grado.pdf ?sequence=1isAllowed=y

[93] D. N. Leonard, G. W. Chandler, and S. Seraphin. Characterization of Materials. *American Cancer Society*, 1–16, 2012, Doi: 10.1002/0471266965

[94] My Scope Scaning Elecetron Microscopy. Revised on Agust 16 - 2020 from: https://myscope.training//SEMlevel_3_1

[95] Weilie Zhou, Robert Apkarian, Zhong Lin Wang and David Joy. Fundamentals of Scanning Electron Microscopy (SEM). *Springer*, pp 1-40, 2006, Doi: 10.1007/978-0-387-29620-0_1

[96] Reimer, L. Scanning Electron Microscopy: Physics of Image Formation and Microanalysis, Second Edition. *Springer*, 11(12), 45, 2000, Doi: 10.1088/0957-0233/11/12/703

[97] Nanakoudis, A. What is SEM? Scanning electron microscope technology explained. *Thermo Fisher Scientific* 2018. Revised on Agust 25 - 2020 From: https://www.nanoscience.com/techniques/scanning-electron-microscopy/: :text=A%20scanning%20electron%20microscope%20(SEM,the%20surface%20topography%20 and%20composition.

[98] Swapp, S.; Microscopy, S. E. University of Wyoming. Scanning Electron Microscopy(SEM), Revised on Agust 28 - 2020 frmo: https://serc.carleton.edu/researcheducation/geochemsheets/techniques/SEM.html

[99] Leili Baghaei Rad, Hanying Feng, Jun Ye, and R. F. W. Pease. Computational scanning electron microscopy. *AIP Conference Proceedings*, 2007, Doi: 10.1063/1.2799427

[100] Kalsoom Akhtar, Shahid Ali Khan, Sher Bahadar Khan and Abdullah M. Asiri. Scanning Electron Microscopy: Principle and Applications in Nanomaterials Characterization. *Springer*, 113–145, 2018, Doi: 10.1007/978-3-319-92955-2

[101] Zhihan Yang, Wanlin Wu, Ling Yu, Xiaoyun Fan and Yang Yu. Fabrication and characterization of magnetically responsive Fe_3O_4@TiO_2 core-shell adsorbent for enhanced thallium removal. *Environmental Science and Pollution Research*, 27(24), 30518-30529, 2020, Doi:10.1007/s11356-020-09144-x

[102] Hammond, Christopher, and Christopher Hammond. The basics of cristallography and diffraction. Vol. 214. Oxford, 2001.

[103] Christopher G. Pope. X-ray diffraction and the Bragg equation. *Journal of chemical education*, 74, 129, 1994.

[104] Ayers, J. The measurement of threading dislocation densities in semiconductor crystals by X-ray diffraction. *Journal of Crystal Growth*, 74(1), 129, 1997, Doi: 10.1021/ed074p129

[105] Guinier, André. X-ray diffraction in crystals, imperfect crystals, and amorphous bodies. Courier Corporation, 1994.

[106] Cullity, Bernard Dennis. Elements of X-ray Diffraction. Addison-Wesley Publishing, 1956.

[107] C. Suryanarayana and M. Grant Norton. X-ray diffraction: a practical approach. *Springer Science Business Media*, 63-64, 2013, Doi: 10.1007/978-1-4899-0148-4_3

[108] Khashan, S., Dagher, S., Tit, N., Alazzam, A., Obaidat, I. Novel method for synthesis of $Fe_3O_4 - SiO_2 - TiO_2$ core/shell nanoparticles. Surface and Coatings Technology, 322, 92–98, 2017, Doi:10.1016/j.surfcoat.2017.05.045

[109] Nguyen Duong, Le Vuong, Nguyen Son, Ho Van Tuyen, Truong Van Chuong. The synthesis of TiO_2 nanoparticlesusing sulfuric acid method with the aid of ultrasound. *Nanomaterials and Energy*, 6(2), 82–88, 2017, Doi: 10.1680/jnaen.17.00009

[110] Amir Hassanjani, Seyed Kazemzadeh, Mohammmad Vaezi, and Ali Shokuhfar. Effect of sonication power on thesonochemical synthesis of titania nanoparticles. *Journal of Ceramic Processing Research*, 12(3), 299–303, 2011.

[111] Li, W.; Ni, C.; Lin, H.; Huang, C.; Shah, S. I. Size dependence of thermal stability of TiO_2 nanoparticles. *Journal of Applied Physics*, 96(11), 6663–6668, 2004, Doi: 10.1063/1.1807520

[112] Didier Devilliers, Mai Thanh Dinh, Eric Mahé, Denise Krulic, Nathalie Larabi and Nicolas Fatouros, N. Behaviour of titanium in sulphuricacid-application to DSAs. *J NewMat Electrochem Sys*, 9, 221–232, 2006,

[113] Maria Vanegas, Veronica Vázquez, Diana Moscoso, Christian Cruzat. Síntesis y caracterización de nanopartículas magnéticasdel tipo Fe$_3O_4/TiO_2$, efecto del pH en la dispersión y estabilización en soluciones acuosas. *Maskana*, 5(1), 43–55, 2012.

[114] Andre. Hubaux and Gilbert. Vos, Gilbert. LDecision and detection limits for calibration curves. *Analytical chemistry*, 42(8), 849-855, 1970, Doi: 10.1021/ac60290a013

[115] Cláudia F. B. Coutinho, Lincoln F. M. Coutinho, Luiz H. Mazo, Suzana L. Nixdorf, Carlos A. P. Camara and Fernando M. Lançasa. Direct determination of glyphosate using hydrophilic interaction chromatography with coulometric detection at copper microelectrode. *Analytica Chimica Acta*, 592(1), 30–35, 2007, Doi: 10.1016/j.aca.2007.04.003

[116] Bing Qu, Wenli Hu, Lin Deng, Weiyi Sun, Sanglan Ding, Zhiwei Gan*, and Shijun Su. Simultaneous Determination of Dithionate Andsulfate in Leaching Solution from SO_2-Leaching Pyrolusite by Ion Chromatography. *Energy Fuels*, 30(10), 8561–8566, 2016, Doi: 10.1021/acs.energyfuels.6b01333

[117] Xianguo Liu, Dianyu Geng, Xiaolei Wang, Song Ma, Han Wang, Da Li, Baiqing Li, Wei Liu and Zhidong Zhang. Enhanced photocatalyticactivity of Mo–001TiO$_2$ core–shell nanoparticles under visible light. *Chemical communications*, 46(37), 6956–6958, 2010, Doi: 10.1039/C0CC02034F

[118] Kadarkarai Murugan, Devakumar Dinesh, Krishnamoorthy Kavithaa, Manickam Paulpandi, Thondhi Ponraj, Mohamad Saleh Alsalhi, Sandhanasamy Devanesan, Jayapal Subramaniam, Rajapandian Rajaganesh, Hui Wei, Suresh Kumar, Marcello Nicoletti and Giovanni Benelli. Hydrothermal synthesis of titanium dioxide nanoparticles: mosquitocidal potential and anticanceractivity on human breast cancer cells (MCF-7). *Springer*, 115(3), 1085–1096, 2016, Doi: 10.1007/s00436-015-4838-8

[119] Cyril Gaudillere and José Manuel Serra. Fabrication of highly porous and hierarchical ceramic supportsfor energy applications. *Boletín de la Sociedad Española de Cerámica y Vidrio*, 55(2), 45–54, 2016, Doi: 10.1016/j.bsecv.2016.02.002

[120] Sharif Ahmad, Ufana Riaz, Ajeet Kaushik and Javed Alam . Soft template synthesis of super paramagnetic Fe$_3$O$_4$ nanoparticles a novel technique. *Journal of Inorganic and Organometallic Polymers and Materials*, 19(3), 355–360, 2009, Doi: 10.1007/s10904-009-9276-6

[121] S. H. Chaki, Tasmira J. Malek, M. D. Chaudhary, J. P. Tailor, and M. P. Deshpande. Magnetite Fe_3O_4 nanoparticles synthesis by wet chemical reduction and their characterization. *Advances in Natural Sciences: Nanoscience and Nanotechnology*, 6(3), 035009, 2015, Doi: 0.1088/2043-6262/6/3/035009

[122] Tianjie Hong, Jun Mao, Feifei Tao, and Mingxuan. Recyclable Magnetic Titania Nanocomposite from Ilmenite with Enhanced Photocatalytic activity. *Molecules*, 22(), 2044, 2017, Doi: 10.3390/molecules22122044

[123] Chenyang Xue, Qiang Zhang, Junyang Li, Xiujian Chou, Wendong Zhang, Hua Ye, Zhanfeng Cui and Peter J. Dobson. High photocatalytic activity of $Fe_3O_4 - SiO_2 - TiO_2$ functional particles with core-shell structure. *Journal of Nanomaterials*, 1-8, 2013, Doi: 10.1155/2013/762423

[124] Mercyrani B., R. Hernandez-Maya, M. Solís-López, Christeena Th-Th and Velumani. Photocatalytic Degradation of Orange G using TiO_2/Fe_3O_4 nanocomposites. *Journal of Materials Science: Materials in Electronics*, 29, 15436-15444, 2018, Doi: 10.1007/s10854-018-9069-1

[125] Congzhi Fu, Xijun Liu and Yuwei Wang. The synthesis and characterization of an $Fe_3O_4@TiO_2$ˇNi/rGO magnetic photocatalyst. *New Journal of Chemistry* , 44, 5755–5761, 2020, Doi: 10.1039/D0NJ00069H

[126] Karaked Tedsree, Natcha Temnuch, Nipaporn Sriplai, Supree Pinitsoontorn. Ag modified $Fe_3O_4@TiO_2$ magnetic core-shell nanocomposites for photocatalytic degradation of methylene blue. *Materials Today: Proceedings*, 4(5), 6576–6584, 2017, Doi: 10.1016/j.matpr.2017.06.170

[127] Khodaparast, P., Ounaies, Z. Influence of dispersion states on the performance of polymer-based nanocomposites. *Smart Materials and Structures*, 23(10), 104004. 2014, Doi:10.1088/0964-1726/23/10/104004

[128] Guan, S., Liu, X., Zhang, Y., Liu, Y., Wang, L., Liu, Y. Synthesis and Characterization of Polycaprolactone Modified Trimellitate Nano-Lubricant. *Materials*, 12(14), 2273, 2019, Doi:10.3390/ma12142273

[129] Govindasamy, G., Murugasen, P., Sagadevan, S. Investigations on the Synthesis, Optical and Electrical Properties of TiO_2 Thin Films by Chemical Bath Deposition (CBD) method. *Materials Research*, 19(2), 413–419, 2016, Doi:10.1590/1980-5373-mr-2015-0411

[130] Khan, M., Naqvi, A. H., Ahmad, M. Comparative study of the cytotoxic and genotoxic potentials of zinc oxide and titanium dioxide nanoparticles. *Toxicology Reports*, 2, 765–774, 2015, Doi:10.1016/j.toxrep.2015.02.004

[131] Salamat, S., Younesi, H., Bahramifar, N. Synthesis of magnetic core–shell $Fe_3O_4@TiO_2$ nanoparticles from electric arc furnace dust for photocatalytic degradation of steel mill wastewater. *RSC Advances*, 7(31), 19391–19405, 2017, Doi:10.1039/c7ra01238a

[132] Zuoli He, Wenxiu Que,Jing Chen, Yucheng He, Gangfeng Wang. Surface chemical analysis on the carbon-doped mesoporous TiO2 photocatalysts after post-thermal treatment: XPS and FTIR characterization. *Journal of Physics and Chemistry of Solids*, 74(7), 924–928, 2013, Doi:10.1016/j.jpcs.2013.02.001

[133] Briceño, S., Brämer-Escamilla, W., Silva, P., Delgado, G. E., Plaza, E., Palacios, J., Cañizales, E. Effects of synthesis variables on the magnetic properties of CoFe$_2$O$_4$ nanoparticles. *Journal of Magnetism and Magnetic Materials*, 324(18), 2926–2931, 2012, Doi:10.1016/j.jmmm.2012.04.051

[134] Nalbandian, L., Patrikiadou, E., Zaspalis, V., Patrikidou, A., Hatzidaki, E., N. Papandreou, C. Magnetic Nanoparticles in Medical Diagnostic Applications: Synthesis, Characterization and Proteins Conjugation. *Current Nanoscience*, 12(4), 455–468, 2016, Doi:10.2174/1573413712666151210230002

[135] Chauhan, Ruby Chauhan, Ashavani Kumar, Ram PalChaudhary. Structural and photocatalytic studies of Mn doped TiO$_2$ nanoparticles. *Spectrochimica Acta Part A: Molecular and Biomolecular Spectroscopy*, 98, 256–264, 2012, Doi: 10.1016/j.saa.2012.08.009

[136] R. A. Spurr and Howard. Myers. Quantitative analysis of anatase-rutile mixtures with an X-ray diffractometer. *Analytical chemistry* 29(5), 760–762, 1957, Doi: 10.1021/ac60125a006

[137] S. Mahshid, M. Askari, M. Sasani Ghamsari. Synthesis of TiO$_2$ nanoparticles by hydrolysis and peptization oftitanium isopropoxide solution. *Journal of Materials Processing Technology*, 189(1-3), 296–300, 2007, Doi: 10.1016/j.jmatprotec.2007.01.040

[138] M. M. Viana, V. F. Soares and N. D. S. Mohallem. Synthesis and characterization of TiO$_2$ nanoparticles. *Ceramics International*, 36(7), 2047–2053, 2010, Doi: 10.1016/j.ceramint.2010.04.006

[139] Gerko Oskam, Abhinav Nellore, R. Lee Penn, and Peter C. Searson. The growth kinetics of TiO_2 nanoparticles from titanium (IV) alkoxide at high water/titanium ratio. *The Journal of Physical Chemistry B*, 107(8), 1734–1738, 2003, Doi: 10.1021/jp021237f

[140] Jesús Vargas Hernández, Sandrine Coste, Antonieta García Murillo, Felipe Carrillo Romoa, Abdelhadi Kassiba. Effects of metal doping (Cu, Ag, Eu)on the electronic and optical behavior of nanostructured TiO_2. *Journal of Alloys and Compounds*, 710, 355–363, 2017, Doi: 10.1016/j.jallcom.2017.03.275

[141] Wei Li, Ahmed Elzatahry, Dhaifallah Aldhayan and Dongyuan Zhao. Core–shell structured titanium dioxide nanomaterials for solar energy utilization. *Chemical Society Reviews*, 47(22), 8203–8237, 2018, Doi: 10.1039/C8CS00443A

[142] Yajuan Li, Chuanqi Zhao, Yujuan Wen, Yuanyuan Wang and Yuesuo Yang. Adsorption performance and mechanism of magnetic reducedgraphene oxide in glyphosate contaminated water. *Environmental Science and Pollution Research*, 25(21), 21036–21048, 2018, Doi: 0.1007/s11356-018-2282-x

[143] Mohammad Muneer and Colin Boxall. Photocatalyzed degradation of a pesticide derivative glyphosate in aqueous suspensionsof titanium dioxide. *International Journal of Photoenergy*, 1-7, 2008, Doi: 10.1155/2008/197346

[144] Wei Zhang, Linda Zou, and Lianzhou Wang. Photocatalytic TiO_2/adsorbent nanocomposites prepared via wet chemicalimpregnation for wastewater treatment: A review. *Applied Catalysis A: General*, 371(1-2), 1–9, 2009, Doi: 10.1016/j.apcata.2009.09.038

[145] Melissa S. Caetano, Teodorico C. Ramalho, Douglas F. Botrel, Elaine F. F. da Cunha, and Walclee Carvalho de Mello. Understanding the inactivationprocess of organophosphorus herbicides: A DFT study of glyphosate metallic complexes with Zn^{2+}, Ca^{2+}, Mg^{2+}, Cu^{2+}, Co^{3+}, Fe^{3+}, Cr^{3+}, and Al^{3+}. *International Journal of Quantum Chemistry*, 112(15), 2752–2762, 2012, Doi: 10.1002/qua.23222

[146] Bernards, M. L. AMS plays a valuable role in preventing glyphosate from binding to hard water ions thatreduce its effectiveness. *Institute of Agriculture and Natural Resources CROPWATCH*, 2007. Revised on Octover 19 - 2020 from: https://cropwatch.unl.edu/ams-what-it-doing-my-tank

[147] Ramrakhiani, L., Ghosh, S., Mandal, A. K., Majumdar, S. Utilizationof multi-metal laden spent biosorbent for removal of glyphosate herbicide from aqueous solution and its mechanism elucidation. Chemical Engineering Journal, 2018, Doi:10.1016/j.cej.2018.12.163

[148] Pankajakshan, A., Sinha, M., Ojha, A. A., Mandal, S. Water-Stable Nanoscale Zirconium-Based Metal–Organic Frameworks for the Effective Removal of Glyphosate from Aqueous Media. ACS Omega, 3(7), 7832–7839, 2018, Doi:10.1021/acsomega.8b00921

[149] Valle, A. L., Silva, A. C., Dantas, N. O., Sabino-Silva, R., Melo, F. C., Moreira, C. S., ... Goulart, L. R. Application of ZnO Nanocrystals as a Surface-Enhancer FTIR for Glyphosate Detection. Nanomaterials, 11(2), 509, 2021, Doi: https://doi.org/10.3390/nano11020509

Abbreviations

AMPA aminomethylphosphonic acid 1
AOP Advance Oxidation Processes ix, 9

BSE backscattered electrons 30

Fe$_3$O$_4$ Magnetic Nanoparticles, Magnetite 2
FTIR Fourier Transform Infrared Spectroscopy iii, x, 51

NPs Nanoparticles ix, 19, 20, 27

PMG Glyphosate (N-phosphonomethyl glycine) 1, 5, 7, 8

SE secondary electrons 30
SEM Scanning Electron Microscopy iii, x, 3, 30, 57

TiO$_2$ Titanium Dioxide iii, 2, 39, 40

UV ultraviolet spectral region 2

XRD X-ray diffraction iii, x, 53